

**PZAS™ at NGCC conditions**

**FEBRUARY 7, 2020**

**TO**

**NATIONAL CARBON CAPTURE CENTER**

**WORK SUPPORTED BY**

**CARBON CAPTURE PROJECT 4**

## Table of Contents

PZAZ™ at NGCC Conditions	p. 2
Measured and Modeled Energy Performance of the Piperazine Advanced Stripper (PZAS™) at NCCC with 4% and 12% CO <sub>2</sub>	p. 15
CO <sub>2</sub> Absorption from Gas Turbine Flue Gas by Aqueous Piperazine with Intercooling	p. 33
Corrosion by Aqueous Piperazine at 40–150 °C in Pilot Testing of CO <sub>2</sub> Capture	p. 66
PZ emissions from PZAS™ on Natural Gas Combined Cycle	p. 91
Piperazine Oxidation in PZAS™ Configuration	p. 99

# **PZAS™ at NGCC conditions**

Pilot plant testing at the National Carbon Capture Center (NCCC)

December 2018 – June 2019

Funded by the Carbon Capture Project (CCP4)

by

Gary T. Rochelle, Tianyu Gao, Ching-Ting Liu, Athreya Suresh, Yuying Xu, Korede Akinpelumi, Eric Chen

McKetta Department of Chemical Engineering

The University of Texas at Austin

Final report for the National Carbon Capture Center

February 7, 2020

## ***Introduction***

With funding from DOE and industrial sponsors, the University of Texas at Austin (UT) has developed the PZAS™ process for CO<sub>2</sub> capture with aqueous, 5 m piperazine (PZ) using the Advanced Stripper. The PZAS™ process was successfully tested in 2018 at coal conditions (11% CO<sub>2</sub>) in the Pilot Solvent Test Unit (PSTU) at the National Carbon Capture Center (NCCC) with a new skid implementing the Advanced Stripper. The specific heat duty (corrected for flow measurement and for heat loss) was 2.35 GJ/tonne CO<sub>2</sub> with 91% CO<sub>2</sub> removal. After 2000 hours of operation the apparent rate of PZ oxidation was 0.1 kg/tonne CO<sub>2</sub>, at the end of the campaign. In the 2018 campaign, unacceptable corrosion of 316L SS and carbon steel was measured with coupons in the hot rich solvent after the steam heater.

The CO<sub>2</sub> Capture Project 4 (CCP4) funded UT to test PZAS™ at flue gas conditions (4.3% CO<sub>2</sub>) of a Natural Gas Combined Cycle (NGCC) in the PSTU using the same Advanced Stripper and starting with the final inventory of aged PZ from the coal campaign. The campaign provided twelve weeks of operation using three different absorber configurations and included several methods to mitigate oxidation as well as corrosion coupon testing to identify suitable materials of construction.

## ***PZAS™ test description***

Figure 1 shows the system configuration and typical operating conditions during the 6+ weeks of long-term testing at the end of the campaign. Coal-fired flue gas was passed through the prescrubber to remove SO<sub>2</sub>. The flue gas was diluted with air to get 4.3% (dry) CO<sub>2</sub> to simulate NGCC flue gas. The PSTU absorber piping was modified to permit pump-around intercooling on the bottom section using two existing intercooling exchangers and pumps.

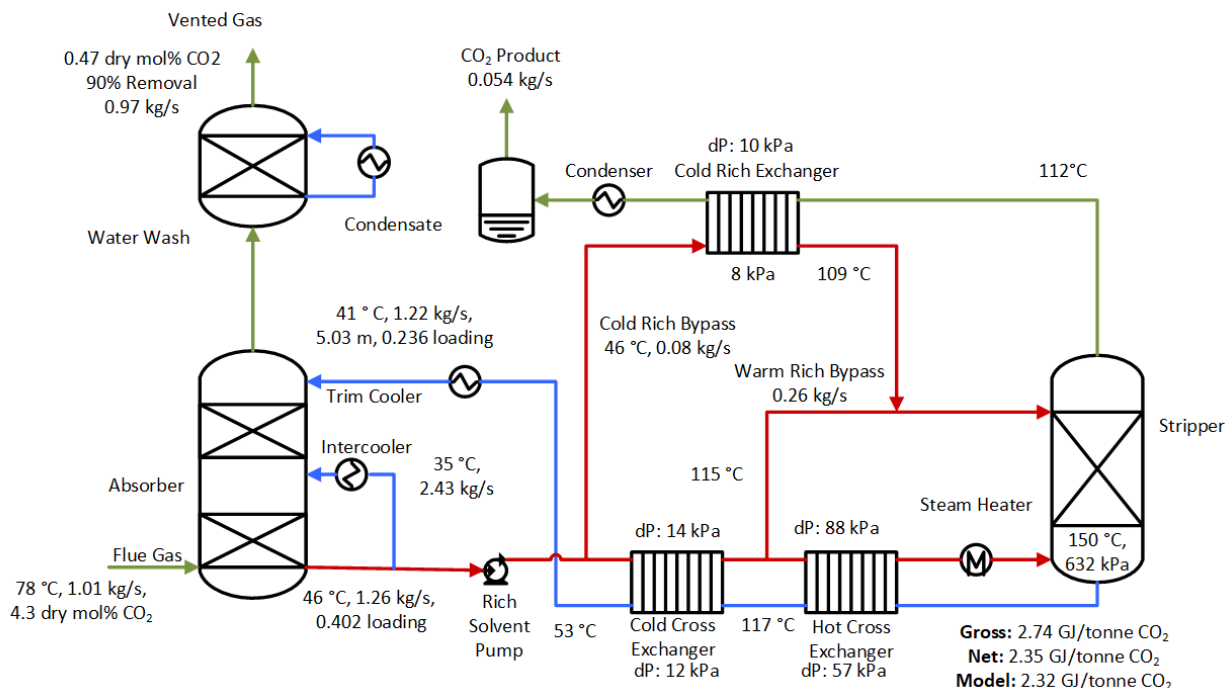


**Figure 1: PZAS™ conditions for long-term testing at NCCC with 4.3% CO<sub>2</sub>**

As shown in Figure 2, three absorber configurations were tested during the campaign:

- 1) In-and-out (I&O) intercooling between two 20-ft beds of packing, flue gas cooled to 40 °C;
- 2) Pump-around (PA) intercooling to 40 °C, flue gas cooled to 40 °C;
- 3) Pump-around intercooling to 35 °C or 40 °C, flue gas uncooled (75–78 °C).

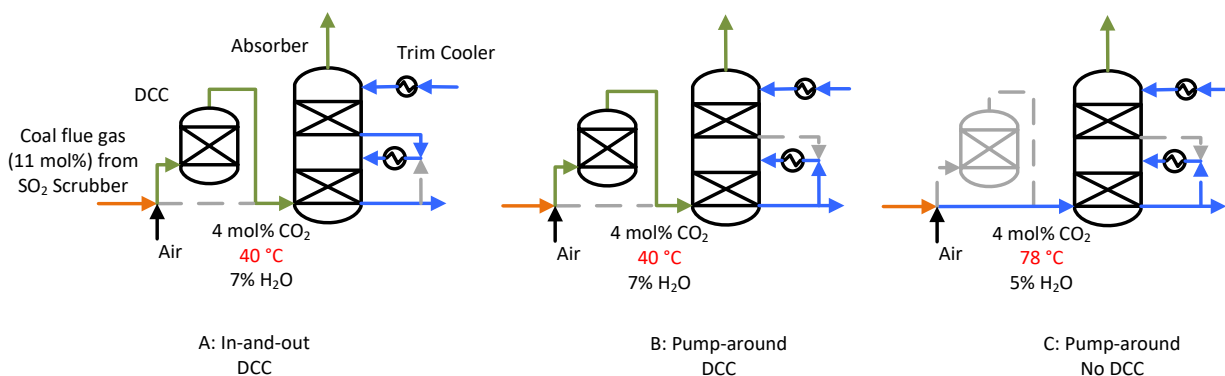


**Figure 2: Three configurations of absorber tested during the 2019 pilot plant campaign**

Four methods were used to minimize PZ oxidation:

- 1) The stripper sump level was maintained at a minimum 20% to minimize solvent residence time at high temperature where oxidation is most likely to occur.
- 2) Nitrogen (2.5 cfm) was sparged into the absorber sump to strip out dissolved oxygen.
- 3) In the second half of the campaign thiosulfate was added to the SO<sub>2</sub> prescrubber to provide sulfite to remove NO<sub>2</sub>, which is known to oxidize piperazine.

- 4) In the last three weeks, 1–5 gpm of cold rich solvent was circulated through the existing carbon bed filter to remove impurities that might catalyze oxidation.

## Timeline

Figure 3 shows the timeline for this campaign. The cumulative operating time with the solvent was 2009 hours (12 weeks) at the NGCC condition. With the operating time from the previous coal campaign, the solvent experienced 4130 hours of exposure to flue gas.

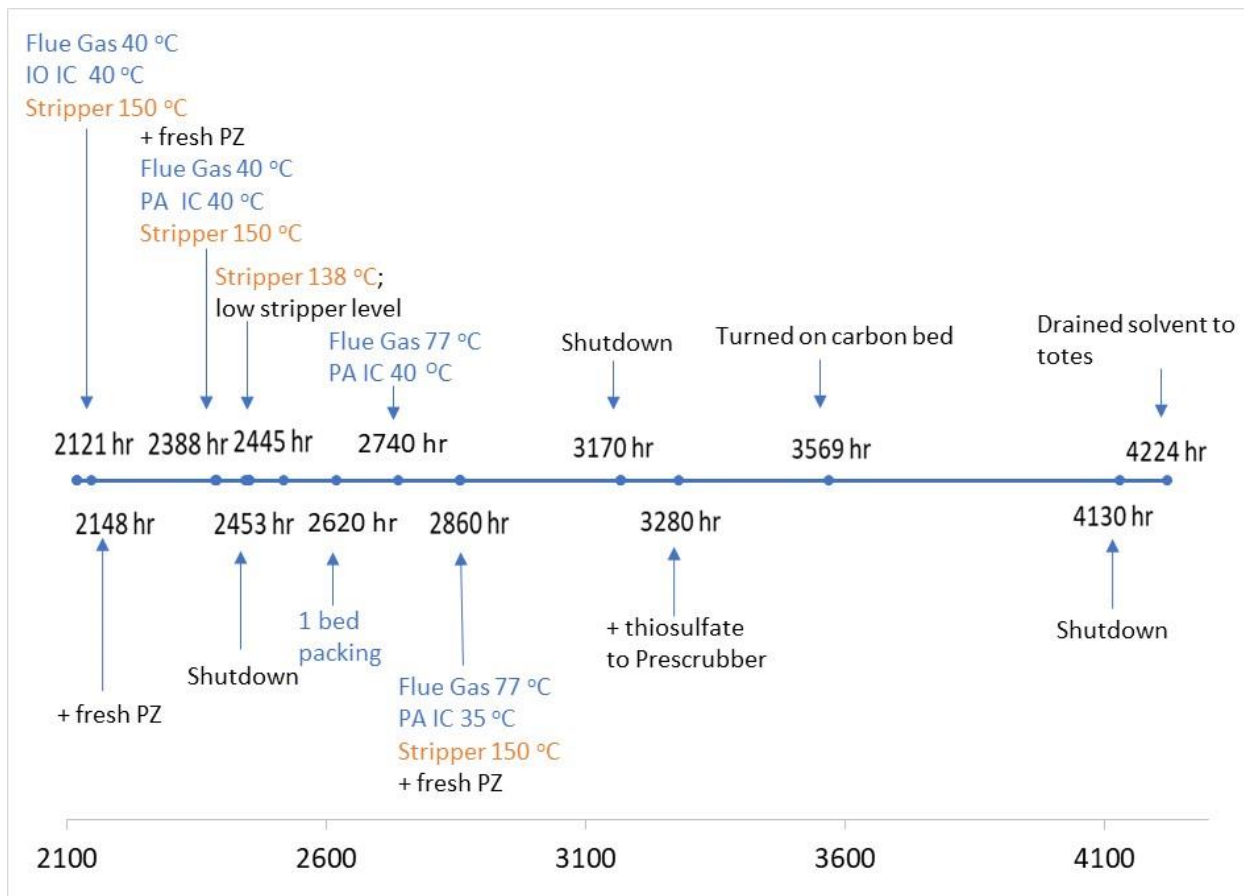


**Figure 3: Timeline for 2019 NGCC campaign as operating hours. Solvent operation started on February 12, 2019 and ended on June 6, 2019.**

## Operational results

The system operated reliably with no apparent problems despite four potentially challenging conditions:

1. There were no precipitation issues with the piperazine solvent. There were two shutdowns with drainage of the solvent to the rich storage tank.
2. The bottom section of the absorber was operated at very high solvent rate without flooding: 8000 lbs/hr flue gas and 29,300 lbs/hr solvent in the packing (including the pump-around).

- Hot flue gas up to 77 °C was directly contacted with rich solvent in the bottom section of absorber packing. No operational issues were associated with the pump-around intercooling.
- The Advanced Stripper was operated from 139 °C/4.5 bara to 160 °C/8 bara, with most runs at 150 °C/6.3 bara.

### Stripper Performance

Figure 4 shows the heat duty of the PZAS™ process in the coal and NGCC campaigns as a function of CO<sub>2</sub> removal. The same data are presented in Figure 5 as a function of rich loading. At a rich loading of 0.403 mol CO<sub>2</sub>/equiv PZ the heat duty was 2.37 GJ/t CO<sub>2</sub> at both the coal and NGCC conditions. In long-term testing at NGCC conditions the greater rich loading of 0.41 mol CO<sub>2</sub>/equiv PZ gave a reduced heat duty of 2.18 GJ/t. Up to 98% CO<sub>2</sub> removal was achieved at coal conditions with little increase in heat duty. However at the NGCC condition the heat duty increased substantially at 95% removal.

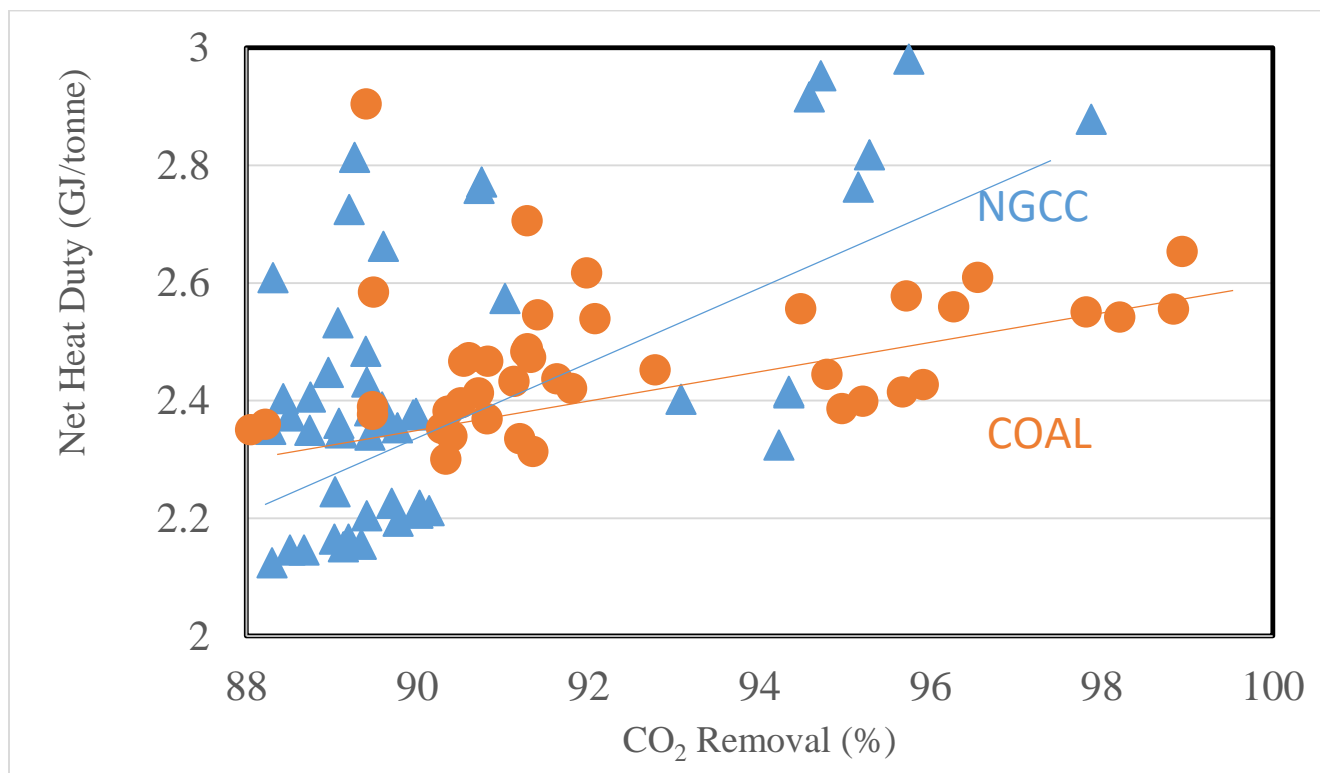


**Figure 4: Net heat duty calculated using measured steam flow corrected for T/P and heat loss**

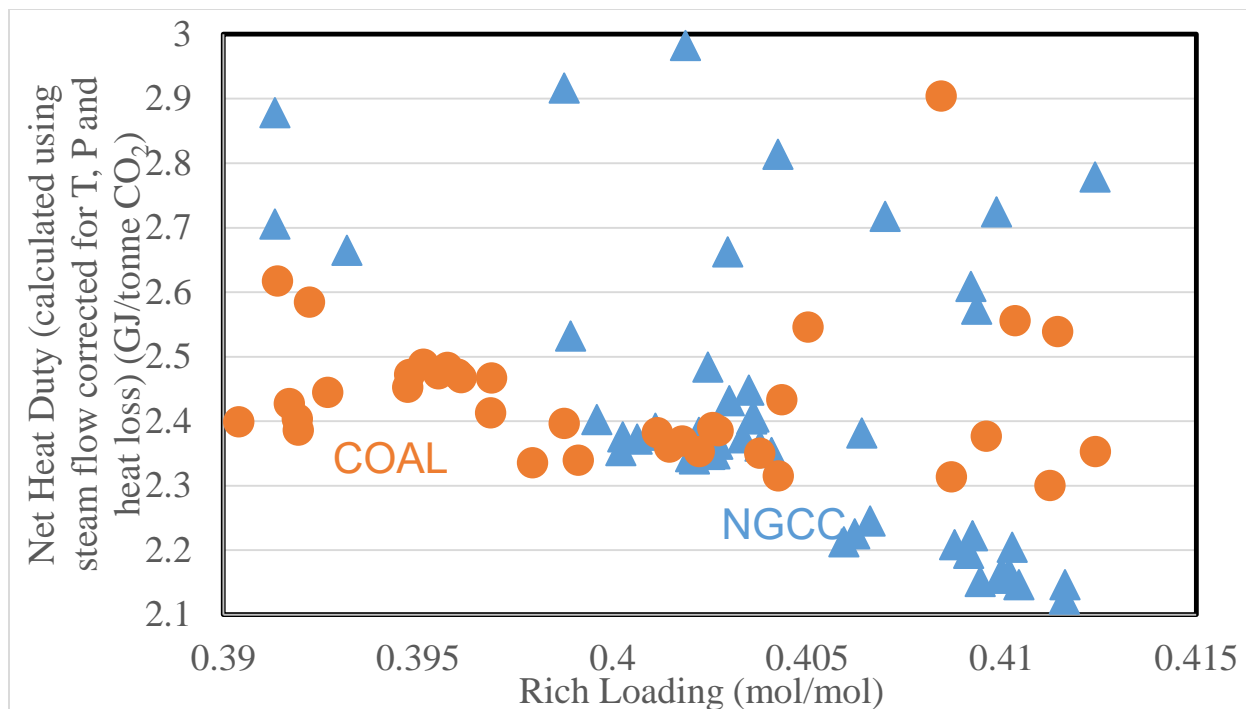


**Figure 5: Net heat duty decreases with increasing rich loading**

The heat duty in Figures 4 and 5 has been reduced from the measured value by the measured heat loss. Because the Advanced Stripper recovers and uses practically all of the steam heat, any heat loss is significant and is expected to increase the measured heat duty. The average heat loss was determined in water testing to be 0.078 GJ/hr during the NGCC campaign, about 30% of the total heat rate.

The measured steam rate in Figures 4 and 5 has been corrected for steam T and P. The vortex flow meter used for steam measurement at the Advanced Stripper was factory calibrated for a steam density of 0.23 lbs/ft<sup>3</sup>. This measurement was corrected by estimating the actual steam density from the locally measured T and P.

A second set of heat duties can also be estimated from a number of steam condensate weight measurements. Twenty weight measurements over a range of steam rate and density were obtained during the coal and NGCC campaigns by collecting and weighing the hot condensate in a tote. These measurements were consistently lower than the measured steam rate, probably because of water vapor loss from the tote. If the vortex meter is recalibrated based on these measurements, the calibration density varies with the measured steam rate from 0.24 to 0.28 lbs/ft<sup>3</sup>. Therefore the reported net heat duty for the NGCC campaign could be as low as 2 to 2.2 GJ/t.

For details on this analysis see the attached report by Suresh.

### **Absorber Performance**

Figure 6 shows that absorber performance during the NGCC campaign was a strong function of the rich loading. The long-term operation with pump-around intercooling at 35 °C with hot inlet flue gas (77 °C) provided 89–90% CO<sub>2</sub> removal while maintaining a rich loading of 0.4 to 0.41 mol CO<sub>2</sub>/equiv PZ. A number of runs with pump-around intercooling at 40 °C and 77 °C with higher solvent rate achieved 95% removal with 0.37–0.38 rich loading.

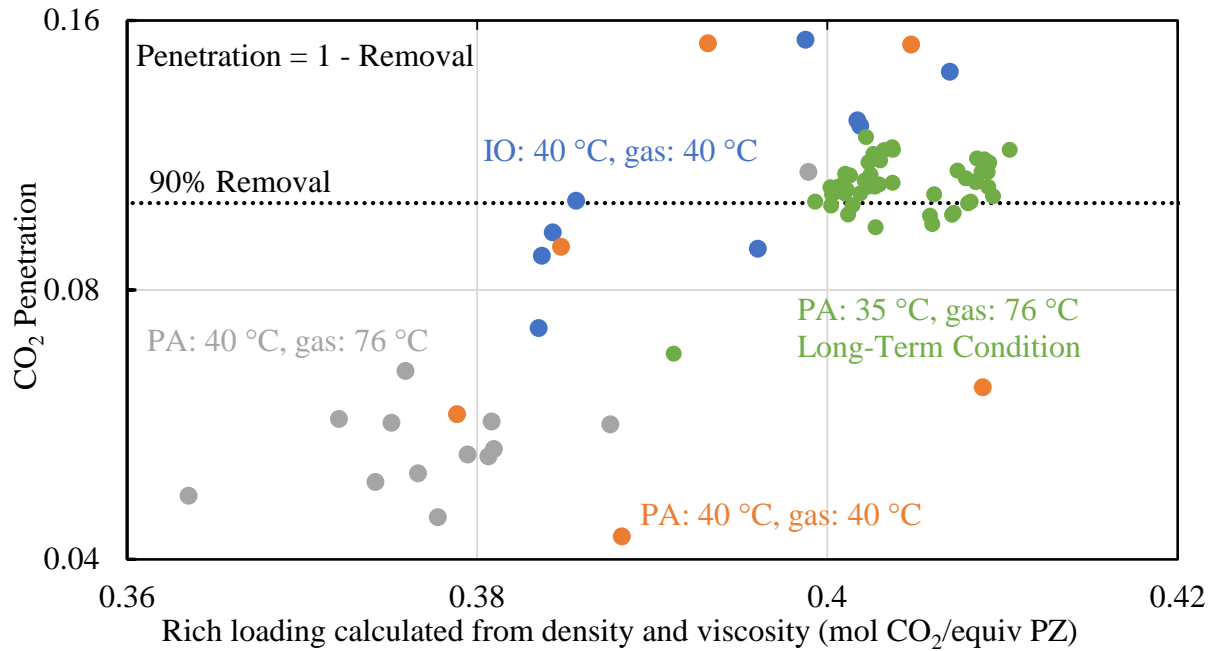


**Figure 6: Experimental absorber performance for NCCC 2019 campaign**

Figure 7 shows the measured and predicted temperature and flux profile for a typical condition from the long-term operation with 35 °C pump-around intercooling flue gas at 76 °C. The rich loading at NGCC conditions for 90% removal is greater than at coal conditions although the CO<sub>2</sub> concentration is lower. This is because of low temperature in the absorber, especially the bottom, and the temperature is low for two reasons:

1. At low CO<sub>2</sub> concentration, there is less heat generated per mass gas, so the magnitude of the temperature bulge is smaller.
2. At low L/G, gas tends to push the heat to the top of the column, so the bottom remains cold, which reduces the solvent equilibrium CO<sub>2</sub> partial pressure and increases the rich loading.

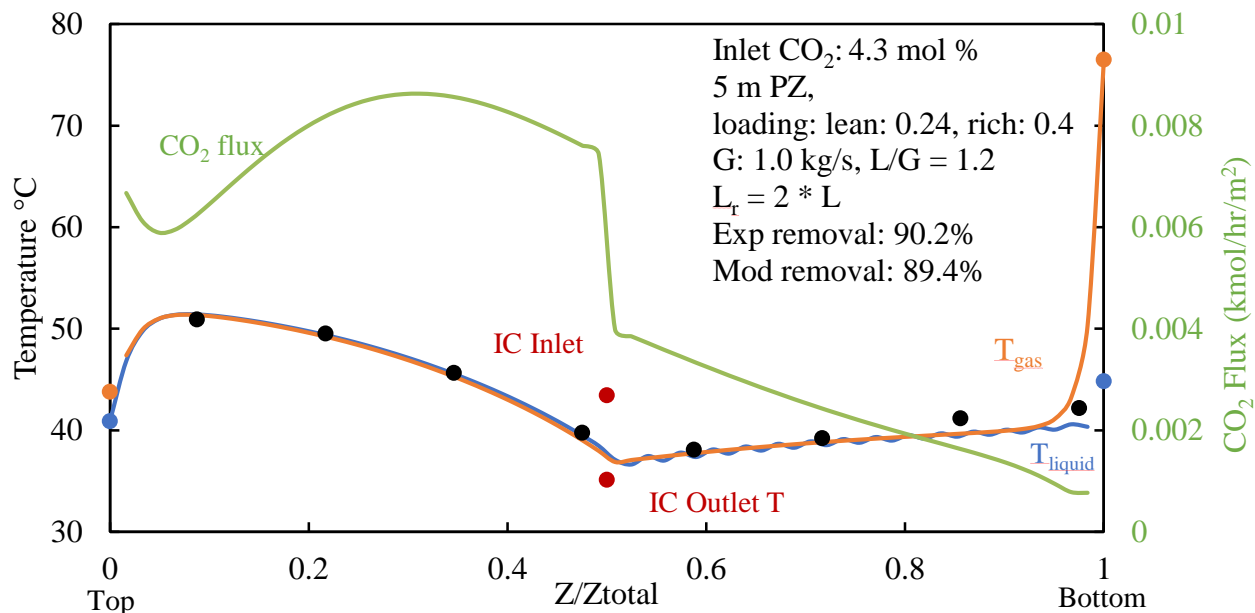


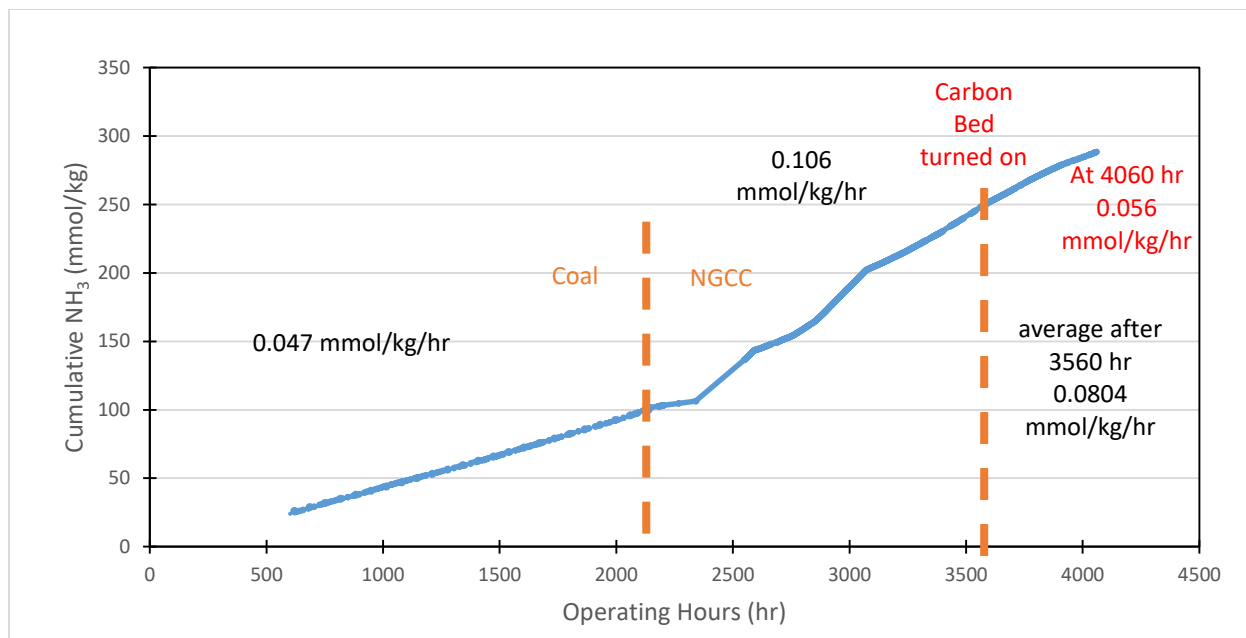
**Figure 7: Absorber profile for pump-around intercooling and 0.24 lean loading. Temperature measurements (points) and model predictions (curve) are shown on the primary axis; CO<sub>2</sub> transfer flux is shown on the secondary axis.**

The excellent performance of the absorber at NGCC conditions was achieved with only 40 ft of packing at almost the maximum gas capacity (8000 lbs/hr). With the pump-around intercooling, Figure 7 shows that the CO<sub>2</sub> flux is approaching zero (a pinch) at the bottom of the absorber, so it is probable that the bottom section of packing could be further reduced to 10 ft with little degradation of the absorber performance. With pump-around intercooling and no direct contact gas cooler, the PZAS™ process should require only 30 feet of Mellapak 252Y packing at maximum gas capacity to achieve superior performance in the NGCC application.

Other details and conclusions on absorber performance are included in the attached manuscript by Gao and Rochelle that has been submitted to *Industrial Engineering Chemistry Research*.

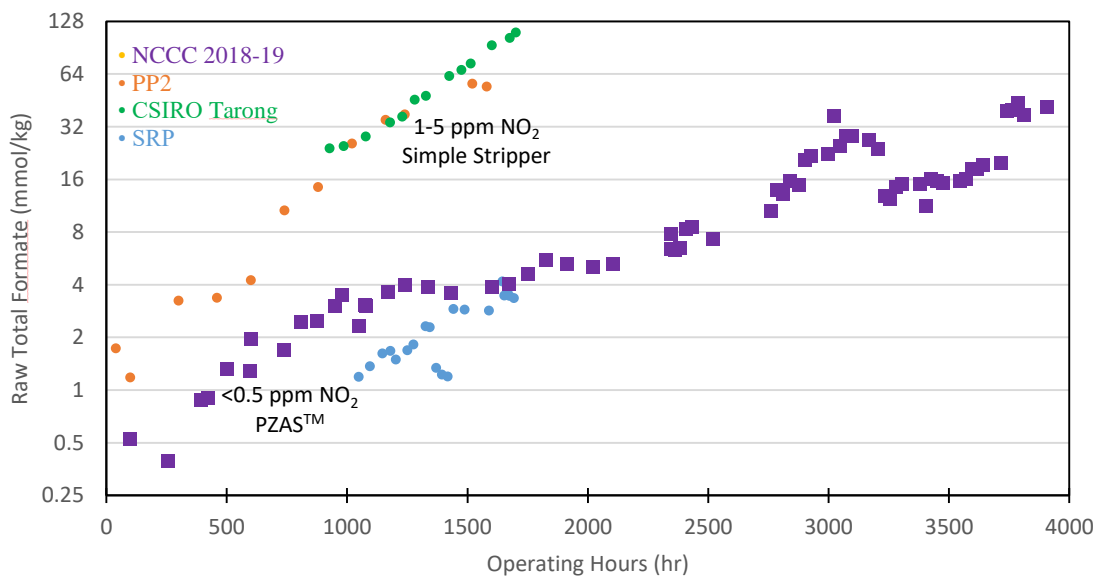
### **Oxidation**

Using NGCC flue gas with 4.3% CO<sub>2</sub> and 15% O<sub>2</sub> resulted in an oxidation rate greater than at coal conditions with only 7% O<sub>2</sub>. Figure 8 shows the cumulative production of ammonia including both campaigns. Assuming one mol NH<sub>3</sub>/mol PZ oxidized, the oxidation rate was 0.106 mmol/kg solvent/hr (0.3 kg PZ/tonne CO<sub>2</sub>). This compares to 0.047 mmol/kg/hr (0.1 kg PZ/tonne CO<sub>2</sub>) during the coal campaign.



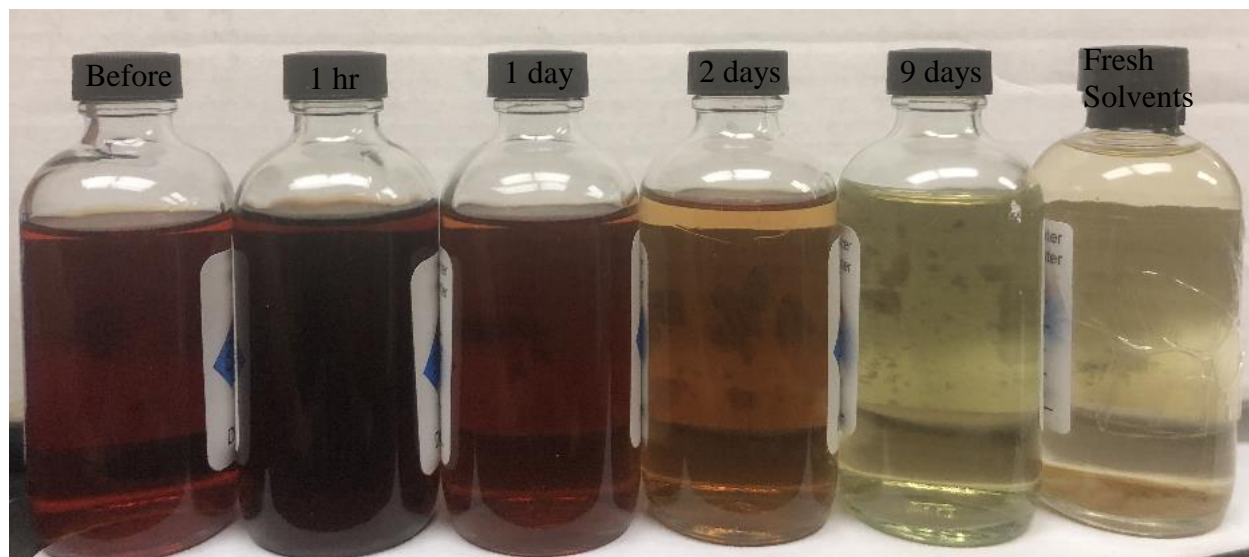
**Figure 8: Cumulative NH<sub>3</sub> over the NCCC 2018–19 Campaign**

Figure 9 compares the accumulation of total formate in the NCCC 2018–19 campaigns to earlier pilot plant work with PZ at pilot plant 2 (PP2), CSIRO Tarong, and the Separations Research Program (SRP). At 1700 hours of operation there was 8 times less formate in this NCCC campaign and in the SRP work, both with very little or no NO<sub>2</sub>, than in PP2 or Tarong, with 1–5 ppm NO<sub>2</sub>.



**Figure 9: Comparison of Raw Total Formate from NCCC 2018–19, PP2, CSIRO, and SRP Campaigns.**

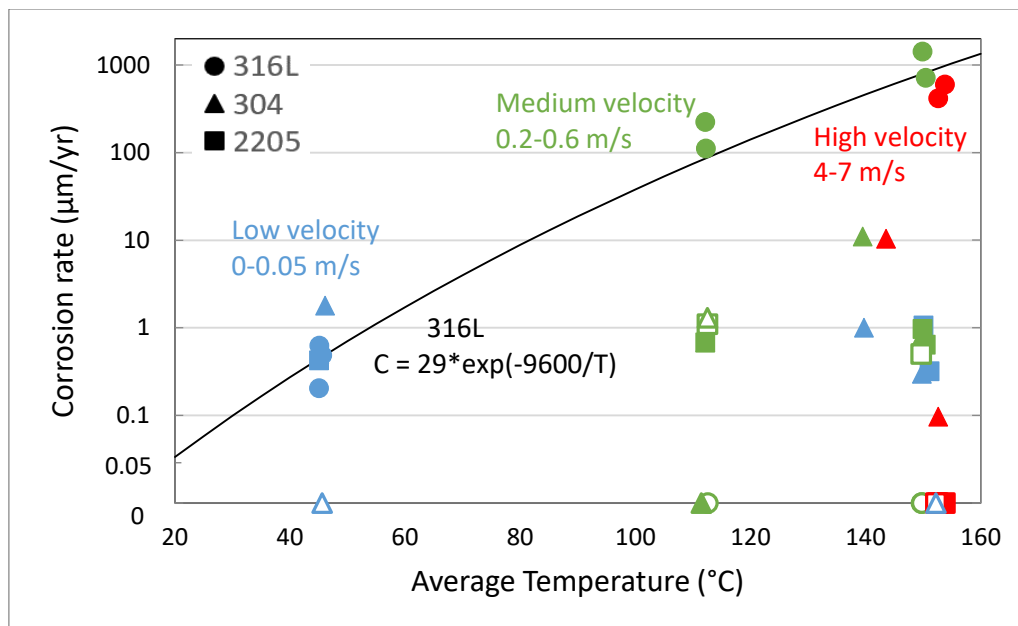
As shown in Figure 10 the use of carbon bed adsorption for 400 hours at the end of the campaign removed the dark degradation products. The carbon bed did not remove Fe as intended, but did reduce the dissolved chromium from 0.13 to 0.06 mmol/kg. Chromium may be an oxidation catalyst and it is an element of concern for classifying spent solvent as a hazardous waste. As shown in Figure 8 the carbon bed appears to reduce the production of ammonia from 0.0804 to 0.056 mmol/kg-hr. It also reduced the corrosion of stainless steel. In Figure 9, with the addition of the carbon bed treating at 3560 hours, the formate doubles. It is possible that the initial surface of the virgin activated carbon included formate from surface oxidation.



**Figure 10: Visual Effects on Solvent by Use of the Carbon Bed**

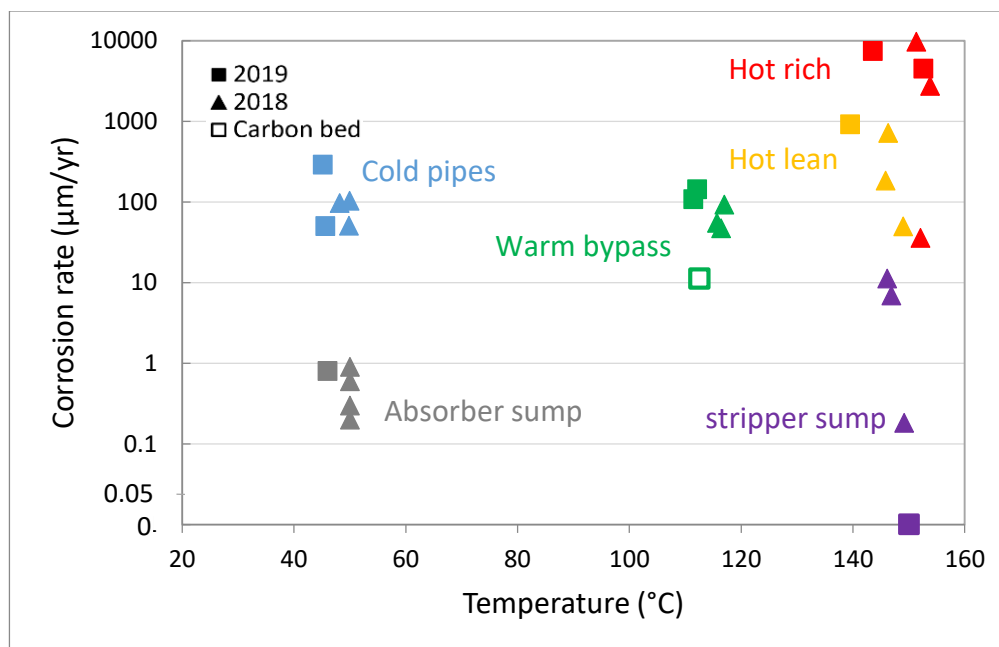
### ***Corrosion***

Figure 11 shows the corrosion performance of stainless steel during the 2019 NGCC campaign. 316L stainless steel experienced unacceptable ( $>100 \mu\text{m}/\text{yr}$ ) corrosion at the higher temperatures (115 and 150 °C) of the stripper. However both 304 stainless steel and 2205 duplex stainless performed well at all temperatures. The unexpected vulnerability of 316L is related to the uniquely high operating temperature of PZ. Degraded PZ also exacerbated 316L corrosion, and removal of PZ degradation products using the carbon adsorption bed appeared to reduce 316L corrosion significantly.



**Figure 11: Stainless steel (●: 316L, ▲: 304, and ■: 2205 duplex) corrosion rates during the 2019 campaign. Blue points are low fluid velocity (0–0.05 m/s) locations, green points are medium velocity (0.2–0.6 m/s) locations, and red points are high velocity (4–7 m/s) locations. Corrosion rate is shown on a complex y-axis (0–0.1 µm/yr: linear-scale; >0.1 µm/yr: log-scale). Open points show the rates measured when the carbon adsorption bed was operating. The solid curve shows the Arrhenius dependence of 316L corrosion rates excluding the data with the carbon bed.**

Carbon steel appears to be an acceptable material (<100 µm/yr) at lower fluid velocities as in the Advanced Stripper sump and at lower temperature (Figure 12). At the elevated temperature carbon steel corrosion was greater in 2019 with increased solvent degradation (Figure 12) because the corrosion is more dependent on protection by a siderite film. Regular, crystalline films formed in stagnant fluid and provided better protection. High-velocity flow might alter the precipitation mechanism of siderite or damage the film and thus result in non-protective films. Carbon steel also performed better with carbon bed adsorption, probably because the carbon bed removes degradation products.



**Figure 12: C1010 corrosion during the 2018(▲) and 2019 (■) campaigns. Blue points are measurements in the cold pipes (cold bypass and cold lean pipe), grey points are in the absorber sump, green points are in the warm bypass, yellow points are in the hot lean stream, red points are in the hot rich stream, and purple points are in the stripper sump. Corrosion rate is shown on a complex y-axis (0–0.1 µm/yr: linear-scale; >0.1 µm/yr: log-scale). Open points show the rates measured when the carbon adsorption bed was operating.**

Hastelloy® C276 and Inconel® did not perform well due to selective dissolution of Ni into PZ in some narrow gaps between alloy and washers.

Additional details on the corrosion measurements and results are given in the attached manuscript by Liu et al. that has been submitted to *IECR*.

### ***Amine vapor and aerosol losses***

During the NGCC campaign the PZ in the gas leaving the water wash (WW) was less than 0.3 ppm up to about 2900 operating hours (Figure 13). After 2900 hours there was a step change in the PZ leaving the water wash to a range of 0.6–1.7 ppm. Higher emissions were observed during most of the coal campaign. The flue gas after the baghouse is diluted by a factor of three to get 4.3% CO<sub>2</sub> for NGCC conditions, so lower emissions associated with residual SO<sub>3</sub> are to be expected.

Previous observations during the coal campaign showed that high emissions of PZ were associated with substandard operation of the baghouse in the parent power plant. However 2900 hours was also the time when the pilot plant operation shifted from using a direct contact cooler to taking hot (77 °C) flue gas directly into the absorber. Quenching the hot flue gas with rich PZ solvent may result in the creation of amine aerosol.

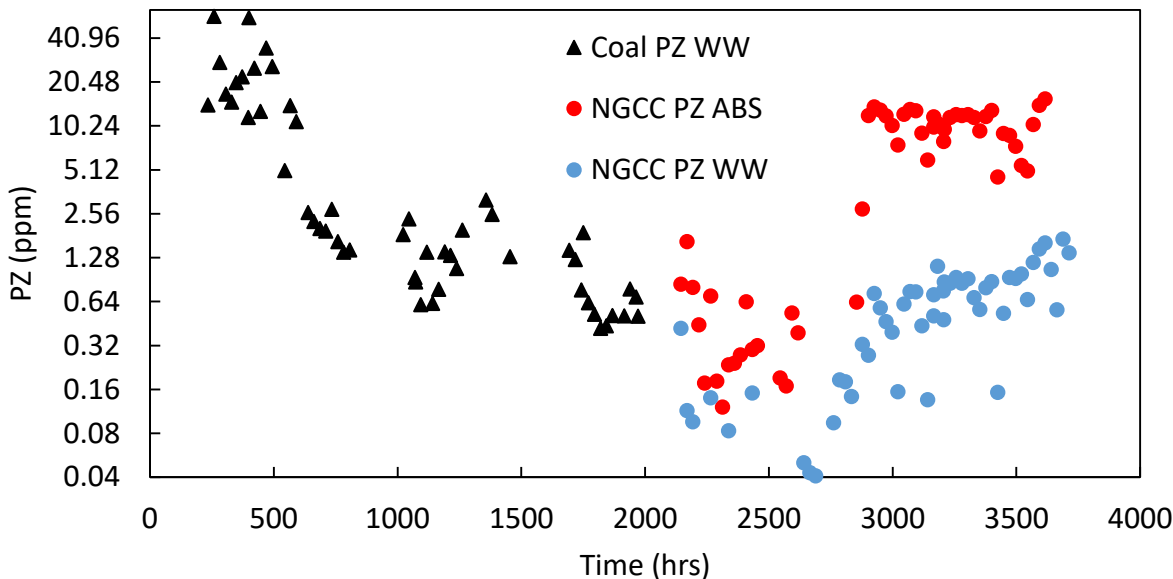


**Figure 13: PZ emission summary for Coal and NGCC campaigns at NCCC. Data points correspond to daily averages of PZ emission.**

No SO<sub>3</sub> was injected and the flue gas was diluted, so the SO<sub>3</sub> carried over with coal-fired flue gas was probably minimized.

Additional details are given in the attached report by Akinpelumi.

## Conclusions

1. PZAS<sup>TM</sup> provided a heat duty of 2.35 GJ/tonne CO<sub>2</sub> with NGCC flue gas (4.3% CO<sub>2</sub>), the same as the heat rate with coal-fired flue gas (11% CO<sub>2</sub>). CO<sub>2</sub> was produced at 6.3 bar from a stripper bottom at 150 °C.
2. 90% CO<sub>2</sub> removal was achieved with only 40 ft of packing at a rich loading providing a heat duty of 2.35 GJ/tonne. Pump-around intercooling at 35 °C in the absorber bottom reliably provided rich solvent at 40 °C with flue gas at 76 °C and significantly enhanced absorber performance.
3. Piperazine oxidation with 4.3% CO<sub>2</sub> was 0.3 kg/tonne CO<sub>2</sub> removed, compared to 0.1 kg/tonne in the earlier campaign with 11% CO<sub>2</sub>. Use of carbon bed treating in the last 3 weeks of the campaign clarified the solvent, appeared to reduce oxidation, and appeared to reduce 316 SS corrosion.
4. The corrosion rate of C1010 (carbon steel) and 316 SS at 150 °C was unacceptable (>400 μm/yr), but 304 SS and 2205 duplex had acceptable rates (<10 μm/yr) at 150 °C. C1010 corrosion was mostly acceptable (<100 μm) at T<120 °C.
5. Piperazine emissions were <0.3 ppm for the first 600 operating hours and <1.7 ppm for the balance of the campaign.

## Future Work

Financial support is available for an additional NCCC campaign at NGCC conditions in 2020 after the gas-fired boiler is operational. This campaign will feed hot flue gas (120 °C) directly to the

absorber with bottom pump-around intercooling. It will further investigate carbon adsorption and other solvent cleanup methods as mitigation methods for oxidation.

# Measured and Modeled Energy Performance of the Piperazine Advanced Stripper (PZAS™) at NCCC with 4% and 12% CO<sub>2</sub>

Quarterly Report for July 1 – September 30, 2019

by Athreya Suresh

Supported by the CO<sub>2</sub> Capture Project and the U.S. Department of Energy,

Office of Fossil Energy through the

CCSI<sup>2</sup> project (Carbon Capture Simulation for Industry

Impact) subcontract 318779 with Los Alamos National Laboratory

McKetta Department of Chemical Engineering

The University of Texas at Austin

October 31, 2019

## **Abstract**

This paper discusses the energy performance of the Piperazine Advanced Stripper (PZAS™) at the National Carbon Capture Center in Wilsonville, Alabama during two test campaigns: one with 12% CO<sub>2</sub> (coal) and the other with 4% CO<sub>2</sub> (NGCC). Heat duty of the process was calculated using two different estimated values of the steam flow rate. The first method used steam flow rate only corrected for temperature and pressure. The second method used steam flow rate calculated by temperature and pressure correction combined with calibration of the steam flow meter with condensate measurements. Heat loss measured using water testing during both campaigns was found to be 30% of the heat rate of the plant (using steam flow rates corrected for temperature and pressure only). Heat duty corrected for this average heat loss, or the net heat rate, under long-term coal conditions was 2.4 GJ/tonne CO<sub>2</sub> and 2.3 GJ/tonne CO<sub>2</sub> under long-term NGCC conditions. The absorber operating condition was found to affect stripper energy performance with the optimal condition being pump-around intercooling at the bottom section with 35 °C intercooling temperature, 90% removal, and 150 °C stripper. The Independence™ model predicted the energy performance of the PZAS™ system with an average error of 6% and predicted long-term heat duties within 5% of the measured values.

## **Introduction**

In amine scrubbing, the steam usage in the stripper is the main contribution to energy use. The intensive energy consumption is one of the major obstacles to the commercial deployment of CO<sub>2</sub> capture. Advanced solvents and process configurations are considered to be promising solutions to reduce the energy requirement. Aqueous piperazine (PZ) is a new standard solvent with twice the absorption rate and greater CO<sub>2</sub> capacity than the conventional alternative, MEA (Rochelle et

al., 2011). PZ has lower volatility and is more resistant to oxidative and thermal degradation, making it usable up to 150 °C (Freeman, 2010). PZ has the ability to reduce energy use while reducing the environmental footprint of the CO<sub>2</sub> capture process.

8 m PZ has been tested at the Separations Research Program (SRP) of The University of Texas at Austin (Lin, 2016) and the Tarong CO<sub>2</sub> capture pilot plant in Australia (Cousins et al., 2016). The lowest heat duty at the Tarong pilot plant was 2.9 GJ/tonne CO<sub>2</sub>, 15% lower than 30 wt % MEA at the same facility. 5 m PZ has sparked interest as it has a wider solid solubility window, lower viscosity, and greater CO<sub>2</sub> absorption rate compared to 8 m PZ (Plaza, 2011).

Alternate stripper configurations have been shown to reduce energy use compared to the simple stripper. Lean vapor compression and the inter-heated stripper have been used with 30 wt% MEA resulting in a heat duty of 2.9–3.5 GJ/tonne CO<sub>2</sub> (Knudsen et al., 2011). The two-stage flash with cold rich solvent bypass was demonstrated with 8 m PZ at UT Austin resulting in a heat duty of 2.7 GJ/tonne CO<sub>2</sub> (Madan, 2013). 5 m PZ with the advanced flash stripper configuration has been shown to improve energy performance over all other alternatives to about 2.0 GJ/tonne CO<sub>2</sub> from simulation data (Lin, 2016). The pilot test of the advanced flash stripper at the Separations Research Program at UT Austin showed a duty of 2.1–2.5 GJ/tonne CO<sub>2</sub> (Lin, 2016).

The advanced flash stripper (the PiperaZine Advanced Stripper or PZAS™) was tested at the National Carbon Capture Center in 2018 (12% CO<sub>2</sub>, coal conditions) and 2019 (4% CO<sub>2</sub>, NGCC conditions). The objective of this paper is to present and interpret energy results from these two campaigns and validate the Independence™ model using pilot plant data. The model will be used to explore optimum operating conditions.

## **Pilot Plant and Campaign Overview**

The integrated absorption-stripping system is located at the National Carbon Capture Center in Wilsonville, Alabama. This 0.5 MW system treats real flue gas from a nearby coal-fired power plant. In 2018, the flue gas contained 12% CO<sub>2</sub>, representing coal conditions and in 2019, the flue gas contained 4% CO<sub>2</sub>, representing natural gas turbine flue gas conditions. In 2019, flue gas containing 12% CO<sub>2</sub> was diluted with air to bring down the CO<sub>2</sub> concentration to 4%. A simplified process flow diagram of a carbon capture system is shown in Figure 1. This figure also shows representative long-term coal and natural gas data to highlight major operational differences.

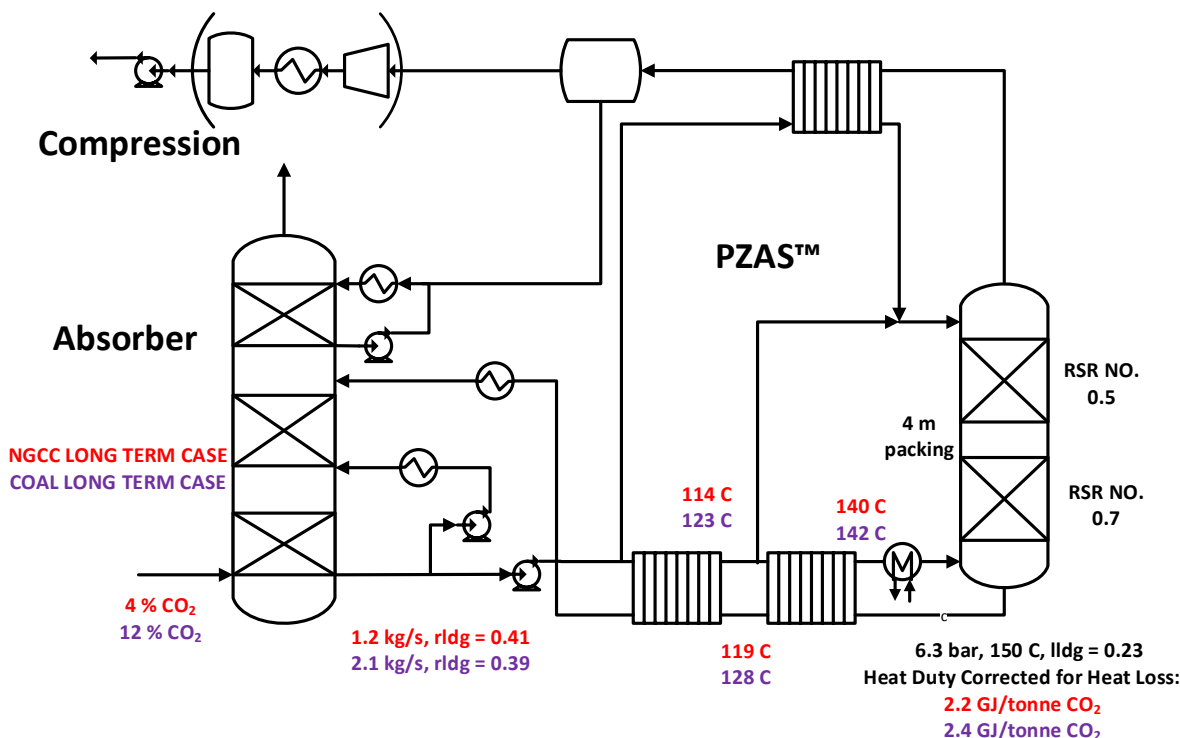


**Figure 1: Simplified process flow diagram of the absorber-PZAS™ at NCCC with representative long-term operation data**

The rich solvent from the absorber is pumped up to stripper pressure by the rich pump, pre-heated in the cross-exchangers, and further heated by the steam heater to flash out the CO<sub>2</sub>. In doing so, two bypass streams are extracted from the rich solvent, the cold rich bypass and the warm rich bypass. The cold rich bypass is used to cool the stripper overhead product, condense some of the water vapor, and recover some of its latent heat. The heated cold rich bypass and the warm rich bypass are then mixed and sent to the top of the stripper.

The total bypass solvent is counter-currently contacted with the vapor in the stripper which contains 2 sections of random packing. The top section contains 2 meters of RSR No. 0.5 packing, and the bottom section contains 2 meters of RSR No. 0.7 packing. High pressure CO<sub>2</sub> is produced in the stripper at about 6 bar which reduces the compression work required for CO<sub>2</sub> sequestration. The heat rate of the steam heater which depends on the steam flow rate and the latent heat of vaporization of steam is inferred as the measured heat duty of the pilot plant.

Table 1 lists the major operational differences between the coal and the NGCC campaigns. Other than the CO<sub>2</sub> concentration, the NGCC case processed about 50% more flue gas compared to the coal case. More parametric tests were done in the NGCC campaign resulting in wider ranges of stripper sump temperature, lean loading, and heat duty. However, under typical long-term conditions of 90% removal in the absorber with a 150 °C stripper sump and a 5 °C approach in the cross exchangers, the heat duties for coal and NGCC cases were almost identical. The long-term

NGCC case gave a lower net heat duty of 2.2 GJ/tonne CO<sub>2</sub> compared to the coal case which gave 2.4 GJ/tonne CO<sub>2</sub>. This is believed to be the effect of increased  $\Delta$ loading in the NGCC case resulting from the usage of pump-around intercooling with a cold intercooling temperature at the absorber bottom. This can be seen in the greater rich loading for the NGCC case compared to the coal case in Figure 1.

**Table 1: Operating conditions of the coal and NGCC campaigns**

Specification	Coal (2018)	NGCC (2019)
CO <sub>2</sub> (mol %)	12.8	3.9
Gas T (°C)	56	117
G (kg/s/MW)	1.1	1.6
Rich Solvent Flow Rate (kg/s)	1.25-2.5	0.57-1.8
Stripper Sump Temperature (°C)	133-155	139-160
Rich Loading (mol/mol)	0.37-0.41	0.36-0.41
Lean Loading (mol/mol)	0.195-0.26	0.18-0.31
CO <sub>2</sub> Removal (%)	88-99	88-96
Measured Heat Duty Corrected for Heat Loss (GJ/tonne CO <sub>2</sub> )	2.3-2.9	2.2-4.0

## **Methods**

### **Steam Flow Reconciliation**

Shown in Figure 2 is the steam flow configuration at NCCC. Intermediate pressure steam from the power plant is sent through a pressure-controlled let-down valve that reduces the steam pressure to about 90 psig. The flow rate of this steam is measured by a vortex flowmeter, FI40508, which converts the velocity of the steam,  $v$ , to a mass flow rate,  $F$ , using a constant area of the device,  $a$ , and standard density referred to as  $\rho_{std}$ . The steam flows through a number of temperature and pressure indicators to the steam heater where it convectively heats the rich solvent to flash out the CO<sub>2</sub>. The steam heater is followed by a steam trap. Steam condensate from the trap is directed to a tote where cumulative weight gain is measured in one-hour intervals. A total of 22 condensate tests were done in the coal and NGCC campaigns. This measurement deviated from the vortex flowmeter by an average of 12%.

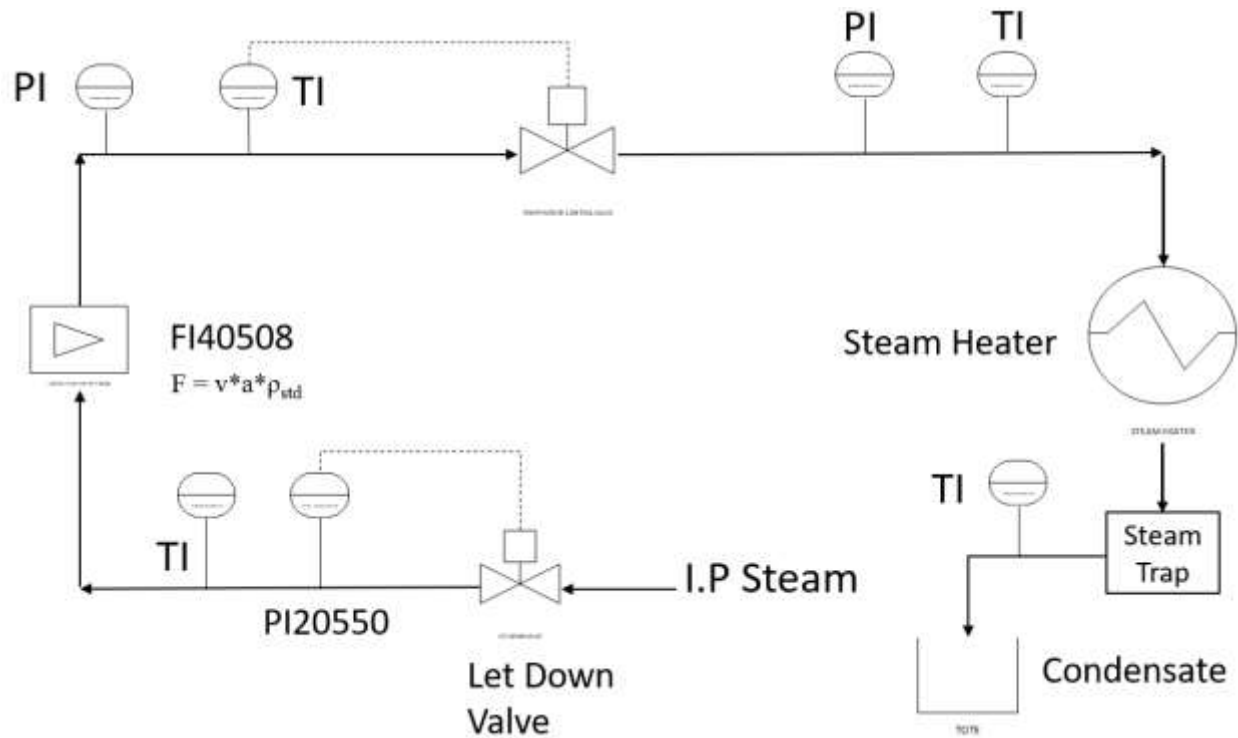


**Figure 2: Steam flow arrangement at NCCC**

The output of the vortex flowmeter was not corrected for the temperature and pressure of the steam, and the flowmeter may also use an incorrect base-density, leading to incorrect measurement of the steam flow rate. The objective of this reconciliation is to verify correction for temperature and pressure, calibrate the steam flow rate with the condensate measurements, and look for any useful trends in the base-density,  $\rho_{std}$ . All heat duty analysis will then be done based on steam flow rates corrected for T, P, and base-density, as well as steam flow rates corrected only for T and P.

### Methods Used to Correct Steam Flow Rate Measurements

Equation 1 shows the first method used to calibrate the steam flow measurements by incorporating the temperature and pressure correction for the flowmeter. This equation is also used to verify the actual value of base-density used by the measurement device. The factory value of this base-density was  $0.23 \text{ lb/ft}^3$ .

$$\frac{F_{corrected}}{F_{measured}} = \frac{\rho_{steam}(T,P)}{\rho_{std}} \quad (1)$$

where:

$F_{corrected}$  = temperature- and pressure-corrected steam flow rate;

$F_{measured}$  = raw steam flow rate measurements from FI40508;

$\rho_{steam}$  = density of steam calculated from let-down pressure measurement (PI20550);

$\rho_{std}$  = value of base-density,  $\rho_{std}$  calculated from condensate tests.

Further analysis based on condensate weight suggested that this base-density was not constant at 0.23lb/ft<sup>3</sup> for this device but varied from 0.2–0.3 lb/ft<sup>3</sup> linearly with the measured steam flow rate, as shown in Figure 3. A correlation from this data has been developed and will be used to update the value of  $\rho_{std}$  at a given measured steam flow rate and this value will then be used to correct the measured steam flow rate value. This method is shown in Equation 2.

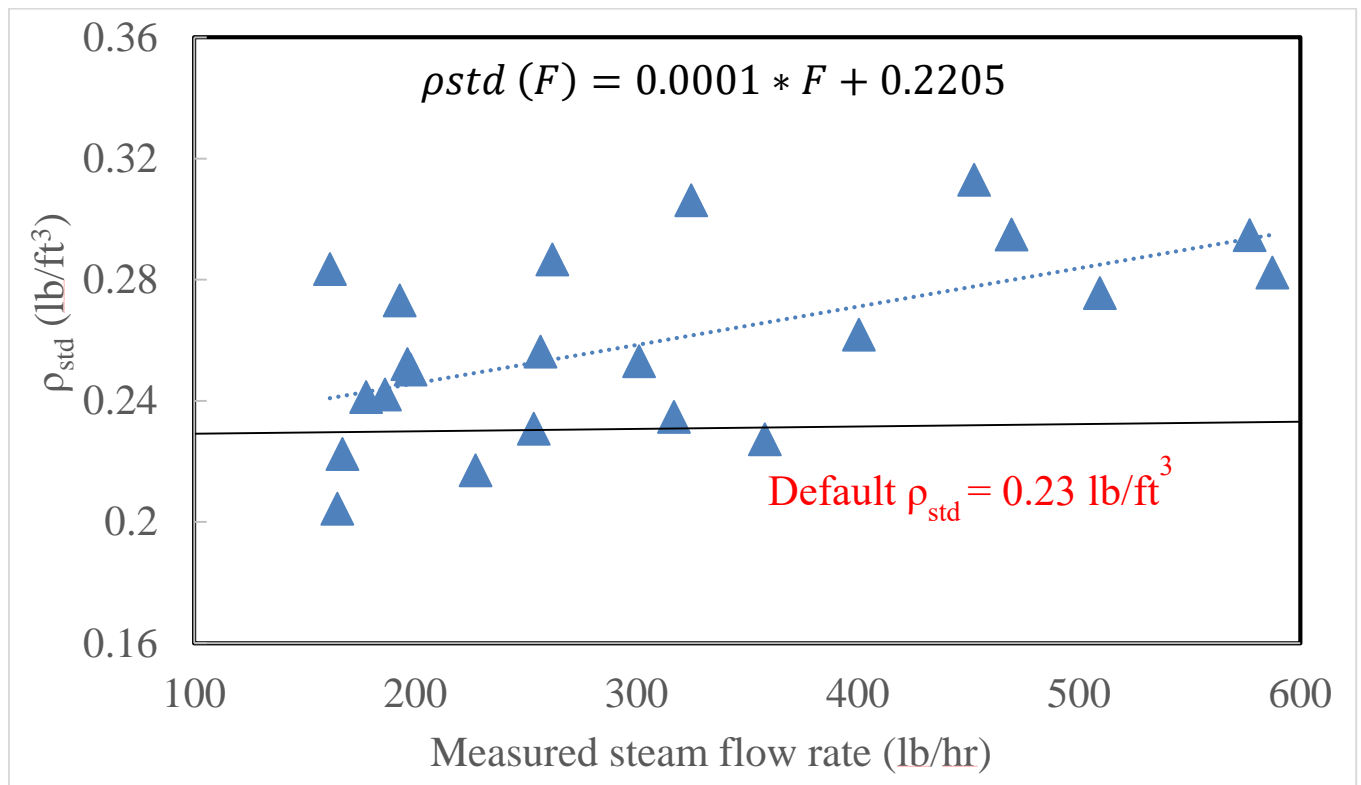


**Figure 3: Base-density of flow rate measurement device linearly correlated with measured flow rate**

$$\frac{F_{corrected}}{F_{measured}} = \frac{\rho_{steam}(T,P)}{\rho_{std}(F)} \quad (2)$$

where:

$F_{corrected}$  = temperature-, pressure-, and density-corrected steam flow rate;

$F_{measured}$  = raw steam flow rate measurements from FI40508;

$\rho_{steam}$  = density of steam calculated from let-down pressure measurement (PI20550);

$\rho_{std}(F)$  = base-density,  $\rho_{std}$  calculated from correlation with measured steam flowrate.

### Heat Loss and Measured Heat Rate Calculation

Heat loss at NCCC was measured using 28 water tests during the coal and NGCC campaigns. Equation 10 was used to measure the heat loss in the plant. All enthalpies were calculated using

measured temperatures from the pilot plant and when required, used a reference temperature of 70 °F. Heat loss was calculated using both methods of correcting steam flow rate measurements.

$$Q_{rich} = L_{rich} * C_{pwater} * (T_{rich} - T_{ref}) \quad (3)$$

$$Q_{steam} = (L_{steam} * \Delta H_{vap}) + (L_{steam} * C_{pwater} * (T_{steamin} - T_{cond})) \quad (4)$$

$$Q_{in} = Q_{steam} + Q_{rich} \quad (5)$$

$$Q_{cw} = L_{cw} * C_{pwater} * (T_{cwout} - T_{cwin}) \quad (6)$$

$$Q_{lean} = L_{lean} * C_{pwater} * (T_{lean} - T_{ref}) \quad (7)$$

$$Q_{condensate} = L_{condensate} * C_{pwater} * (T_{condensate} - T_{ref}) \quad (8)$$

$$L_{condensate} = L_{rich} - L_{lean} \quad (9)$$

$$Q_{loss} = Q_{in} - (Q_{cw} + Q_{lean} + Q_{condensate}) \quad (10)$$

$$Q_{net} = Q_{steam} - \frac{\sum Q_{loss}}{N} \quad (11)$$

where:

$C_{pwater}$  = specific heat capacity of water;

$L_{rich}$  = measured rich side water flow rate;

$T_{rich}$  = outlet temperature of rich side water;

$Q_{rich}$  = enthalpy of rich side water;

$T_{ref}$  = reference temperature;

$L_{steam}$  = measured steam flow rate;

$T_{ref}$  = reference temperature;

$T_{steamin}$  = measured inlet temperature of steam;

$T_{cond}$  = steam condensate temperature;

$Q_{steam}$  = measured heat rate;

$\Delta H_{vap}$  = heat of vaporization of steam;

$Q_{cw}$  = sensible heat associated with cooling water;

$L_{cw}$  = measured cooling water flow rate;

$T_{cwout}$  = cooling water outlet temperature;

$T_{cwin}$  = cooling water inlet temperature;

$Q_{lean}$  = enthalpy associated with lean side water;

$T_{lean}$  = outlet temperature of lean side water;

$L_{lean}$  = lean side water flow rate;

$L_{condensate}$  = calculated condensate flow rate;

$T_{condensate}$  = measured condensate temperature;

$Q_{condensate}$  = enthalpy of condensate;

$Q_{loss}$  = heat loss;

$Q_{net}$  = net heat rate of pilot plant (heat rate corrected for heat loss);

$N$  = number of heat loss tests.

The term  $Q_{steam}$  in the above equations is interpreted as the measured heat rate of the pilot plant. The heat of vaporization of steam is calculated at the inlet pressure of steam. It is now possible to correct the heat rate of the pilot plant for the heat loss and find the fraction of the total heat rate that is lost to the surroundings as heat loss. All heat loss calculations have been done using water, as its specific heat capacity value is well established. Using piperazine to calculate heat loss would allow for uncertainties related to the values of specific heat capacity and heat of absorption of  $CO_2$  in the solvent.

The average heat loss coefficients from solvent and water runs were found to be closely matched at about  $100 \text{ WK}^{-1}$  for the 0.1 MW pilot plant at the Separations Research Program at UT Austin (Lin, 2016). This consistent heat loss constant of the amine and water system assures the validity of the measured heat loss. Moreover, the heat loss is believed to be only a function of the total exposed area of the pilot plant and hence, the magnitude of heat loss should be the same whether calculated using water or piperazine.

### Rate-Based Modeling Methodology

Modeling of the Piperazine Advanced Stripper (PZAS<sup>TM</sup>) was done using Aspen Plus<sup>®</sup> v 10.0. The thermodynamic framework used by the model was the Independence<sup>TM</sup> model (Frailie, 2011) which was developed in Aspen Plus<sup>®</sup> RateSep<sup>TM</sup> and contains the  $CO_2$  solubility, kinetics, specific heat capacity, and amine volatility regressed within the e-NRTL framework. The mass transfer model was developed by Wang (2015) and contains the interfacial area ( $a$ ), liquid-phase mass-transfer coefficient ( $k_L$ ), and gas-phase mass-transfer coefficient ( $k_G$ ) regressed for random packings.

The rich and lean loadings and piperazine concentration used by the model were calculated from density-viscosity correlations developed by Freeman (2011). Solving these two equations simultaneously yields the  $CO_2$  and piperazine concentrations, which are then used as inputs to the model. Finally, a packing adjustment factor of 0.16 was used in the stripper column to account for deviations in model diffusivities of piperazine compared to experimentally measured values.

Figure 4 is the process flow diagram of the PZAS<sup>TM</sup> system with the key model inputs and model outputs highlighted. The model accepts all the measured properties of the rich solvent such as flow rate, temperature, pressure, rich loading, and PZ concentration as input. In addition to this, the properties of the bypasses are completely specified to be the measured values at NCCC. The stripper sump temperature is adjusted using a design specification to match the measured sump temperature. The heat exchangers are modeled as pairs of heater blocks to reduce model complexity and for ease of convergence. The main model outputs are the heat rate of the plant, interpreted to be equal to the duty of the stripper sump from the model, and the stripper overhead

CO<sub>2</sub> flow rate. Using the two values, the modeled heat duty of the pilot plant can be found in GJ/tonne CO<sub>2</sub>.

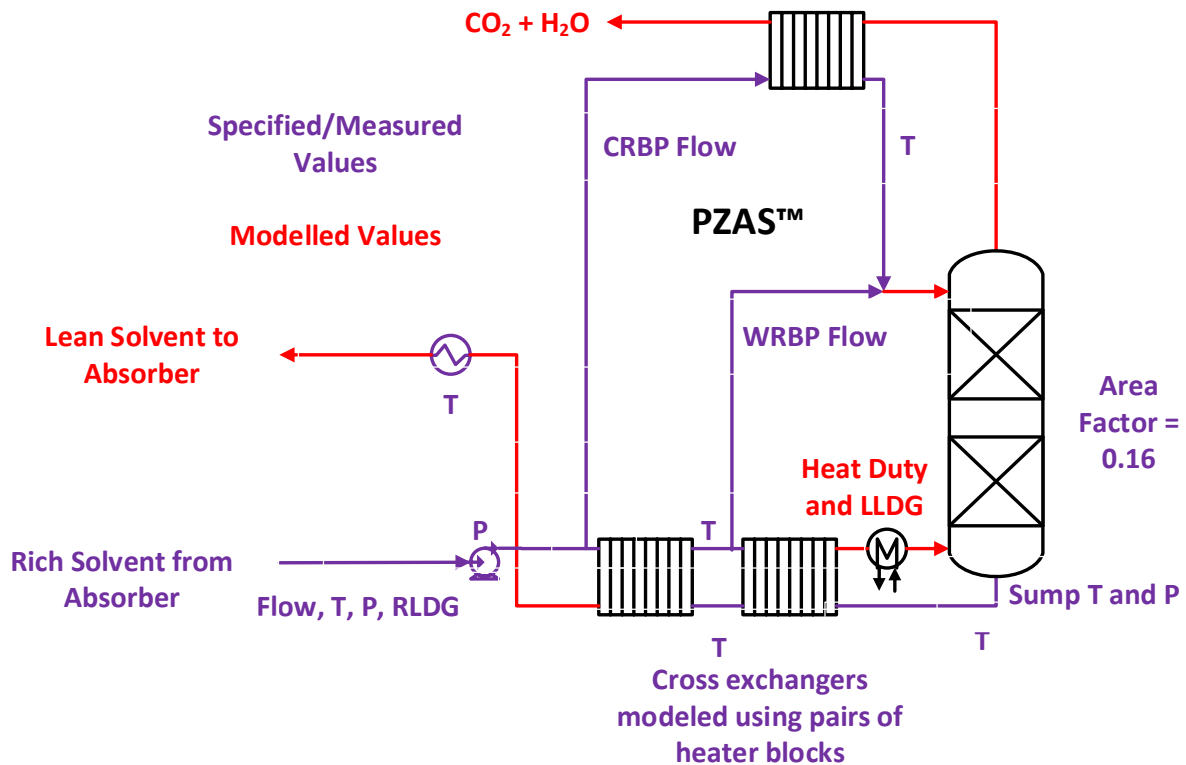


Figure 4: Key model inputs (purple) and outputs (red) to the PZAS™ model

## Results

### Heat Loss at NCCC

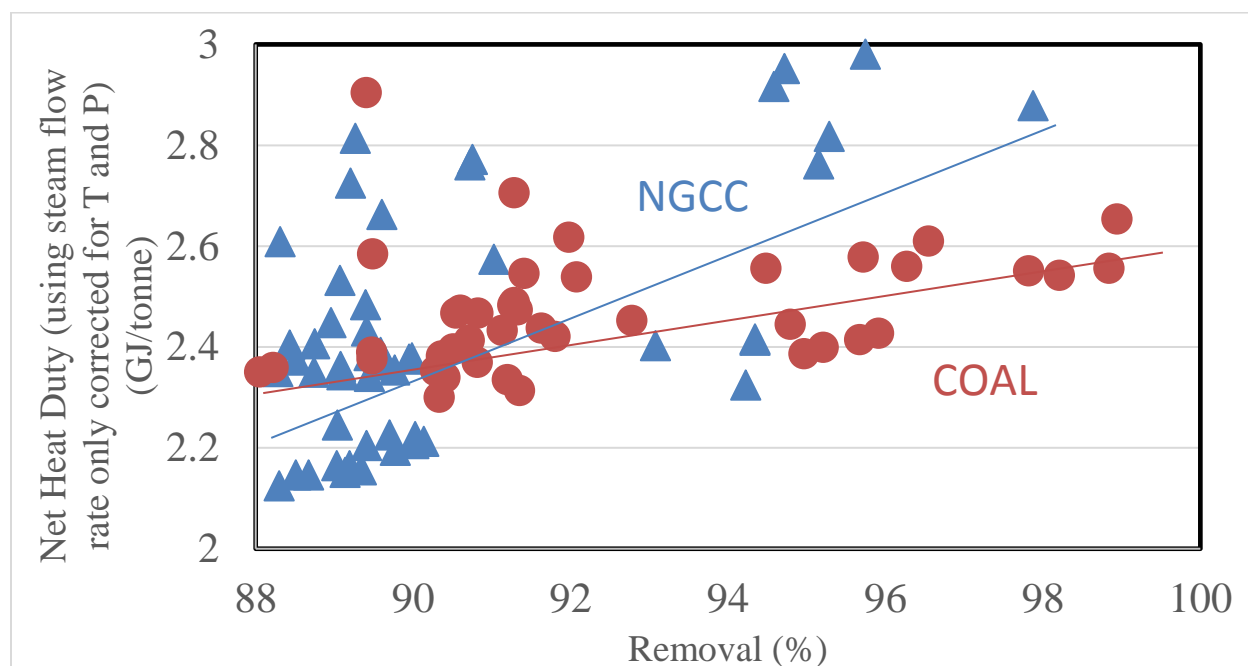
Heat loss was measured at NCCC from 28 water tests in the coal and NGCC campaigns. However, not all runs were representative of typical long-term operating conditions where both bypasses are operational and the stripper sump temperature is between 150 and 160 °C. Out of these 28 tests, the average heat loss was calculated from the final 12 runs where the cold rich bypass was about 500 lb/hr, the warm rich bypass was 1000 lb/hr, and the stripper sump temperature was maintained between 150 and 160 °C. Average heat loss was calculated using both steam flow rate corrected for temperature and pressure only, as well as steam flow rate corrected for temperature, pressure, and base-density.

When steam flow rate only corrected for temperature and pressure was used, the average heat loss was calculated to be 73,800 BTU/hr (0.078 GJ/hr) which was about 30% of the total steam heater heat rate. When steam flow rate was also corrected for the base-density, the average heat loss was calculated to be 61,000 BTU/hr (0.06 GJ/hr) which was about 28% of the total heat rate supplied by the steam heater.

Heat loss was reported to be about 10–20% of the total heat supplied to the reboiler at the 0.1 MW pilot plant located at the Separations Research Program at UT Austin (Seibert et al., 2011). The NCCC pilot plant is about 5 times larger in capacity than the Separations Research Program pilot plant and hence could result in greater heat loss. Correction of the steam flow rate measurement for base-density reduces the fraction of heat rate that is heat loss by about 2%.

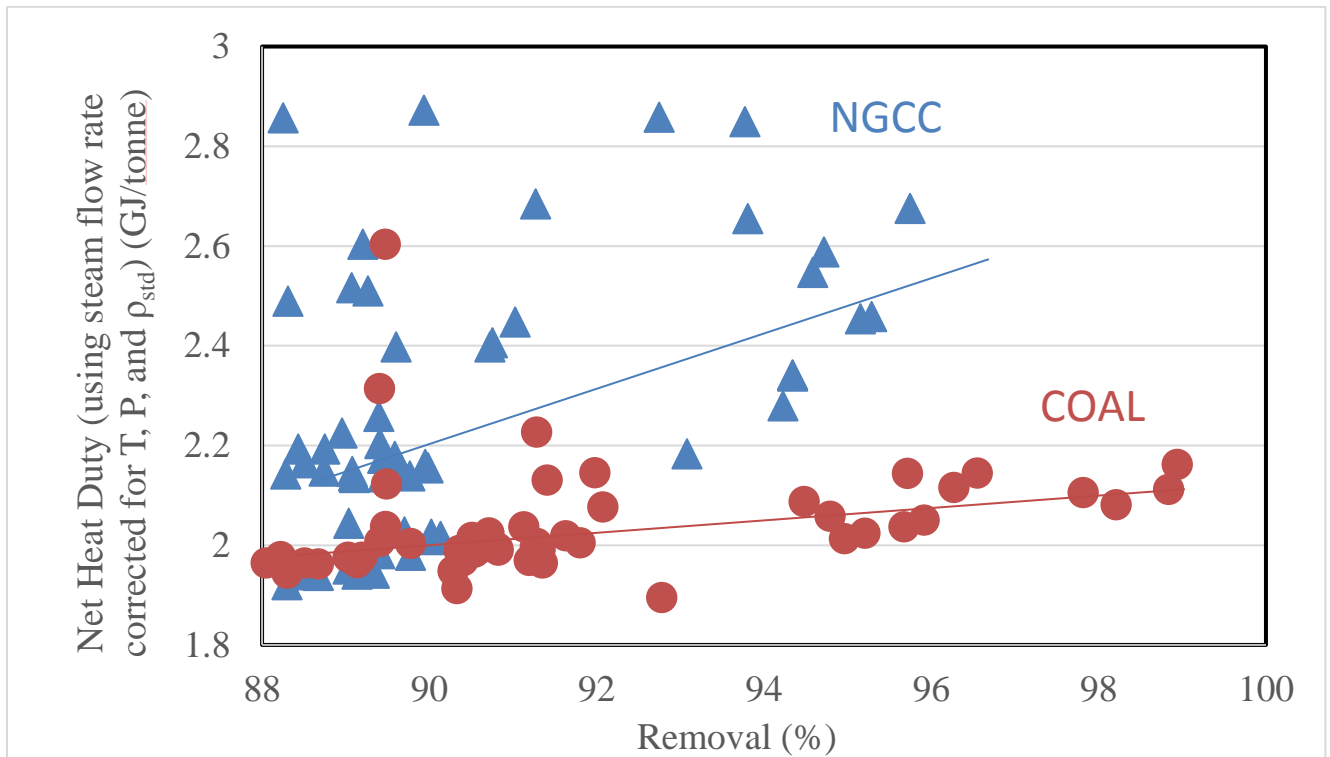
### Net Heat Duty Increases with Capture Efficiency

Figure 5 shows the net heat duty as a function of the capture efficiency for both the coal and NGCC campaigns. Net heat duty in this figure is calculated using the steam flow rates only corrected for temperature and pressure. Net heat duty is found to increase with capture efficiency due to the increased solvent circulation at high removal rates. Associated with this are the greater sensible heats in the cross exchangers and greater heat required to flash out the CO<sub>2</sub> in the steam heater. In the coal case, higher removal can be achieved with a much lower penalty in energy performance compared to the NGCC case. There is also more scatter seen in the NGCC data due to the greater number of parametric tests done in the NGCC campaign compared to the coal campaign. Under long-term conditions of 90% removal, the average net heat duty for the NGCC campaign is about 2.3 GJ/tonne CO<sub>2</sub> and about 2.4 GJ/tonne CO<sub>2</sub> for the coal campaign.



**Figure 5: Net heat duty calculated using steam flow rate corrected only for T & P increases with capture efficiency**

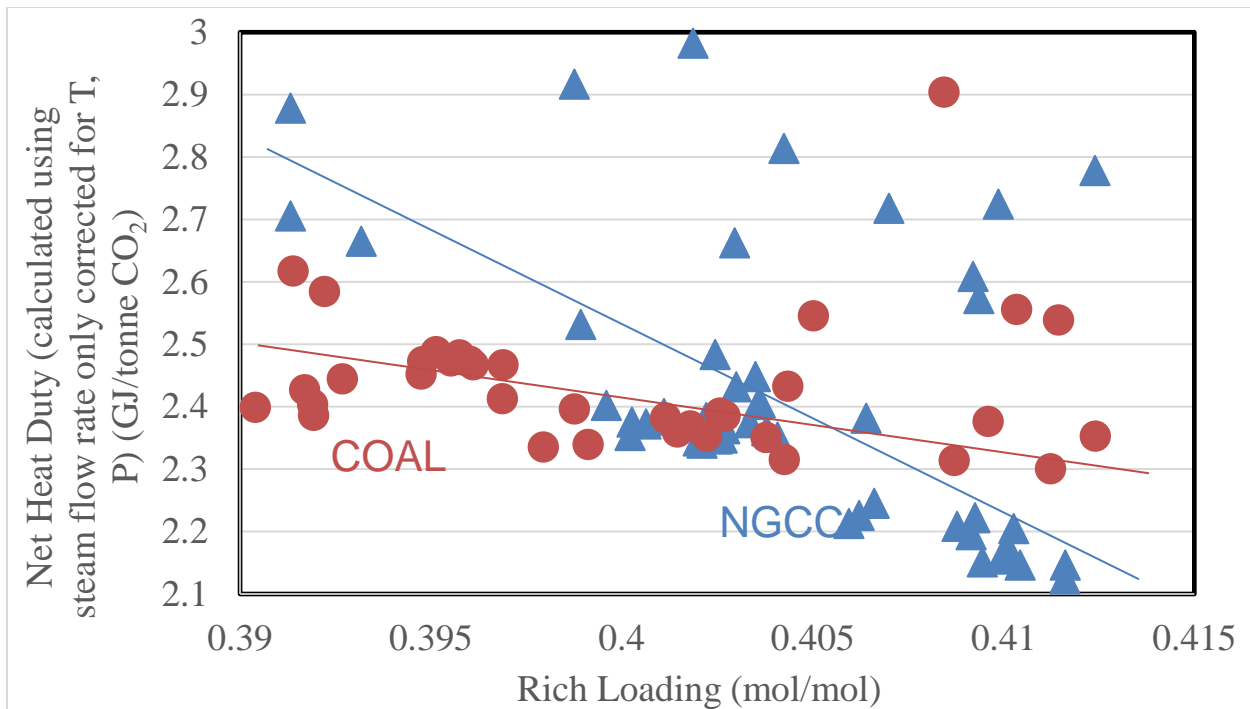
When net heat duty is calculated using steam flow rates corrected for temperature, pressure, and base-density, the long-term average net heat duty is about 9% lower for the NGCC case at 2.1 GJ/tonne CO<sub>2</sub>, and about 16% lower for the coal case at 2 GJ/tonne CO<sub>2</sub>. However, net heat duty still appears to be increasing with removal for both NGCC and coal cases. This is shown in Figure 6.



**Figure 6: Net heat duty using steam flow rate corrected for T, P, and  $\rho_{std}$  reduces compared to when steam flow rates are corrected only for T and P.**

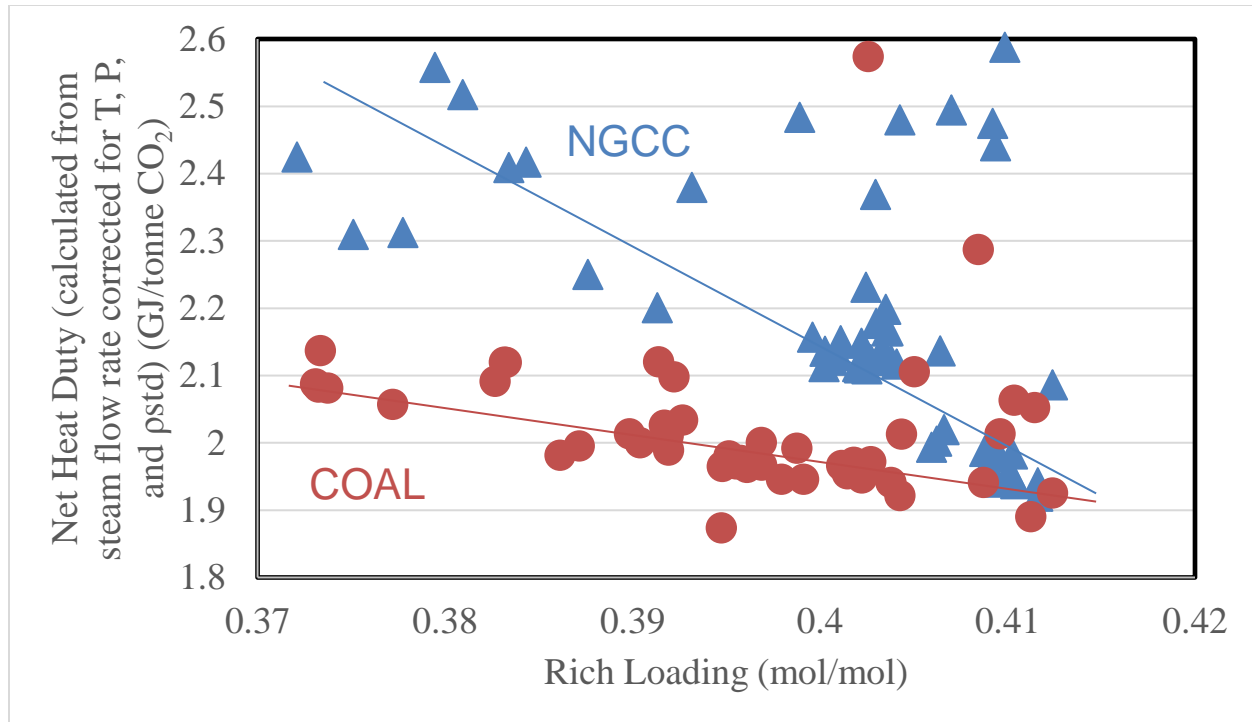
### Improved Energy Performance at Greater Rich Loading

Figure 7 shows net heat duty as a function of rich loading for both the coal and NGCC campaigns. Heat duty and heat loss have been calculated using the steam flow rate corrected for temperature and pressure only. In general, there is improved energy performance at greater rich loading. This is because a greater rich loading gives a greater delta loading and less solvent needs to be circulated between the absorber and stripper systems for a given removal. This reduces the sensible heat requirement. At long-term conditions of 90% removal and 0.403 rich loading, the heat duty corrected for heat loss for both NGCC and coal conditions is 2.35 GJ/tonne CO<sub>2</sub>. However, the NGCC campaign includes a number of points during long-term testing at a rich loading of 0.41 proving a lower heat duty of 2.15 GJ/tonne.



**Figure 7: Net heat duty reduces with increasing rich loading when steam flow rate is only corrected for T and P**

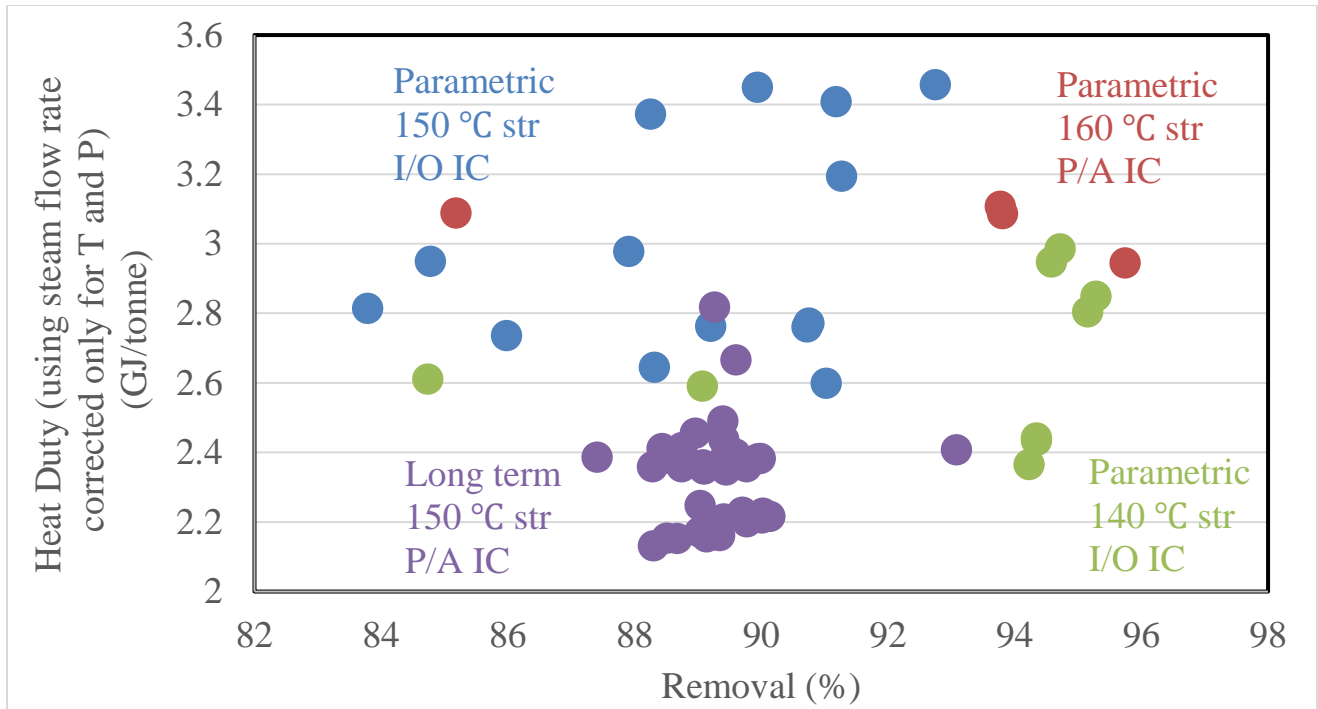
When the Figure 7 is reproduced using net heat duty calculated using steam flow rates only corrected for temperature and pressure, a similar decrease in net heat duty is observed in both NGCC and coal cases as is seen in Figure 6. Even in this case, the heat duty decreases at greater rich loading. This is shown in Figure 8.



**Figure 8: Correcting steam flow rate for T and P only reduces heat duty compared to T, P, and  $\rho_{std}$  correction**

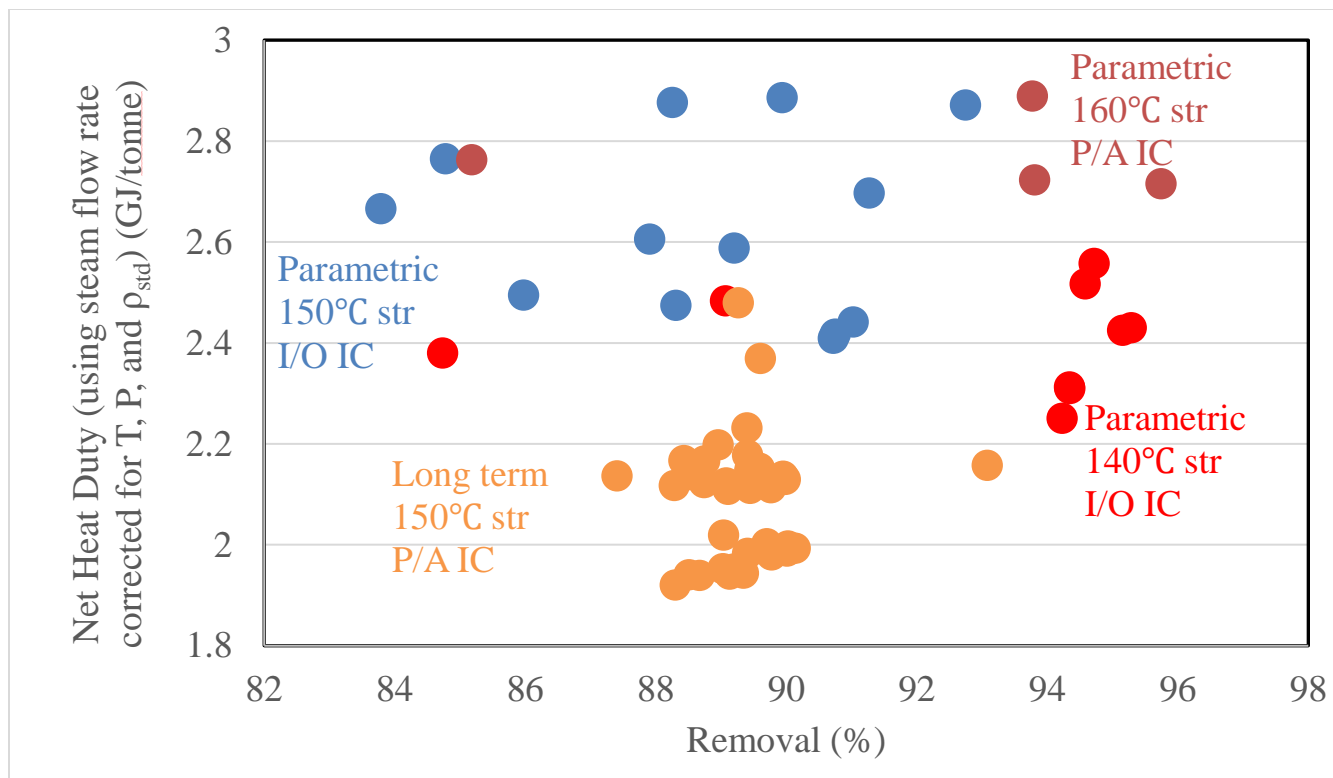
### Optimal Operating Conditions for NGCC CO<sub>2</sub> Capture & Effect of Carbon Bed

Figure 9 shows the net heat duty calculated using steam flow rates corrected for temperature and pressure only. The data have been color coded to represent different types of operating conditions. These are broadly categorized into parametric tests and long-term tests. It is apparent that long-term conditions of about 90% removal, 150 °C stripper sump, and pump-around intercooling in the bottom section of the absorber gave the lowest average net heat duty of about 2.3 GJ/tonne CO<sub>2</sub> compared to the parametric tests where different combinations of stripper sump temperature and intercooling configurations were employed. The data are shown by the purple dots in Figure 9.



**Figure 5: Net heat duty is the lowest with 150 °C stripper and pump-around intercooling with 35 °C intercooling temperature in absorber**

Figure 10 shows heat rates calculated using steam flow rates corrected for temperature, pressure, and base-density. The most optimum configuration in this case remains the same. The heat duty at the most optimum configuration is lower by 9% at 2.1 GJ/tonne CO<sub>2</sub>.



**Figure 10: Net heat duty with the most optimal process configuration reduces to 2 GJ/tonne CO<sub>2</sub>**

In the above two figures, there exist two patches of the long-term data. Although both patches correspond to the same stripper sump temperature (and lean loading), pump-around configuration, and removal, the net heat duty corrected for heat loss is lower for the lower patch.

This step change in heat duty is believed to be the effect of including a carbon bed in the process. The carbon bed began operation on May 14 and was used to remove degradation products from a rich amine slip stream after the absorber. The treated rich amine was recycled and mixed with the rest of the untreated rich amine and sent to the regeneration system. The measured viscosity of the rich solvent decreased with time following the use of the carbon bed. This is most strongly related to a decrease in piperazine concentration. This could be related to the carbon bed removing high molecular weight and high viscosity degradation products from the amine or water balance issues in the carbon bed.

However, during this time, the CO<sub>2</sub> concentration measured analytically remained unchanged. The coupled effect of this was an increase in rich loading which gave rise to an increase in the delta loading under long-term operating conditions. As a consequence of this, the heat duty was reduced to about 2.2 GJ/tonne CO<sub>2</sub> when steam flow rates were corrected for temperature and pressure only. When the steam flow rates were corrected for temperature, pressure, and base-density, the heat duty reduced to about 2 GJ/tonne CO<sub>2</sub>.

## Model Validation

The data from the coal and NGCC campaigns were used to validate the Independence™ model. A total of 122 steady state runs for coal and NGCC conditions were identified and modeled. Figure 11 shows the model error or the ratio of model-predicted heat duty to the measured net heat duty as a function of the measured rich loading at the pilot plant. The measured net heat duty is calculated using steam flow rates corrected only for temperature and pressure. The model performs well at predicting long-term NGCC data and almost all the coal data with only about 5% error. On average, the model underpredicts the measured energy performance by 6%.

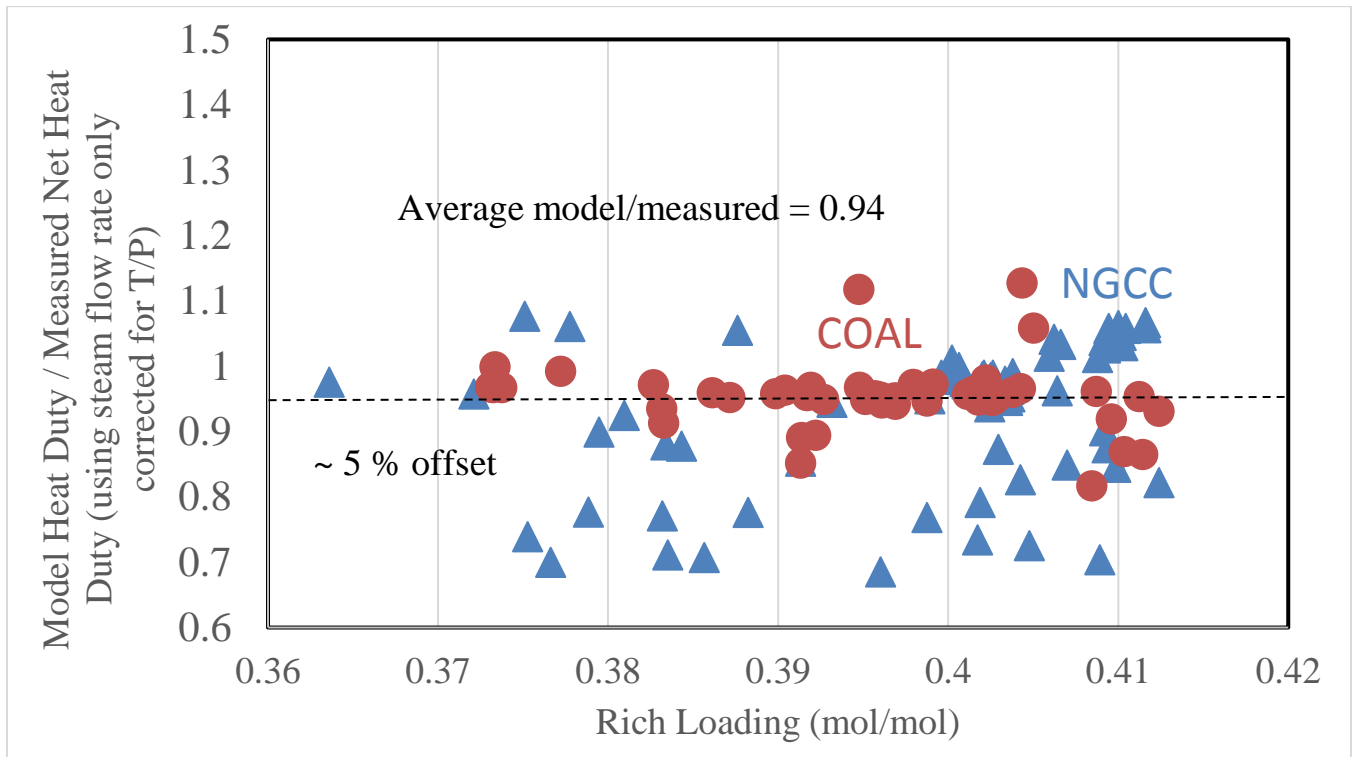


**Figure 11: Model predicts long-term energy performance within 5% when steam flow rate is only corrected for T and P**

When the heat duty and heat loss is calculated using steam flow rates corrected for temperature, pressure, and base-density, the average model error for long-term NGCC and coal data increases to 15%. On average, the model now overpredicts the measured net heat duty by 8%. The model agrees best with the measured heat rate corrected for T and P and heat loss. Therefore it is probable that the additional adjustment of the heat rate based on the condensate weight measurement is not correct.

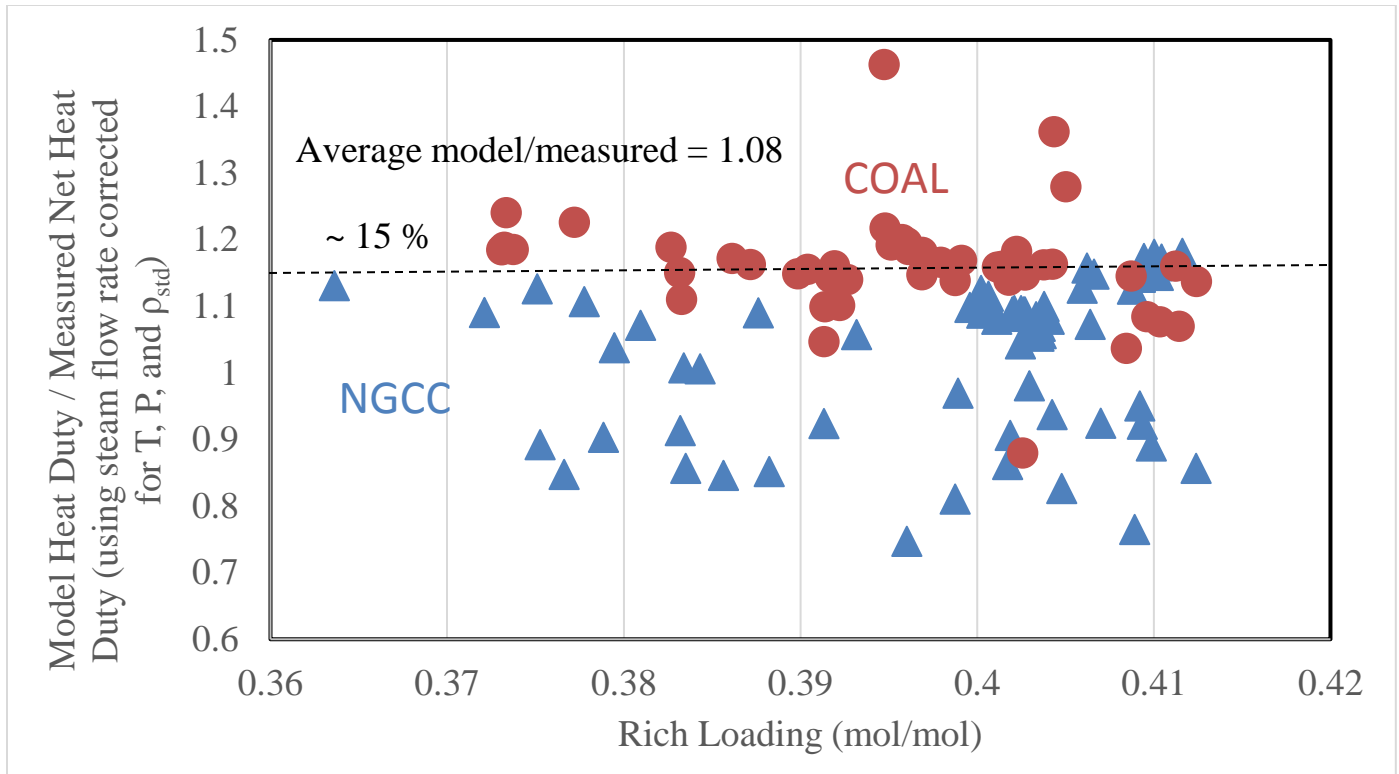


**Figure 12: Long-term model error increases to 15% when steam flow rate is corrected for T, P and  $\rho_{std}$**

Conclusions When the steam flow rate was only corrected for temperature and pressure, the long-term heat duty for NGCC was 2.2 to 2.4 GJ/tonne CO<sub>2</sub> and was 2.2 to 2.35 GJ/tonne CO<sub>2</sub> for coal. An additional correction for the base-density lowered the net heat duty of the PZAS™ system by 9–16%. Under this condition, the long-term average net heat duty was 2 GJ/tonne CO<sub>2</sub> for coal and 2.1 GJ/tonne CO<sub>2</sub> for NGCC. It is likely that the calibration of the steam flow measurement with condensate measurements underestimated the true steam rate. Therefore, steam flow rates corrected for temperature and pressure should be sufficient for future analysis of heat duty.

Rich loading played a major role in determining the net heat duty of the regeneration system. Net heat duty was reduced to 2.2 GJ/tonne CO<sub>2</sub> by using pump-around intercooling at 35 °C in the absorber bottom with a 150 °C stripper sump along with the carbon bed. Net heat duty also increased with capture efficiency of the pilot plant.

The Independence™ model was validated with the pilot plant data. The model predicted long-term net heat duty for both NGCC and coal with only 5% error, when steam flow rates were corrected only for temperature and pressure. The model error increased to 15% for the long-term data, when steam flow rates were corrected for base-density also. Overall, the model was capable of predicting measured net heat duties within  $\pm 8\%$ .

## References

- Cousins A et al. "Pilot-scale parametric evaluation of concentrated piperazine for CO<sub>2</sub> capture at an Australian coal-fired power station." *Greenhouse Gases: Science and Technology* 2.6 (2015): 408-418.
- Frailie P et al. "Modeling piperazine thermodynamics." *Energy Proc.* 4:2011:35-42.
- Freeman SA, Rochelle GT. "Density and viscosity of aqueous (piperazine+ carbon dioxide) solutions." *J Chem & Engin Data* 56.3;2011:574-581.
- Freeman SA, Davis J, Rochelle GT. "Degradation of aqueous piperazine in carbon dioxide capture." *IJGGC.* 4.5:2010:756-761.
- Knudsen JN et al. "Evaluation of process upgrades and novel solvents for the post combustion CO<sub>2</sub> capture process in pilot-scale." *Energy Proc.* 4:2011:1558-1565.
- Lin Y-J, Rochelle GT. "Approaching a reversible stripping process for CO<sub>2</sub> capture." *Chem Enging J.* 283:2016:1033-1043.
- Lin Y-J, Chen E, Rochelle GT. "Pilot plant test of the advanced flash stripper for CO<sub>2</sub> capture." *Faraday Disc.* 192:2016:37-58.
- Madan T et al. "Modeling pilot plant results for CO<sub>2</sub> stripping using piperazine in two stage flash." *Energy Proc.* 37:2013:386-399.
- Plaza JM, Rochelle GT. "Modeling pilot plant results for CO<sub>2</sub> capture by aqueous piperazine." *Energy Proc.* 4;2011:1593-1600.
- Rochelle GT et al. "Aqueous piperazine as the new standard for CO<sub>2</sub> capture technology." *Chem engin J.* 171.3:2011:725-733.
- Wang C. *Mass transfer coefficients and effective area of packing.* The University of Texas at Austin. Ph.D. Dissertation. 2015.
- Seibert F et al. "UT/SRP CO<sub>2</sub> capture pilot plant—Operating experience and procedures." *Energy Proc.* 4:2011:1616-1623.

# CO<sub>2</sub> Absorption from Gas Turbine Flue Gas by Aqueous Piperazine with Intercooling

*Tianyu Gao, Gary T. Rochelle*

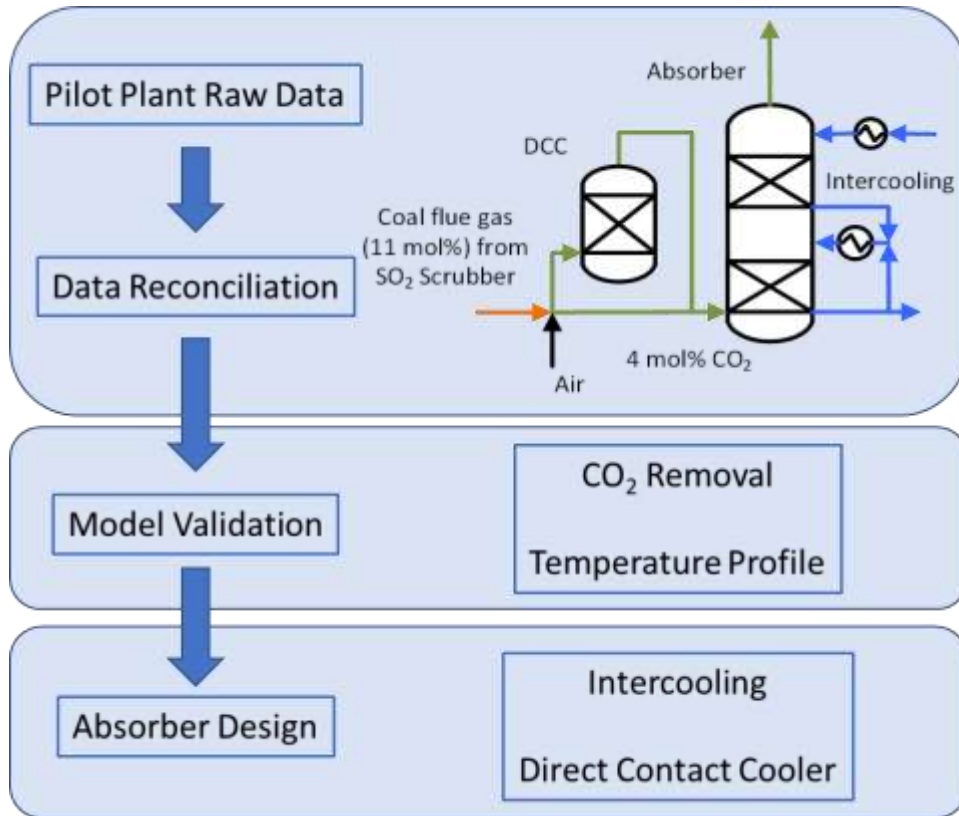
The University of Texas at Austin, McKetta Department of Chemical Engineering, 200 E. Dean  
Keeton St., C0400, Austin, TX 78712-1589, USA

KEYWORDS Amine Scrubbing, Piperazine, Absorber, Pilot Scale, NGCC

## ABSTRACT

Amine scrubbing is the most mature technology for post-combustion carbon capture. Much bench- and pilot-scale work has been focused on CO<sub>2</sub> capture from coal-fired flue gas. Because natural gas is inexpensive and readily available in the United States and other countries, the natural gas combined-cycle (NGCC) has been replacing coal for electricity generation. Carbon capture for NGCC is therefore an important technology for modern power plants. The Piperazine (PZ) Advanced Stripper (PZAS<sup>TM</sup>) technology has been established as a benchmark system for second-generation amine scrubbing for CO<sub>2</sub> capture from coal-fired flue gas. It has a fast absorption rate, good energy performance, and strong resistance to thermal degradation and oxidation. PZAS<sup>TM</sup> was operated with simulated NGCC flue gas (4.3 mol % (dry) CO<sub>2</sub>) at the National Carbon Capture Center (NCCC) in Wilsonville, Alabama in 2019. The absorber was tested with in-and-out and pump-around intercooling. The variable operating conditions included lean loading (0.19–0.25 m CO<sub>2</sub>/mol alkalinity), gas temperature (40, 76 °C), and intercooling temperature (35, 40 °C). Using 5 m PZ, CO<sub>2</sub> removal from 82% to 96% was achieved with intercooling and only 12 m of packing. A rigorous, rate-based absorber model accurately predicted the CO<sub>2</sub> removal and temperature profile. The model shows that the delta loading of the solvent at NGCC conditions for 90% removal is greater than at coal conditions, but high CO<sub>2</sub> removal (99%) is more difficult to achieve with NGCC gas than with coal-fired flue gas. The pump-around intercooling was effective, and the intercooling temperature had a large impact on the absorber performance. With pump-around, the delta loading penalty for hot gas feed into the absorber without a direct contact cooler was less than 5%.

## GRAPHIC ABSTRACT



## 1. Introduction

In the US, carbon emissions from the power sector accounted for the second largest portion (27.5%) of total emissions, following transportation (28.9%), in 2017<sup>1</sup>. In the electricity sector, coal and natural gas produce 65% and 33% of the carbon emissions, respectively. Natural gas contains less carbon than coal and results in less carbon emission per unit of electricity. In countries where it is readily available, gas has been replacing coal in the power sector for both economic and environmental reasons. In the US, natural gas usage for power generation surpassed coal in 2016 and currently provides approximately 33% of all electricity. In December 2018, the US Environmental Protection Agency (EPA) proposed a GHG emission regulation for new, modified, and reconstructed power plants. It is projected that most of the fossil fuel electricity-generating capacity added in the US through 2050 will be Natural Gas Combined-Cycle (NGCC). Therefore, carbon capture for gas application is an important pathway to carbon neutrality for modern power plants.

Various second-generation (2G) amine solvents and processes have been tested for CO<sub>2</sub> capture from coal flue gas (~12 mol % CO<sub>2</sub>). With the fast absorption, good energy performance, and high resistance to thermal and oxidative degradation, piperazine (5 m, 30 wt % PZ) with the Advanced Stripper (PZAS)<sup>TM</sup> has been demonstrated as a benchmark 2G amine scrubbing process<sup>2</sup>. The process has been tested in the pilot plants at the Separations Research Program (SRP) of the University of Texas at Austin and at the National Carbon Capture Center (NCCC). At SRP, over 2000 hours of operation through seven campaigns have tested the 0.43-inch ID absorber with in-and-out and spray intercooling using synthetic flue gas<sup>3-6</sup>. The CO<sub>2</sub> content was varied between 3.5% and 20 mol % for different applications<sup>6-9</sup>. In 2018, PZAS<sup>TM</sup> was tested at the NCCC for

about 2000 hours of operation with coal flue gas (11 mol % CO<sub>2</sub>). 90–99% CO<sub>2</sub> removal was achieved with 12 m packing and simple in-and-out intercooling<sup>10-11</sup>.

Previous research work and pilot demonstrations have shown the feasibility of CO<sub>2</sub> capture from coal flue gas<sup>10, 12</sup>. The low CO<sub>2</sub> content in NGCC flue gas is a challenge for many technologies, and only a few pilot-scale demonstrations or research can be found in open literature<sup>7, 13-15</sup>. Fluor deployed a commercial NGCC capture plant in Massachusetts from 1991 to 2005. The Econamine FG Plus<sup>SM</sup> process used MEA-based solvent and achieved a capture rate between 85% and 95% for 40 MW gas<sup>16</sup>. The plant was shut down because of the high price of natural gas at the time. This paper reports the pilot plant absorber performance and modeling results using PZAS<sup>TM</sup> with advanced intercooling with 4.3% CO<sub>2</sub> to demonstrate feasibility for the gas turbine application.

## 2. Methodology

### 2.1. Pilot Plant Overview

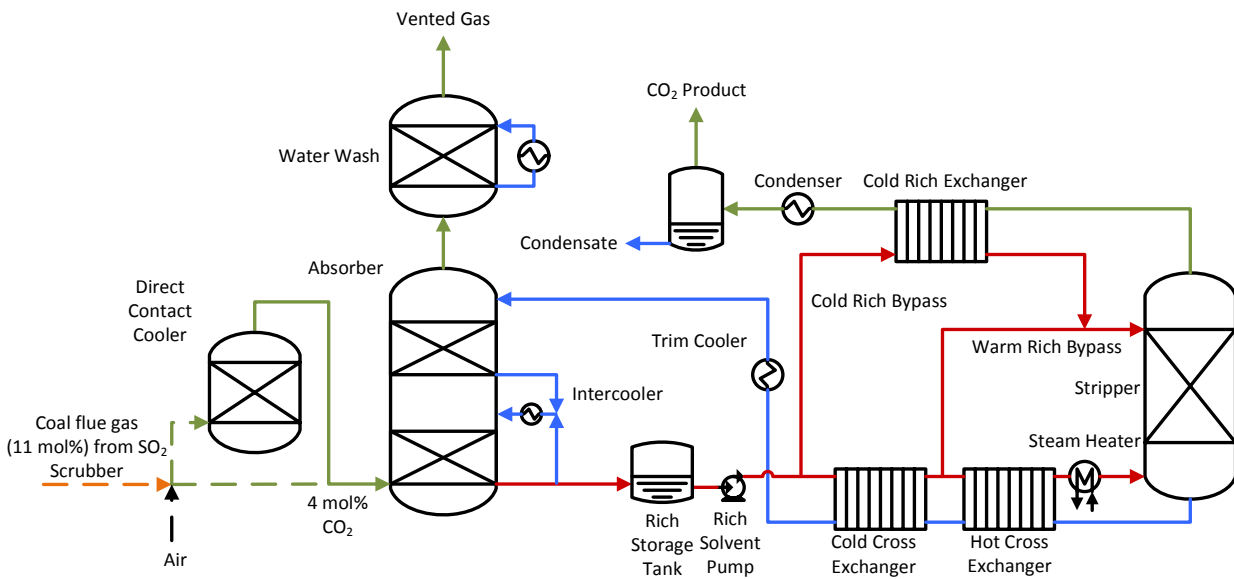


**Figure 1.** Process flow diagram for PZAS<sup>TM</sup> tested at NCCC

The Pilot Solvent Test Unit (PSTU) at the NCCC was modified to test PZAS<sup>TM</sup> with 4.3 dry mol % CO<sub>2</sub>. The flue gas pretreatment and PZAS<sup>TM</sup> process are shown in Figure 1. Coal-fired flue gas containing about 11 mol % CO<sub>2</sub> was fed to a NaOH scrubber to remove SO<sub>2</sub>. The gas was then diluted with air to reduce the CO<sub>2</sub> to about 4.3 mol % to simulate NGCC flue gas. The diluted gas could be cooled in the direct contact cooler (DCC) and saturated with water at 40 °C or sent directly to the absorber. In bypass mode, the flue gas was heated to 76 °C by the blower to partially simulate hot NGCC gas conditions. Both simple in-and-out and advanced pump-around intercooling were tested. Figure 2 shows the three absorber configurations: (A) absorber with in-and-out intercooling and DCC, (B) with pump-around intercooling and DCC, and (C) with pump-around intercooling but no DCC. When the DCC was online, the mixed gas was cooled and saturated with water at 40 °C and when it was bypassed, the gas was heated to 76 °C and fed directly to the absorber column.

The absorber column has three beds of packing, but the top bed was not used for absorption. For the in-and-out cooling loop, solvent was removed from the bottom of the middle bed, intercooled, and returned to the top of the bottom bed. For the pump-around, solvent was recycled from the bottom of the bottom bed, cooled, and fed to the top of the bottom bed.

The flue gas flowed upward in the absorber and counter-currently contacted the solvent. The CO<sub>2</sub>-scrubbed gas was washed with water to remove entrained solvent and control amine emissions, and then vented. The rich solvent leaving the absorber bottom was pumped to the stripper for regeneration. The solvent was split into cold rich bypass and warm rich bypass for heat recovery. After two cross exchangers, the rich stream was heated to 150–155 °C by a steam heater. The bypass stream was fed to the stripper to condense the water vapor and recover the latent heat in the stripper overhead. Table 1 summarizes the detailed specifications of the test facilities.

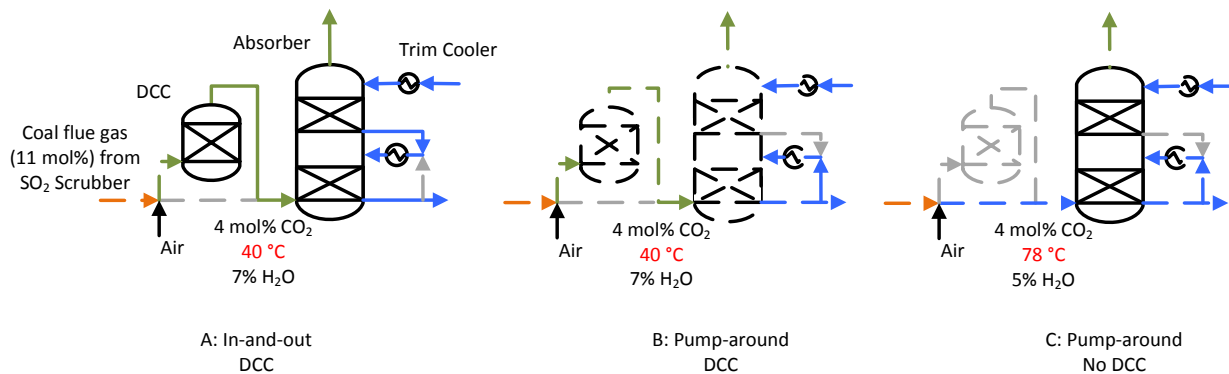


**Figure 2.** Three configurations of absorber tested during the 2019 pilot plant campaign

**Table 1.** Summary of equipment specifications

Absorber	Column Inner Diameter ( <i>meters</i> )	0.66
	Packing Height ( <i>meters</i> )	2 × 6.10
	Packing type	M252Y
	Material	Stainless Steel
Stripper	Packing Height ( <i>m</i> )	2 × 2
	Packing Type	RSR #0.5, #0.7
	Material	Stainless Steel
	Cold Cross Exchanger Area ( <i>m</i> <sup>2</sup> )	114.0
	Hot Cross Exchanger Area ( <i>m</i> <sup>2</sup> )	31.9
	Cold Rich Exchanger Area ( <i>m</i> <sup>2</sup> )	8.5

## 2.2. Measurement Methods

The methods for measuring gas and solvent compositions were the same as the NCCC 2018 campaign described in previous papers<sup>10-11</sup>. The gaseous CO<sub>2</sub> was measured continuously by online non-dispersive infrared (NDIR) analyzers. Liquid PZ and CO<sub>2</sub> were analyzed by online auto-titration about every 70 minutes. Samples were collected daily and analyzed by gas

chromatography (GC) and total inorganic carbon (TIC) analyzers for PZ and CO<sub>2</sub>, respectively. Solvent density and viscosity were measured continuously by online flowmeters and viscometers and were used for calculating PZ and CO<sub>2</sub> concentration. The correlations were described previously<sup>10</sup>.

### 2.3. Modeling Methods

The rigorous “Independence” model in Aspen Plus<sup>®</sup> was used to simulate the absorber performance. It consists of several sub-models, including solvent properties and packing characterization. The “Independence” model includes physical properties, thermodynamics, and kinetics models regressed from bench-scale experiments. The thermodynamics were built in the electrolyte non-random two liquid (e-NRTL) framework<sup>2</sup>. The packing characterization model includes interfacial area, and liquid- and gas-side mass transfer coefficients developed by Song<sup>17</sup> from pilot-scale measurements with various random and structured packings. All the model parameters were regressed independently and were not tuned to match the campaign data.

## 3. Results and Discussion

### 3.1. NGCC and coal flue gas

Table 2 shows the typical parameters of coal and NGCC flue gas<sup>18</sup>.

**Table 2.** Typical flue gas parameters<sup>18</sup>

	Coal (Supercritical pulverized coal)	NGCC (F-Class)
CO <sub>2</sub> (mol %)	12.88	3.91
H <sub>2</sub> O (mol %)	14.51	8.41
N <sub>2</sub> (mol %)	68.54	74.42
O <sub>2</sub> (mol %)	3.25	12.38

Temperature (°C)	56	117
Gross Power (MW)	550	630
Flowrate (kg/s)	601.5	1029.7
Flowrate (kg/s/MW)	1.09	1.58

---

Gas emitted from a coal flue contains about 13 mol % CO<sub>2</sub>, while that from a gas turbine contains only ~4 mol %. The first challenge of carbon capture from NGCC is associated with the low CO<sub>2</sub>, which reduces the partial pressure driving force for absorption. For NGCC conditions, 90% removal requires a lean CO<sub>2</sub> partial pressure below 0.4 kPa, which is the same partial pressure required for about 97% removal for the coal case. This means the lean solvent needs more overstripping to provide adequate mass transfer driving force for the gas application. It also makes >99% capture more difficult for NGCC. For coal, it has been demonstrated feasible to achieve high removal with reasonable energy and economic penalties<sup>11,19</sup>. However, for NGCC flue gas, high CO<sub>2</sub> removal (95–99%) may experience a greater penalty or may even be infeasible.

The second challenge for capturing CO<sub>2</sub> from NGCC flue gas is the absorber column size. The flue gas flow rate per unit of electricity for NGCC is more than 60% greater than for coal-fired flue gas, which requires a greater absorber diameter and increases the capital cost. For the NGCC application, the absorber dominates the total capital cost of the capture plant. Therefore, the absorber design and optimization become more important for NGCC.

The third challenge for the NGCC application is related to the low liquid to gas (L/G) ratio and the heat of absorption. The low CO<sub>2</sub> content requires significantly less solvent circulation. The column temperature is mainly determined by the gas. The benefits of simple in-and-out intercooling are diminished because it is the gas that carries most of the enthalpy into the column. Cooling the

solvent at such a low flow rate is not effective. Therefore, pump-around intercooling becomes necessary because it enhances the solvent rate and increases the cooling ability of the solvent.

Along with these challenges, NGCC flue gas capture also provides opportunities for absorber optimization. The natural gas flue gas is “cleaner” than coal flue gas. There is no SO<sub>2</sub> or fly ash, so flue gas pre-treating is less expensive. Secondly, the water content in NGCC flue gas is only about 8 mol %. The water balance in the absorber column can be maintained by running the water wash section at about 43 °C with 8% inlet water. A direct contact cooler (DCC) is not necessary to knock out excess water. By removing the DCC and using pump-around intercooling, the bottom section of the absorber serves the purposes of both cooling and capturing.

### 3.2. Pilot Plant Campaign Results

PZAS<sup>TM</sup> was tested for about 4 months and 2100 operating hours. The starting solvent inventory had 2120 operating hours from the 2018 NCCC campaign with coal flue gas. The steady-state runs were defined based on flue gas rate, CO<sub>2</sub> concentration, lean solvent flow, feed temperature, intercooling temperature, solvent loading, and CO<sub>2</sub> removal. Table 3 summarizes the pilot plant steady-state conditions.

**Table 3.** Summary of NCCC 2019 campaign operating conditions

CO <sub>2</sub> in flue gas (mol % dry)	4.0–4.3%
PZ molality (m)	3.5–5.6
Flue gas rate (kg/s)	0.63–1.01
Solvent rate (kg/s)	0.61–1.77
CO <sub>2</sub> removal	80.0–95.8%
Lean loading (mol CO <sub>2</sub> /mol alkalinity)	0.186–0.254

Rich loading (mol CO <sub>2</sub> /mol alkalinity)	0.364–0.410
Absorber solvent inlet T (°C)	40.3–53.5
Absorber gas inlet T (°C)	39.7–83.0
Absorber intercooling T (°C)	34.9–42.6

---

### 3.2.1. Material Balance

The CO<sub>2</sub> material balance was studied to check the consistency of measurements. Three CO<sub>2</sub> rates were calculated: CO<sub>2</sub> removed from the gas phase, CO<sub>2</sub> captured in the liquid phase, and stripper overhead production. The gas phase balance was based on inlet and outlet flowmeters and NDIR measurements. The solvent loading was calculated from density and viscosity measurements. The stripper overhead product was assumed to be pure CO<sub>2</sub>. As shown in Figure 3, the liquid phase removal rate matches the overhead production rate. The gas phase removal rate is consistently 3% higher. The error bars show the standard deviation associated with all the measurements. The liquid rate shows the least uncertainty because of the good reproducibility of the online density and viscosity measurements. The greater uncertainty of the overhead production was caused by fluctuation in the flowrate.

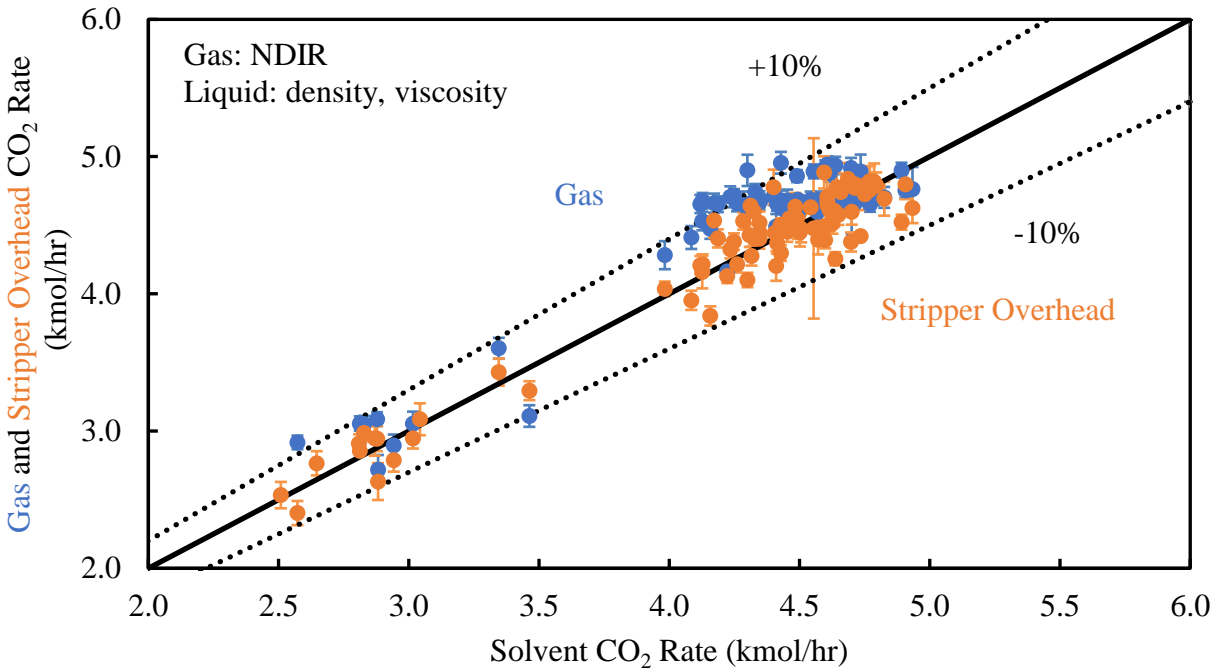


**Figure 3.** CO<sub>2</sub> transfer rate in the gas and liquid phases and the CO<sub>2</sub> production rate.

### 3.2.2. Absorber Performance

Data from 80 absorber steady-state runs were obtained over 2100 operating hours in 2019. The first 22 runs were parametric tests, which examined the absorber performance over a wide range of conditions, and the rest were from long-term testing designed to study the system stability, solvent oxidation, and other problems. There were four major absorber operating conditions tested during the campaign: in-and-out (40 °C) with 40 °C gas, pump-around (40 °C) with 40 °C gas, pump-around (40 °C) with 76 °C gas, and pump-around (35 °C) with 76 °C gas. The CO<sub>2</sub> removal (defined by Equation 1) varied between 85% and 96% with lean loading from 0.19 to 0.25 mol CO<sub>2</sub>/mol alkalinity. CO<sub>2</sub> penetration and number of transfer units (NTU) as defined in Equation 2 were used to evaluate absorber performance.

$$Removal = 1 - \frac{N_{out,CO_2}}{N_{in,CO_2}} \quad \text{Equation 1}$$

$$NTU = -\ln(\text{Penetration}) = -\ln(1 - \text{Removal}) \quad \text{Equation 2}$$

Figure 4 shows the experimental absorber performance grouped with four operating conditions. The rich loading varied between 0.36 and 0.41, and it shows correlation with CO<sub>2</sub> penetration: the rich loading decreases from 0.4 to 0.38 as the removal increases from 90% to 95%. The delta loading reflects the energy penalty for high CO<sub>2</sub> removal at the NGCC condition. The long-term runs achieved rich loading exceeding 0.4, which is greater than the rich loading from the 2018 campaign at coal conditions<sup>11</sup>. This means that low CO<sub>2</sub> in the NGCC flue gas does not necessarily lead to a lower rich loading, nor to worse energy performance. This is because the column temperature is well-managed with pump-around intercooling, which increases the rich loading even at the low CO<sub>2</sub> partial pressure.

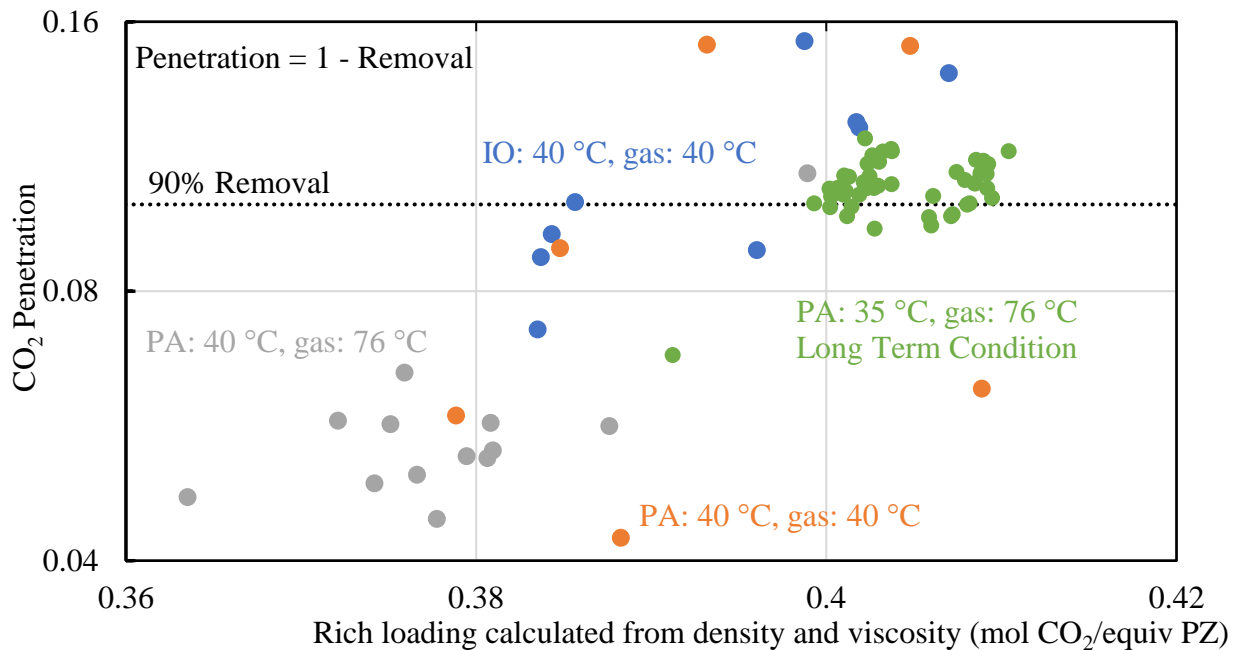


**Figure 4.** Experimental absorber performance for NCCC 2019 campaign

### 3.3. Model Results

### 3.3.1. Model Validation

The absorber performance was modeled rigorously using Aspen Plus<sup>®</sup>. The CO<sub>2</sub> and PZ concentration for model inputs were calculated from density and viscosity. The calculated PZ was increased by a factor of 1.08 to provide a better representation of the pilot plant data. This adjustment could be consistent with systematic analytical error or with systematic degradation of the solvent. Figure 5 compares the measured and modeled absorber NTU in chronological order with color coding for the four major absorber conditions. The pump-around data are more scattered because the viscosity measurements showed a greater variation at these conditions. The relative difference in NTU between the model and the experiments shows a decreasing trend during the long-term testing, and it reflects the extent of solvent degradation. Figure 6 shows the NTU ratio at different nominal L/G conditions (lean solvent rate to gas rate), and the model predictions are independent of L/G. Overall, the model is validated at different absorber configurations and operating conditions.

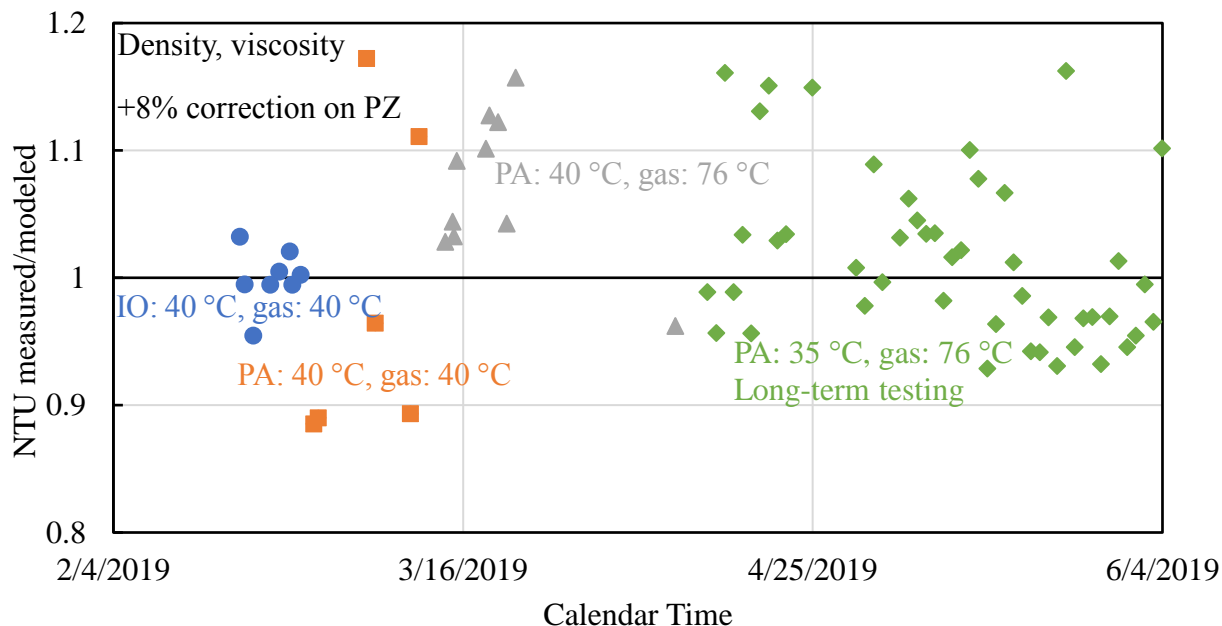


**Figure 5.** Absorber model validation for 2019 campaign. Points are color-coded for 4 major operating conditions.

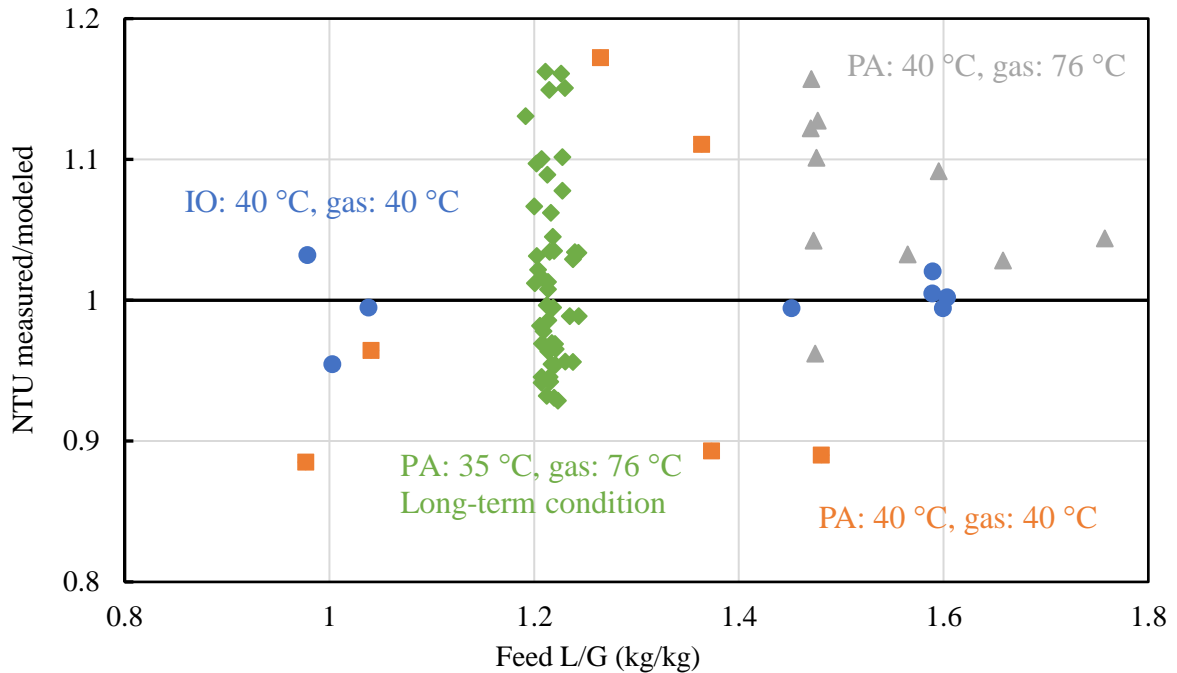


**Figure 6.** Comparison of experimental and modeled absorber NTU at variable L/G. Points are color-coated for different operating conditions.

The measured temperature profile was also compared to the model predictions. Figures 7, 8, and 9 show results for 3 representative cases. In all figures, the temperature on the primary axis is plotted against the relative position, with 0 and 1 representing the top and bottom of the absorption column. The calculated CO<sub>2</sub> flux is shown on the secondary axis.

As shown in the three figures, the shape of the temperature profile varies with the conditions of lean loading, L/G, and intercooling. At low lean loading and L/G, the gas carries the heat of

absorption, pushes the temperature bulge to the top of the column, and leads to a cold bottom. 90% removal is achievable because the over-stripped solvent provides adequate CO<sub>2</sub> driving force even at elevated temperature, and the rich loading is high because of the cold rich temperature. Therefore, the low lean loading leads to a greater solvent capacity and can reduce the solvent circulation significantly.

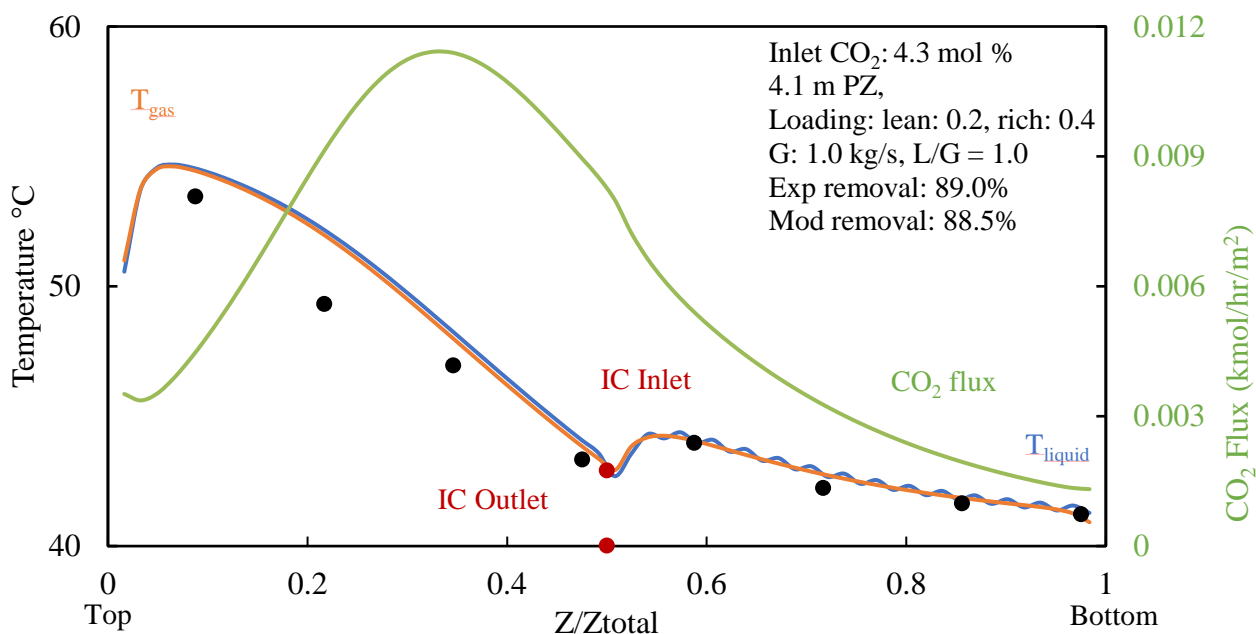


**Figure 7.** Absorber profile for in-and-out intercooling and 0.24 lean loading. Temperature measurements (points) and model predictions (curve) are shown on the primary axis; CO<sub>2</sub> transfer flux is shown on the secondary axis.

With 0.24 lean loading and in-and-out intercooling (Figure 8), more solvent is needed to achieve 90% CO<sub>2</sub> removal. At the same time, the solvent pushes the reaction heat into the bottom of the column, but the simple in-and-out intercooling cannot cool the gas effectively given the L/G ratio, and the rich loading decreases at this high temperature. This leads to a significant increase of solvent circulation (about 50%) compared to 0.20 lean loading.

With pump-around intercooling, the solvent rate in the bottom section can be enhanced to provide effective cooling. As shown in Figure 9, the solvent rate in the bottom section is 2 times greater than the top. At this solvent rate, the intercooling is sufficient, and the temperature is low even with a hot flue gas inlet. As a result, the pump-around intercooling increases the rich loading and reduces the solvent requirement by 30% compared to in-and-out.

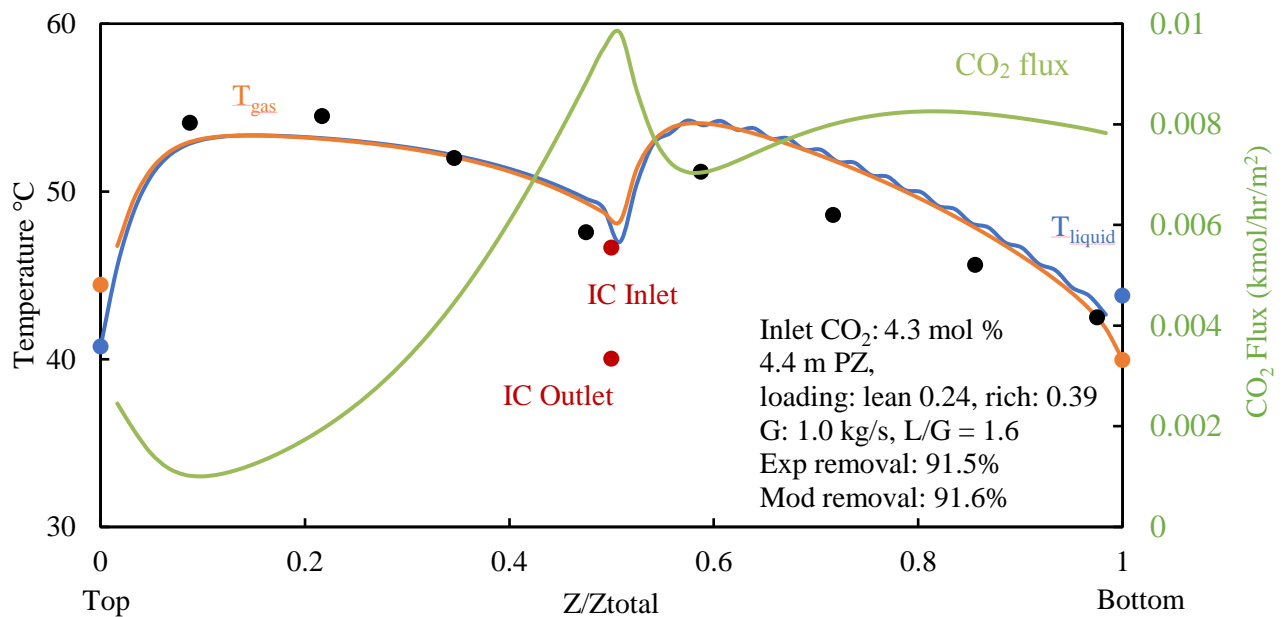


**Figure 8.** Absorber profile for in-and-out intercooling and 0.24 lean loading. Temperature measurements (points) and model predictions (curve) are shown on the primary axis; CO<sub>2</sub> transfer flux is shown on the secondary axis.

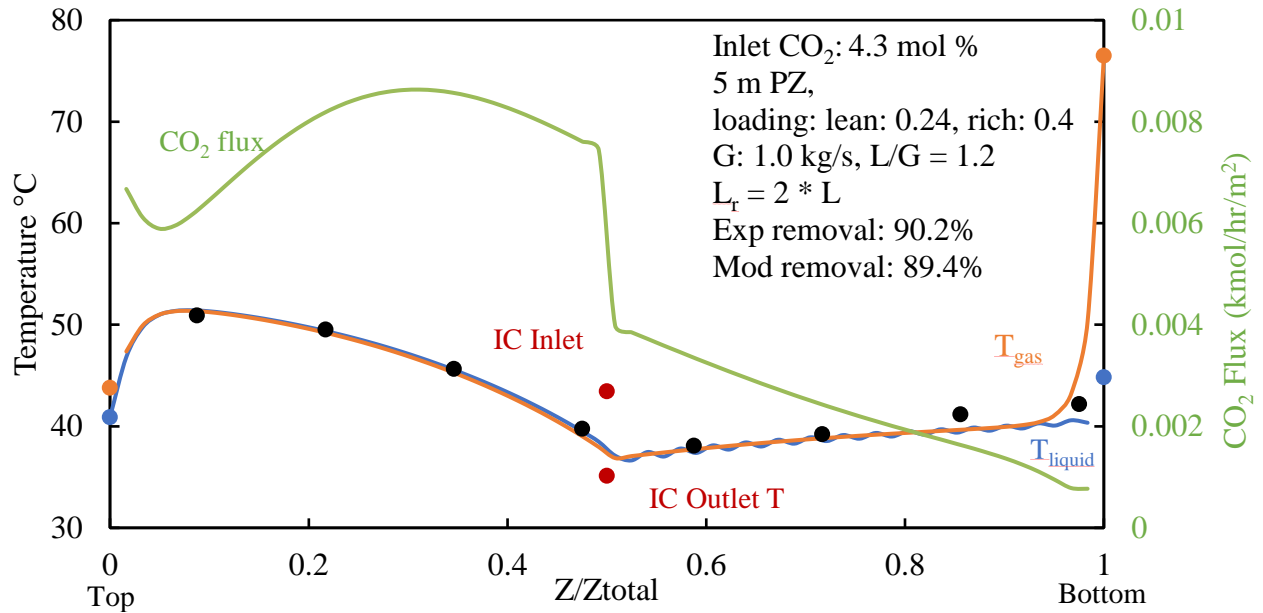


**Figure 9.** Absorber profile for pump-around intercooling and 0.24 lean loading. Temperature measurements (points) and model predictions (curve) are shown on the primary axis; CO<sub>2</sub> transfer flux is shown on the secondary axis.

Generally, a temperature bulge at NGCC conditions tends to occur in the top section, given the low L/G. The maximum temperature is less than 55 °C (near the top), which is much lower than the maximum in coal conditions (about 68 °C near the bottom). At NGCC conditions, the heat generated per volume (or mass) gas is only a third of that at coal conditions; thus, the column temperature is generally lower. This is beneficial because it reduces the solvent equilibrium CO<sub>2</sub> pressure, compensating for the low CO<sub>2</sub> concentration, and increases the rich loading and solvent cyclic capacity.

### 3.3.2. Insights from the model

#### 3.3.2.1. Effect of CO<sub>2</sub> penetration

Along with the validated absorber model, the effects of CO<sub>2</sub> penetration, intercooling, and lean loading are evaluated in this section. At constant lean loading, the delta loading is a direct indicator

of the energy performance. Given fixed CO<sub>2</sub> removal, delta loading is inversely proportional to solvent circulation: the greater delta loading means less solvent, thus less sensitive heat loss through cross exchangers. At greater rich loading, the stripper also performs better because CO<sub>2</sub> can be stripped more easily when the solvent has a greater equilibrium partial pressure. Figure 10 shows the delta loading as a function of penetration for NGCC and coal conditions. The coal conditions were validated with the data from the 2018 NCCC campaign. At 90% removal, the NGCC shows a greater delta loading than coal, even though the CO<sub>2</sub> concentration is three times less. At NGCC conditions, the absorber temperature bulge tends to move to the top and the rich solvent is colder than at coal conditions, which compensates for the low CO<sub>2</sub> partial pressure. Therefore, the energy performance is even better than coal. However, the delta loading at NGCC conditions shows a strong dependence on CO<sub>2</sub> penetration. At low CO<sub>2</sub>, the energy performance is sensitive to removal and the energy penalty is significant at high removal. The NGCC curve starts to bend at 0.024 penetration, where the equilibrium driving force at the lean end is depleted and a higher removal rate becomes impossible. On the other hand, the coal curve is almost flat for penetration between 0.1 to 0.013 and bends at a removal greater than 98%.

The delta loading and energy penalty for high CO<sub>2</sub> removal is less at higher CO<sub>2</sub> concentration. The temperature bulge affects the ability to reach high removal: at NGCC conditions, the temperature bulge moves to the top and it increases the solvent equilibrium partial pressure at the lean end. But for coal, the top section at high removal is cold so it is easier to achieve high removal. If the CO<sub>2</sub> removal for the NGCC and coal capture system were both optimized, the optimal removal at NGCC would be lower than that at coal conditions.

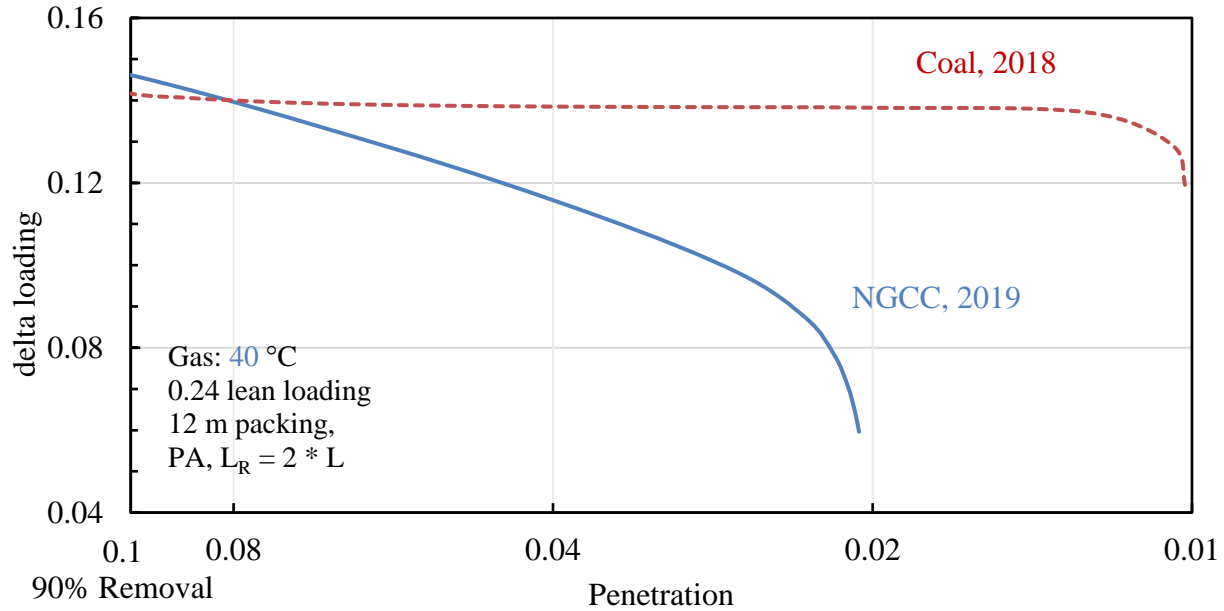


**Figure 10.** Solvent delta loading as a function of CO<sub>2</sub> penetration for absorber with coal<sup>11</sup>(red dashed line, in-and-out) and NGCC (blue solid line, pump-around) flue gas.

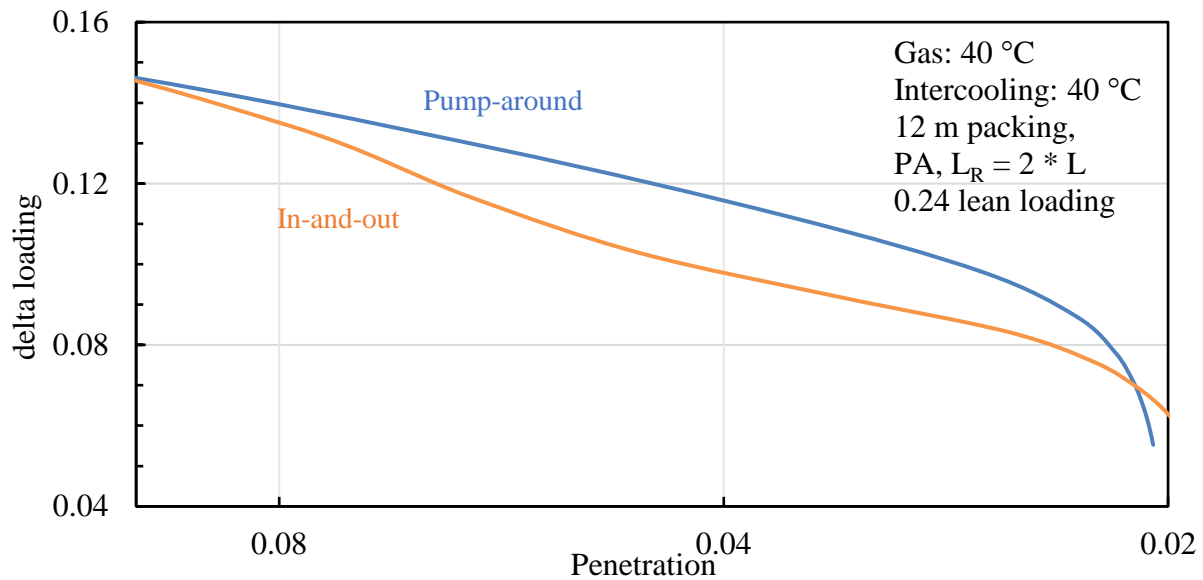


**Figure 11.** Solvent delta loading as a function of CO<sub>2</sub> penetration for pump-around (blue) and in-and-out (orange) intercooling.

### 3.3.2.2. Effect of pump-around and in-and-out intercooling

Pump-around and in-and-out intercooling are compared in Figure 11. At 40 °C gas inlet and intercooling temperature, the delta loading of pump-around intercooling is generally greater than

in-and-out. With enhanced solvent recycle, pump-around is able to cool the rich end and to increase the equilibrium rich loading, except with removal below 90% or greater than 98%. When the removal is low, the bottom of the column is cold because the low L/G leads to a temperature bulge at the top, so the benefits are not significant. At high removal, L/G increases, making cooling by in-and-out sufficient, and the solvent back-mixing caused by pump-around overshadows the cooling effect.

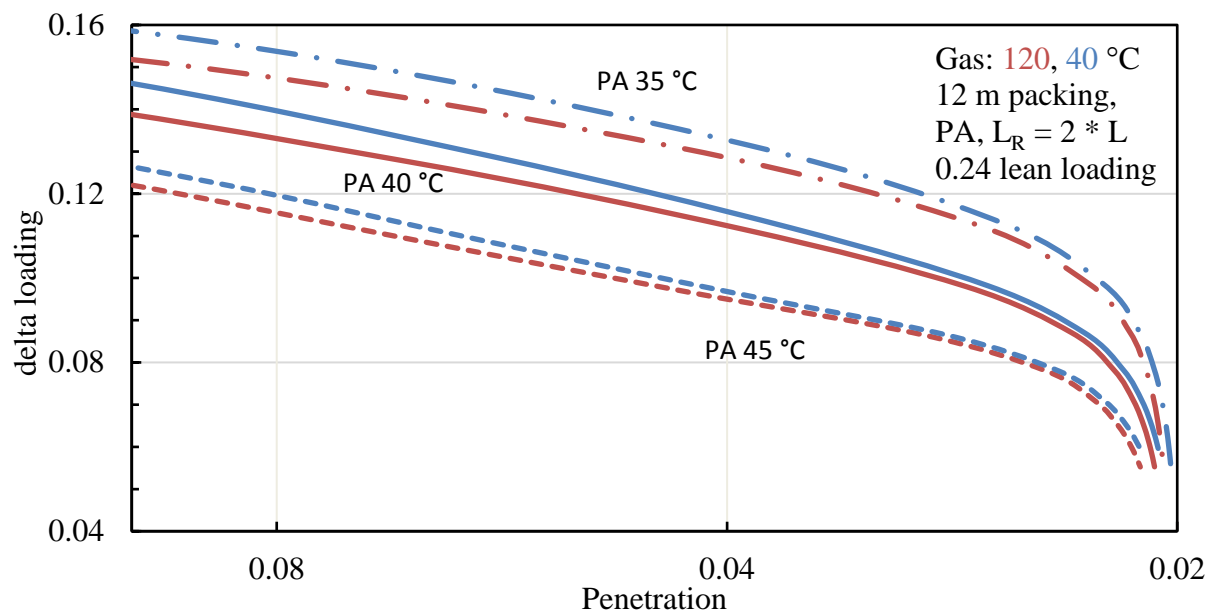


**Figure 12.** Absorber delta loading as a function of CO<sub>2</sub> penetration with pump-around intercooling at 35 °C (dash dot), 40 °C (solid line), and 45 °C (dashed line). Gas feed temperatures are 40 °C (blue) and 120 °C (red).

### 3.3.2.3. Effect of gas temperature and intercooling temperature

The effects of gas feed temperature and intercooling temperature are shown in Figure 12. Two gas temperatures of interest are 40 °C and 120 °C. The 40 °C gas is saturated with water (7 mol %) to represent the DCC upstream and the 120 °C gas contains 8 mol % water as a result of stoichiometry combustion of natural gas. The difference in delta loading between the 40 °C and 120 °C curves therefore represents the delta loading and energy penalty for taking out the DCC column, and it is

less than 5%. This is because the 120 °C case is undersaturated with water and has a low enthalpy. It picks up water in the bottom of the absorber and is cooled quickly. The gas temperature only has a minor effect on the absorber performance. The water balance can also be maintained for the undersaturated flue gas by running the water wash at about 42 °C so that the CO<sub>2</sub> gas leaving the absorber has the same amount of water as the inlet.

The intercooling temperature, on the other hand, affects the absorber significantly. The delta loading can be enhanced by 10% when the intercooling temperature is reduced by 5 °C. The temperature in the bottom section is primarily set by the pump-around temperature and it can dramatically change the equilibrium rich loading. Therefore, running colder is especially beneficial for pump-around intercooling.

#### 3.3.2.4. Effect of lean loading

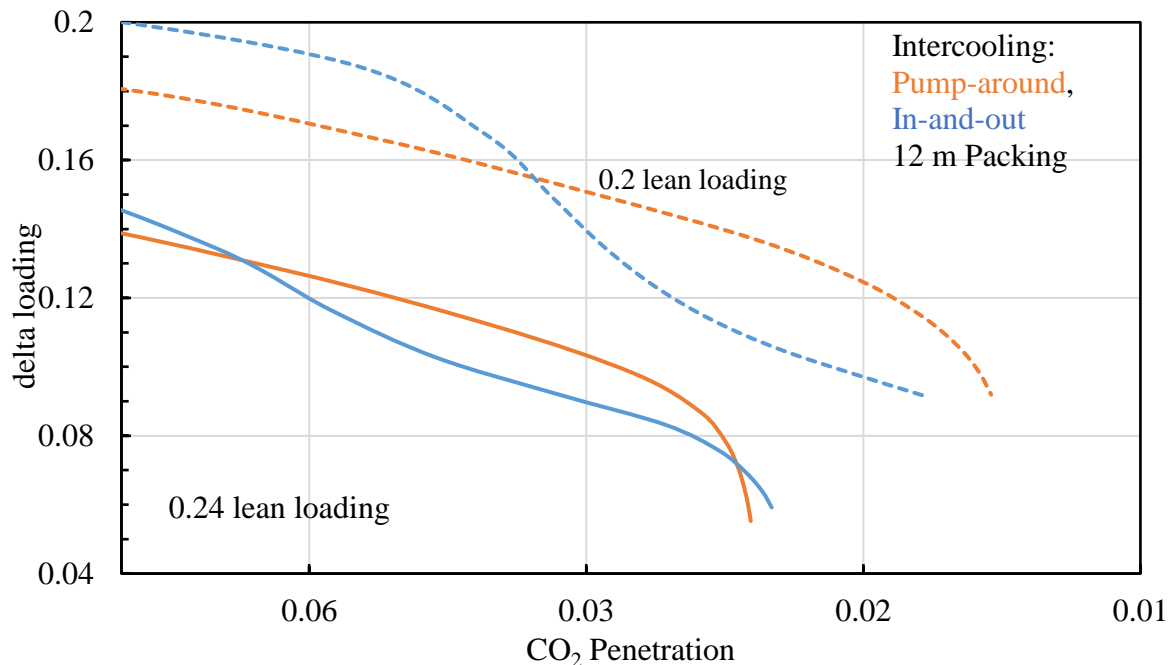


**Figure 13.** Absorber delta loading as a function of CO<sub>2</sub> penetration with pump-around (orange) and in-and-out (blue) intercooling at 0.2 (dashed line) and 0.24 (solid line) lean loadings. The gas feed temperatures for the pump-around and in-and-out are 120 and 40 °C.

Figure 13 shows the absorber performance at 0.2 and 0.24 lean loading for both in-and-out and pump-around intercooling. The rich loading for pump-around cases is about the same and the lower lean loading increases the solvent capacity by about 30%. The lower lean loading also leads to a greater maximum removal because it provides greater CO<sub>2</sub> transfer driving force at the lean end. At low lean loading, in-and-out performance is better than pump-around because the temperature bulge moves to the absorber top at this low L/G condition and the extra cooling at the bottom becomes marginal. The energy consumption for getting lower lean loading is greater because more water vapor will be stripped out, but the advanced stripper is capable of recovering the heat from water vapor in the stripper overhead. For PZ, operating at low lean loading could be risky because of solid precipitation, but during the 2018 and 2019 campaigns, the system was operated at a lean loading of 0.19 without precipitation.

#### 4. Conclusion

A rigorous PZ absorber model has been validated using the steady-state data from the NCCC 2019 campaign at NGCC conditions. The operating conditions included lean loading (0.19–0.25 m CO<sub>2</sub>/mol alkalinity), gas temperature (40, 76 °C), and intercooling temperature (35, 40 °C). With 12 m of packing and intercooling, CO<sub>2</sub> removal from 82% to 96% was achieved using 5 m PZ. The model is able to predict the absorber NTU and temperature profile accurately for both in-and-out and pump-around intercooling.

1. The delta loading at NGCC conditions for 90% removal is greater than the coal conditions although the CO<sub>2</sub> concentration is lower. This is because of low temperature in the absorber, especially the bottom, and it is low for two reasons:
  - a. At low CO<sub>2</sub> concentration, there is less heat generated per mass gas, so the magnitude of the temperature bulge is smaller.
  - b. At low L/G, gas tends to push the heat to the top of the column, so the bottom remains cold, which reduces the solvent equilibrium CO<sub>2</sub> partial pressure and increases the rich loading.
2. At NGCC conditions, high CO<sub>2</sub> removal leads to a greater penalty in the delta loading compared to coal conditions. The CO<sub>2</sub> transfer driving force will be depleted at the lean end because of the low CO<sub>2</sub> partial pressure and the high temperature.
3. Pump-around intercooling is almost always better than in-and-out at NGCC conditions because it cools the gas effectively with an enhanced solvent flow. With pump-around intercooling, the delta loading penalty for removing the DCC column is less than 5%.
4. At NGCC conditions, the absorber bottom temperature is dominated by the intercooling temperature and lowering that temperature can improve the performance dramatically: reducing the intercooling temperature by 5 °C increases the delta loading by 10%.

Because of the low CO<sub>2</sub> concentration and high gas rate at NGCC conditions, the absorber dominates the total capital cost of the capture plant. With a fast solvent such as PZ, the absorber performance is not degraded at low CO<sub>2</sub> concentration because the column can be cooled effectively with intercooling. Therefore, PZ is excellent for the NGCC application because it reduces the packing requirements and the absorber cost.

## ACKNOWLEDGMENT

Financial support was provided by the CO<sub>2</sub> Capture Project and the U.S. Department of Energy, Office of Fossil Energy through the CCSI<sup>2</sup> project (Carbon Capture Simulation for Industry Impact) (subcontract 318779 with Los Alamos National Laboratory). Aspen Plus<sup>®</sup> proprietary software was provided by an academic license from AspenTech<sup>®</sup>. AspenTech<sup>®</sup> and Aspen Plus<sup>®</sup> are trademarks of Aspen Technology, Inc. All rights reserved.

Operational support for the pilot plant was provided by the team of the National Carbon Capture Center of Southern Company.

## REFERENCES

1. EPA *Inventory of U.S. Greenhouse Gas Emissions and Sinks*; 2019.
2. Frailie, P. T. Modeling of Carbon Dioxide Absorption/Stripping by Aqueous Methyl-diethanolamine/Piperazine. Ph.D. Dissertation., The University of Texas at Austin, 2014.
3. Sachde, D.; Chen, E.; Rochelle, G. T., Modeling Pilot Plant Performance of an Absorber with Aqueous Piperazine. *Energy Proc* **2013**, *37*, 1987-2001.
4. Rochelle, G. T.; Chen, E.; Freeman, S.; Van Wagener, D.; Xu, Q.; Voice, A., Aqueous piperazine as the new standard for CO<sub>2</sub> capture technology. *Chem. Eng. J.* **2011**, *171* (3), 725-733.
5. Chen, E.; Fulk, S.; Sache, D.; Lin, Y.; Rochelle, G. T., Pilot Plant Activities with Concentrated Piperazine. *Energy Proc* **2014**, *63*, 1376-1391.
6. Zhang, Y.; Sachde, D.; Chen, E.; Rochelle, G., Modeling of absorber pilot plant performance for CO<sub>2</sub> capture with aqueous piperazine. *Int. J. Greenh. Gas Con.* **2017**, *64*, 300-313.
7. Pun, B.; Jadhav, R.; Selinger, J.; Rochelle, G. In *Advancing CO<sub>2</sub> Capture from Natural Gas Combined Cycle with Piperazine Scrubbing*, 14th Greenhouse Gas Control Technologies Conference Melbourne, 2018; pp 21-26.
8. Lin, Y.-J.; Chen, E.; Rochelle, G. T., Pilot plant test of the advanced flash stripper for CO<sub>2</sub> capture. *Faraday Discuss.* **2016**, *192*, 37-58.
9. Zhang, Y. Absorber and Aerosol Modeling in Amine Scrubbing for Carbon Capture. Ph.D. Dissertation, The University of Texas at Austin, 2018.
10. Rochelle, G. T.; Wu, Y.; Chen, E.; Akinpelumi, K.; Fischer, K. B.; Gao, T.; Liu, C.-T.; Selinger, J. L., Pilot plant demonstration of piperazine with the advanced flash stripper. *Int. J. Greenh. Gas Con.* **2019**, *84*, 72-81.
11. Gao, T.; Selinger, J. L.; Rochelle, G. T., Demonstration of 99% CO<sub>2</sub> removal from coal flue gas by amine scrubbing. *Int. J. Greenh. Gas Con.* **2019**, *83*, 236-244.
12. Morgan, J. C.; Soares Chinen, A.; Omell, B.; Bhattacharyya, D.; Tong, C.; Miller, D. C.; Buschle, B.; Lucquiaud, M., Development of a Rigorous Modeling Framework for Solvent-Based CO<sub>2</sub> Capture. Part 2: Steady-State Validation and Uncertainty Quantification with Pilot Plant Data. *Industrial & Engineering Chemistry Research* **2018**, *57* (31), 10464-10481.
13. *Cansolv Testing of Cansolv DC-201 CO<sub>2</sub> Capture System with Simulated Natural Gas Testing*; 2015.
14. Sachde, D.; Rochelle, G. T., Absorber Intercooling Configurations using Aqueous Piperazine for Capture from Sources with 4 to 27% CO<sub>2</sub>. *Energy Proc* **2014**, *63*, 1637-1656.
15. Zhang, Y.; Freeman, B.; Hao, P.; Rochelle, G. T., Absorber modeling for NGCC carbon capture with aqueous piperazine. *Faraday Discuss.* **2016**, *192*, 459-477.
16. Reddy, S.; Gilmartin, J. In *Fluor's Econamine FG PlusSM Technology for Post Combustion CO<sub>2</sub> Capture*, GPA Gas Treatment Conference, Amsterdam, The Netherlands, 2008.
17. Song, D. Effect of Liquid Viscosity on Liquid Film Mass Transfer for Packings. Ph.D. Dissertation, The University of Texas at Austin, 2017.
18. NETL *Cost and Performance Baseline for Fossil Energy Plants Volume 1a: Bituminous Coal (PC) and Natural Gas to Electricity Revision 3*; 2015.
19. Yasuhide Nakagamia; Takashi Nojoa; Takuya Hiratab; Tatsuya Tsujiuchib; Takashi Kamijoc; Shinya Kishimotoc; Kawasakic, S. In *Near-Zero Emission Thermal Power Plant using*

*Advanced KM CDR Process<sup>TM</sup>*, Post Combustion Capture Conference 5, Kyoto, Japan, Kyoto, Japan, 2019.

## Appendix: Experimental Runs

Run	Gas Inlet T	Gas Outlet T	Solvent Inlet T	Solvent Outlet T	Intercooling (IC)	IC 1 Inlet T	IC 1 Outlet T	IC 1 flow
	°C	°C	°C	°C		°C	°C	* 10 <sup>-3</sup> m <sup>3</sup> /s
1	40.1	47.9	41.1	43.7	IO			
2	40.1	47.8	40.9	43.3	IO			
3	39.9	48.0	40.9	43.7	IO			
4	40.0	46.5	41.0	44.9	IO			
5	39.9	45.4	41.0	45.0	IO			
6	39.9	44.8	40.8	44.1	IO			
7	40.0	44.8	40.7	44.3	IO			
8	40.0	44.4	40.7	43.8	IO			
9	39.9	44.6	40.3	38.5	IO			
10	40.0	47.4	41.7	50.9	PA	42.7	40.1	1.17
11	40.0	43.1	41.4	49.7	PA	45.0	40.1	1.17
12	39.7	45.9	41.0	47.6	PA	44.8	40.0	1.39
13	39.9	46.1	41.3	44.4	PA	41.4	38.1	1.39
14	40.5	44.1	40.9	45.1	PA	43.7	40.0	1.39
15	39.9	43.3	40.7	45.3	PA	43.9	39.9	1.39
16	75.7	45.2	41.1	45.2	PA	43.5	40.1	1.13
17	75.8	41.5	41.1	46.6	PA	45.1	40.0	1.14
18	76.6	43.2	41.0	46.2	PA	44.7	40.0	1.14
19	73.9	43.2	40.9	48.3	PA	47.1	40.0	0.55
20	83.0	40.2	40.5	49.5	PA	48.1	40.0	1.38
21	82.7	41.4	40.5	48.8	PA	47.6	40.1	1.39
22	82.6	41.9	40.6	47.6	PA	46.3	40.0	1.39
23	80.0	44.0	40.7	46.3	PA	45.7	40.0	1.39
24	80.4	42.4	40.7	46.2	PA	45.6	40.0	1.38
25	79.6	42.4	40.7	46.4	PA	45.8	39.9	1.39
26	77.9	42.5	40.6	46.6	PA	45.8	40.0	1.38
27	76.8	41.6	40.8	46.1	PA	45.4	40.0	1.39
28	75.8	41.4	40.7	45.2	PA	44.7	40.0	1.39
29	78.8	52.8	53.5	47.1	PA	45.6	42.6	1.10
30	77.8	42.5	40.7	47.0	PA	45.2	34.9	1.09
31	79.1	44.0	40.8	46.2	PA	44.1	35.0	1.07
32	78.2	43.5	40.8	46.3	PA	44.3	34.9	1.13
33	78.9	43.9	40.7	46.3	PA	44.2	35.0	1.13
34	78.5	43.5	40.8	46.7	PA	44.6	34.9	1.13
35	76.0	43.0	41.0	43.8	PA	42.3	35.0	1.14
36	79.1	43.7	41.0	45.1	PA	43.1	34.9	1.14
37	77.4	43.4	40.8	45.4	PA	43.4	35.1	1.14

38	77.9	43.6	40.8	46.1	PA	44.0	34.9	1.15
39	76.9	43.3	41.0	45.8	PA	44.1	34.9	1.14
40	74.9	43.2	40.9	43.7	PA	41.7	35.1	1.17
41	76.0	43.5	40.9	44.1	PA	42.1	35.0	1.18
42	76.5	43.8	40.9	44.8	PA	42.9	34.9	1.18
43	77.6	43.8	40.8	46.0	PA	44.1	35.0	1.16
44	77.9	45.4	40.7	46.0	PA	43.8	35.0	1.18
45	78.4	44.1	40.7	46.6	PA	44.3	35.1	1.16
46	78.2	50.4	40.7	46.6	PA	44.4	35.1	1.17
47	78.3	46.1	40.7	46.5	PA	44.3	35.1	1.17
48	77.2	43.9	40.9	45.9	PA	43.8	35.0	1.19
49	77.5	44.2	40.8	45.4	PA	43.4	35.0	1.18
50	77.4	43.9	40.7	46.3	PA	44.1	35.1	1.13
51	77.7	45.7	40.7	46.6	PA	44.5	35.0	1.11
52	78.3	43.8	40.8	46.8	PA	44.8	35.0	1.11
53	77.7	44.0	40.7	46.2	PA	44.3	35.1	1.12
54	78.8	45.4	40.8	46.7	PA	44.6	35.0	1.15
55	78.4	43.3	40.8	46.3	PA	44.2	34.9	1.15
56	78.3	44.0	40.8	46.1	PA	44.0	35.0	1.16
57	77.5	43.8	40.8	45.1	PA	43.2	35.0	1.13
58	76.4	43.8	40.7	45.1	PA	43.9	34.9	1.00
59	76.9	44.3	40.6	45.7	PA	44.3	34.9	1.08
60	76.3	44.2	40.7	45.7	PA	44.2	35.0	1.07
61	76.7	44.8	40.7	45.9	PA	44.2	34.9	1.11
62	77.1	44.5	40.7	45.8	PA	44.0	34.9	1.13
63	77.2	44.7	40.7	45.8	PA	44.0	35.0	1.13
64	77.7	51.3	40.7	46.4	PA	44.6	35.1	1.13
65	77.5	45.0	40.7	45.8	PA	44.0	35.1	1.14
66	77.4	45.1	40.8	45.8	PA	44.0	34.9	1.13
67	77.8	45.0	40.7	46.6	PA	44.8	35.1	1.13
68	77.9	45.3	40.5	46.5	PA	44.7	34.9	1.13
69	77.3	45.9	40.7	46.4	PA	44.5	34.9	1.13
70	77.7	45.4	40.5	46.5	PA	44.6	35.0	1.13
71	77.6	46.1	40.6	46.0	PA	44.1	35.0	1.14
72	77.4	44.9	40.6	45.9	PA	44.1	35.0	1.13
73	78.1	44.9	40.6	45.8	PA	44.2	35.0	1.13
74	78.0	45.5	40.5	45.9	PA	44.0	35.0	1.13
75	77.8	45.5	40.6	45.5	PA	43.4	35.1	1.13
76	77.8	45.6	40.6	45.6	PA	43.7	35.0	1.13
77	78.0	45.6	40.7	45.9	PA	43.9	35.0	1.14
78	77.1	45.3	40.5	45.0	PA	43.2	35.0	1.13
79	77.9	45.6	40.6	45.6	PA	43.4	34.9	1.13
80	78.1	45.2	41.0	48.7	PA	47.6	35.1	1.14

Continued

Runs	IC 2 Inlet T	IC 2 Outlet T	IC 2 Flow	Solvent Inlet	Solvent Outlet	Gas Inlet	Gas Outlet	CO <sub>2</sub> Inlet	CO <sub>2</sub> Outlet
	°C	°C	* 10 <sup>-3</sup> m <sup>3</sup> /s	kg/s	kg/s	kg/s	kg/s	dry mol%	dry mol%
1	42.3	38.7	0.64	0.80	0.82	0.82	0.78	4.31	0.61
2	43.1	40.0	0.89	1.05	1.06	1.01	0.96	4.32	0.53
3	43.3	39.9	0.91	1.01	1.06	1.01	0.97	4.30	0.53
4	44.1	40.0	0.75	0.86	0.88	0.63	0.60	4.28	0.65
5	45.9	39.9	0.77	0.91	0.94	0.63	0.60	4.28	0.38
6	46.9	39.9	1.45	1.60	1.64	1.01	0.96	4.31	0.40
7	47.1	40.1	1.45	1.60	1.64	1.01	0.96	4.34	0.31
8	46.9	40.0	1.45	1.61	1.64	1.01	0.97	4.30	0.38
9	46.4	39.8	1.09	1.62	1.64	1.01	0.96	4.31	0.43
10	42.8	39.9	1.17	0.61	0.63	0.63	0.61	4.31	0.27
11	44.9	40.1	1.16	0.93	0.95	0.63	0.60	4.31	0.18
12				1.28	1.31	1.01	0.95	4.33	0.25
13	41.4	39.3	1.39	1.05	1.07	1.01	0.97	4.30	0.65
14	43.6	40.0	1.39	1.38	1.41	1.01	0.96	4.00	0.60
15	43.8	39.9	1.39	1.37	1.41	1.01	0.97	3.99	0.36
16	43.5	40.0	1.13	0.84	0.84	0.63	0.61	4.31	0.47
17	45.0	40.0	1.14	1.07	1.07	0.63	0.60	4.30	0.19
18	44.6	40.1	1.13	0.97	0.97	0.63	0.60	4.30	0.24
19	46.9	39.9	0.58	1.04	1.05	0.63	0.60	4.29	0.24
20	48.0	40.1	1.38	1.77	1.81	1.01	0.96	4.31	0.20
21	47.5	40.0	1.39	1.58	1.64	1.01	0.97	4.31	0.25
22	46.2	40.0	1.38	1.61	1.64	1.01	0.97	4.34	0.28
23	45.6	39.9	1.39	1.49	1.51	1.01	0.99	4.29	0.24
24	45.6	40.1	1.39	1.49	1.51	1.01	0.99	4.31	0.23
25	45.7	40.1	1.39	1.48	1.51	1.01	0.99	4.31	0.22
26	45.8	40.0	1.39	1.48	1.51	1.01	0.98	4.30	0.23
27	45.4	39.9	1.39	1.48	1.51	1.01	0.98	4.33	0.21
28	44.7	40.0	1.39	1.48	1.51	1.01	0.99	4.30	0.21
29	45.5	43.5	1.13	1.49	1.52	1.01	1.05	4.32	0.88
30	45.0	34.9	1.13	1.34	1.39	1.01	0.98	4.32	0.29
31	44.1	35.0	1.14	1.23	1.26	1.01	1.00	4.31	0.45
32	44.2	35.1	1.13	1.25	1.26	1.01	0.98	4.27	0.42
33	44.1	34.9	1.13	1.24	1.26	1.01	0.98	4.31	0.44
34	44.4	34.9	1.13	1.24	1.26	1.01	0.98	4.31	0.44
35	42.2	35.1	1.13	1.24	1.26	1.01	0.99	4.31	0.45
36	43.1	35.0	1.14	1.25	1.26	1.01	0.98	4.30	0.45
37	43.3	35.0	1.13	1.25	1.26	1.01	0.97	4.31	0.46
38	43.9	34.9	1.13	1.25	1.26	1.01	0.97	4.31	0.45

39	43.9	34.9	1.14	1.20	1.26	1.01	0.97	4.26	0.42
40	41.8	35.1	1.13	1.24	1.26	1.01	0.99	4.33	0.46
41	42.1	34.9	1.13	1.25	1.26	1.01	0.98	4.30	0.45
42	42.8	35.0	1.13	1.25	1.26	1.01	0.98	4.34	0.44
43	44.0	34.9	1.12	1.22	1.26	1.01	0.97	4.35	0.45
44	43.9	34.9	1.13	1.22	1.26	1.01	0.97	4.32	0.49
45	44.1	35.0	1.13	1.22	1.26	1.01	0.97	4.30	0.51
46	44.3	35.0	1.13	1.22	1.26	1.01	0.97	4.31	0.43
47	44.2	34.9	1.13	1.22	1.26	1.01	0.97	4.33	0.48
48	43.6	35.1	1.14	1.21	1.26	1.01	0.99	4.31	0.50
49	43.2	35.0	1.13	1.23	1.26	1.01	0.97	4.30	0.49
50	44.1	35.0	1.13	1.23	1.26	1.01	0.97	4.29	0.44
51	44.3	35.0	1.13	1.23	1.26	1.01	0.97	4.32	0.45
52	44.5	35.0	1.13	1.23	1.26	1.01	0.96	4.32	0.45
53	44.1	35.0	1.13	1.22	1.26	1.01	0.97	4.33	0.46
54	44.5	35.1	1.14	1.22	1.26	1.01	0.97	4.31	0.48
55	44.0	34.9	1.13	1.21	1.26	1.01	0.98	4.31	0.48
56	43.9	35.0	1.13	1.22	1.26	1.01	0.98	4.32	0.49
57	43.1	35.0	1.13	1.24	1.26	1.01	0.99	4.32	0.47
58	43.6	35.0	1.14	1.23	1.26	1.01	0.99	4.31	0.46
59	44.1	35.1	1.13	1.22	1.26	1.01	0.98	4.33	0.42
60	43.8	35.0	1.13	1.21	1.26	1.01	0.98	4.34	0.44
61	44.1	35.1	1.13	1.21	1.26	1.01	0.97	4.33	0.42
62	43.8	35.1	1.13	1.22	1.26	1.01	0.97	4.33	0.41
63	43.9	35.0	1.13	1.23	1.26	1.01	0.97	4.32	0.42
64	44.4	35.0	1.13	1.22	1.26	1.01	0.97	4.31	0.43
65	43.8	35.0	1.13	1.23	1.26	1.01	0.97	4.30	0.44
66	43.7	35.0	1.13	1.23	1.26	1.01	0.97	4.31	0.43
67	44.6	35.2	1.13	1.22	1.26	1.01	0.97	4.30	0.42
68	44.4	34.8	1.14	1.22	1.26	1.01	0.97	4.32	0.46
69	44.2	34.9	1.13	1.22	1.26	1.01	0.97	4.33	0.45
70	44.4	35.0	1.13	1.22	1.26	1.01	0.96	4.34	0.46
71	43.8	34.9	1.13	1.22	1.26	1.01	0.97	4.32	0.49
72	43.7	35.0	1.13	1.23	1.26	1.01	0.97	4.30	0.47
73	43.8	35.0	1.13	1.22	1.26	1.01	0.99	4.33	0.46
74	43.9	35.0	1.13	1.22	1.26	1.01	0.98	4.31	0.47
75	43.3	35.0	1.14	1.23	1.26	1.01	0.99	4.32	0.48
76	43.4	35.0	1.14	1.23	1.26	1.01	0.99	4.33	0.47
77	43.8	35.1	1.13	1.23	1.26	1.01	0.98	4.31	0.48
78	43.0	34.9	1.14	1.24	1.26	1.01	0.98	4.32	0.48
79	43.2	35.0	1.13	1.23	1.26	1.01	0.98	4.32	0.48
80	47.4	35.2	1.13	1.21	1.26	1.01	0.95	4.19	0.39

Continued

Runs	CO <sub>2</sub> Production	PZ Molality	Lean Loading	Rich Loading	Removal
	kg/s	m	m/equiv	m/equiv	%
1	0.042	4.2	0.197	0.407	86.0
2	0.051	4.1	0.195	0.402	87.8
3	0.051	4.0	0.186	0.402	87.6
4	0.032	4.2	0.233	0.399	84.8
5	0.034	4.3	0.241	0.396	91.1
6	0.055	4.2	0.241	0.384	90.7
7	0.057	4.4	0.234	0.384	92.7
8	0.056	4.4	0.239	0.384	91.3
9	0.055	4.2	0.242	0.386	89.9
10	0.036	5.4	0.198	0.409	93.8
11	0.040	5.6	0.228	0.388	95.8
12	0.052	4.9	0.215	0.379	94.2
13	0.047	4.6	0.215	0.405	85.0
14	0.050	4.9	0.254	0.393	84.9
15	0.048	4.8	0.250	0.385	91.1
16	0.029	4.8	0.251	0.399	89.2
17	0.036	4.9	0.248	0.378	95.5
18	0.035	4.9	0.246	0.388	94.3
19	0.036	5.0	0.246	0.375	94.3
20	0.058	5.0	0.249	0.364	95.3
21	0.054	5.1	0.246	0.372	94.3
22	0.055	5.0	0.248	0.376	93.5
23	0.056	4.9	0.239	0.381	94.3
24	0.054	5.0	0.238	0.379	94.8
25	0.054	5.0	0.238	0.381	94.8
26	0.055	5.1	0.233	0.381	94.7
27	0.053	5.0	0.239	0.374	95.1
28	0.050	4.9	0.246	0.377	95.0
29	0.049	3.5	0.231	0.383	79.7
30	0.056	5.4	0.250	0.391	93.2
31	0.056	5.4	0.237	0.401	89.6
32	0.055	5.3	0.245	0.400	90.1
33	0.054	5.2	0.242	0.400	89.8
34	0.056	5.2	0.240	0.401	89.7
35	0.051	5.0	0.251	0.403	89.5
36	0.052	5.1	0.243	0.402	89.5
37	0.054	5.1	0.247	0.402	89.2
38	0.055	5.2	0.241	0.402	89.6

39	0.054	5.2	0.248	0.401	90.1
40	0.052	5.0	0.251	0.404	89.5
41	0.052	5.0	0.244	0.403	89.6
42	0.053	5.1	0.244	0.402	89.7
43	0.054	5.1	0.249	0.401	89.6
44	0.053	5.0	0.242	0.403	88.6
45	0.055	5.1	0.243	0.402	88.1
46	0.054	5.1	0.244	0.399	90.0
47	0.054	5.0	0.240	0.402	88.9
48	0.054	5.0	0.243	0.404	88.5
49	0.054	4.9	0.246	0.404	88.5
50	0.054	5.1	0.244	0.401	89.7
51	0.054	5.1	0.242	0.401	89.6
52	0.055	5.1	0.242	0.400	89.6
53	0.054	5.1	0.239	0.401	89.3
54	0.055	5.0	0.241	0.403	88.8
55	0.057	5.0	0.242	0.403	88.8
56	0.056	5.0	0.248	0.403	88.5
57	0.055	4.9	0.245	0.401	89.2
58	0.055	5.2	0.237	0.402	89.4
59	0.056	5.1	0.235	0.401	90.3
60	0.057	5.1	0.235	0.406	89.8
61	0.058	5.0	0.236	0.406	90.3
62	0.059	5.0	0.235	0.406	90.5
63	0.059	5.0	0.232	0.407	90.3
64	0.059	5.0	0.230	0.408	90.0
65	0.059	4.9	0.235	0.409	89.8
66	0.058	4.9	0.231	0.408	90.0
67	0.058	4.8	0.245	0.407	90.2
68	0.059	4.8	0.232	0.408	89.4
69	0.059	4.8	0.232	0.409	89.6
70	0.059	4.8	0.232	0.408	89.4
71	0.059	4.8	0.232	0.410	88.5
72	0.058	4.7	0.234	0.409	89.2
73	0.060	4.7	0.235	0.408	89.3
74	0.058	4.7	0.231	0.409	89.2
75	0.058	4.7	0.232	0.409	88.9
76	0.057	4.7	0.234	0.407	89.1
77	0.057	4.7	0.234	0.409	88.8
78	0.057	4.6	0.242	0.409	88.9
79	0.057	4.7	0.232	0.409	88.8
80	0.055	4.6	0.237	0.403	90.6

# Corrosion by Aqueous Piperazine at 40–150 °C in Pilot Testing of CO<sub>2</sub> Capture

*Ching-Ting Liu, Kent B. Fischer, and Gary T. Rochelle\**

The University of Texas at Austin, McKetta Department of Chemical Engineering, 200 E Dean  
Keeton St. Stop C0400, Austin, TX 78712, USA.

## Abstract

Corrosion data are presented from two pilot plant campaigns for CO<sub>2</sub> capture with 5 m (30 wt %) aqueous piperazine (PZ) and the Advanced Stripper (the PZAS<sup>TM</sup> process). 316L stainless steel experienced high corrosion at high temperature, and the corrosion rate showed strong dependence on temperature. PZ degradation also increased 316L corrosion. 304 stainless steel and 2205 duplex stainless steel performed well at all temperatures and can be good alternative construction materials for PZAS<sup>TM</sup>. Stagnant fluid in the sumps allowed for the formation of compact, protective films on carbon steel while high-velocity flow seemed to inhibit such film formation. Selective dissolution of Ni from Ni-based alloys into PZ occurred in narrow gaps between alloy and washers. Such localized corrosion can make these alloys not ideal at the joints in piping.

## 1. Introduction

Significant reduction in CO<sub>2</sub> emissions is necessary to prevent the worst effects of climate change. Post-combustion carbon capture (PCCC) removes CO<sub>2</sub> from power plant flue gas, so it can be permanently sequestered underground. Among the CCS technologies, post-combustion carbon capture (PCCC) with amine scrubbing is one of the most promising; it is a mature technology that can be deployed quickly enough to achieve ambitious CO<sub>2</sub> emission reduction targets.<sup>1-3</sup> Careful solvent selection and process optimization has improved the energy performance of the amine-scrubbing process. A process using 30 wt % aqueous piperazine (PZ) with the Advanced Stripper (PZAS™) has been demonstrated to have significant energy benefits compared to systems using the first-generation, benchmark solvent, monoethanolamine (MEA).<sup>4</sup> One reason for the better energy performance of PZ is that it has greater thermal stability and can be regenerated at 160 °C and elevated pressure, thus saving compression energy to reach pipeline pressure for injection. Despite these advances, cost is still the main obstacle to commercial implementation of PCCC.<sup>5</sup>

Reducing plant capital costs will be a crucial way to reduce the cost and to promote widespread deployment of PCCC. Capital cost is largely affected by the selection of construction materials, in which appropriate corrosion performance of materials is often a major consideration. Improving understanding of corrosion in PCCC plants will allow for optimal choices of construction materials to balance capital costs and the maintenance cost for corroded equipment.

Current corrosion data for amine-scrubbing processes are mostly for MEA, while some research has shown that several second-generation solvents such as PZ are intrinsically less corrosive.<sup>6,7</sup> Research has also demonstrated that carbon steel can be protected by a siderite (FeCO<sub>3</sub>) film in PZ<sup>8-10</sup> and that such protective films do not form in MEA at comparable conditions,<sup>8,11</sup> except at very high CO<sub>2</sub> loading<sup>12</sup> or at strictly controlled pH.<sup>13</sup> However, bench-scale work has shown that

the protection could fail when the concentration of ethylenediamine (EDA), which is a major degradation product of PZ, in the solvent increased to a critical value.<sup>10</sup> This suggests solvent degradation has an important effect on carbon steel corrosion in a PZ unit. Due to the complicated pathways of PZ degradation, which are not easy to replicate at bench-scale, the effect of PZ degradation on corrosion needs to be studied at fully representative pilot plant conditions.

Most of the current PCCC pilot plants are constructed with stainless steel with the assumption, based on previous experience with MEA, that stainless steel is always passivated at operating conditions. Although stainless steel has been suggested as a substitute for carbon steel on the regeneration side of the PCCC process,<sup>14</sup> most data for stainless steel corrosion in amines are available at temperatures only up to 135 °C<sup>15,16</sup>, mostly below 80 °C.<sup>17-19</sup> A bench-scale study demonstrated that stainless steel can be attacked at high temperature, O<sub>2</sub>-depleted conditions in PZ at 150 °C,<sup>20</sup> although the study environment may have been more reducing and corrosive than a real plant. The lack of high temperature measurements and the limited investigation of stainless steel behavior in second generation amines means that measuring stainless steel corrosion in a pilot PZ system is critical to improving the PZAS<sup>TM</sup> process.

Corrosion in amine units for CO<sub>2</sub> capture has been measured at several pilot plants.<sup>17,21-26</sup> These studies all investigated MEA, and as a consequence are typically limited to operation at 120 °C. To date there are limited published data on pilot scale corrosion in second generation solvents. To fill up the knowledge gap, corrosion measurements were made in two pilot plant campaigns, one in 2018 and the other in 2019, at the National Carbon Capture Center (NCCC) in Wilsonville, AL.

Corrosion was evaluated at the NCCC pilot plant between February and August 2018 (the 2018 campaign). This campaign captured CO<sub>2</sub> from a 0.6 MWe equivalent coal flue gas starting with fresh 5 m (30 wt %) aqueous PZ. The pilot unit used a conventional absorber and an advanced

stripper configuration. Detailed operating conditions and corrosion measurements have been published.<sup>4,26–28</sup>

Corrosion was also evaluated at NCCC between February and June 2019. During this campaign (the 2019 campaign), the pilot unit operated with a synthetic flue gas composed of coal flue gas and air to simulate the CO<sub>2</sub> concentration in the flue gas at natural gas combined cycle (NGCC) conditions. The NGCC flue gas contained 4.3% CO<sub>2</sub> and 15% O<sub>2</sub>. The solvent was the inventory of 5 m PZ retained from the 2018 campaign.

## 2. Experimental Methods

### 2.1 Corrosion coupons

Corrosion coupons were used to evaluate corrosion at the NCCC pilot plant by weight loss measurement and to characterize the corrosion products. Coupons were mounted in the pipes and equipment and exposed to process conditions for 1 to 4 weeks. Once removed, coupons were rinsed with deionized H<sub>2</sub>O, dried, weighed, and then imaged by a FEI Quanta 650 scanning electron microscope (SEM). Energy-dispersive X-ray spectroscopy (EDS) mapping was also performed using a Bruker EDS system integrated into the FEI Quanta 650. Afterward, any corrosion product was scraped off and analyzed by powder X-Ray diffraction (XRD) using a Rigaku R-Axis Spider instrument with a Cu tube source. Any residual corrosion product was removed using concentrated HCl inhibited with N, N'-Dibutylthiourea, and a final weight loss was calculated. Corrosion rates were calculated based on these weight loss measurements.

### 2.2 NCCC corrosion measurement locations

Corrosion measurements were made in both campaigns at the 10 locations shown in Figure 1. In the absorber system, coupons were installed at 5 locations, including in the absorber sump, between packing sections one and two, between packing sections two and three, at the absorber

top, and in the cold lean solvent pipe. In the Advanced Stripper (AS), coupon measurements were made at 5 locations, including the cold rich bypass, the warm rich bypass, the hot rich stream, the hot lean stream, and the stripper sump. C1010 carbon steel, 304 stainless steel, and 316L stainless steel were evaluated in the 2018 campaign. During the 2019 campaign, in addition to the carbon and stainless steels, several higher-grade alloys, including 2205 duplex stainless steel, Hastelloy<sup>®</sup> C276, and Inconel<sup>®</sup> 625 (I625) were evaluated in the Advanced Stripper.

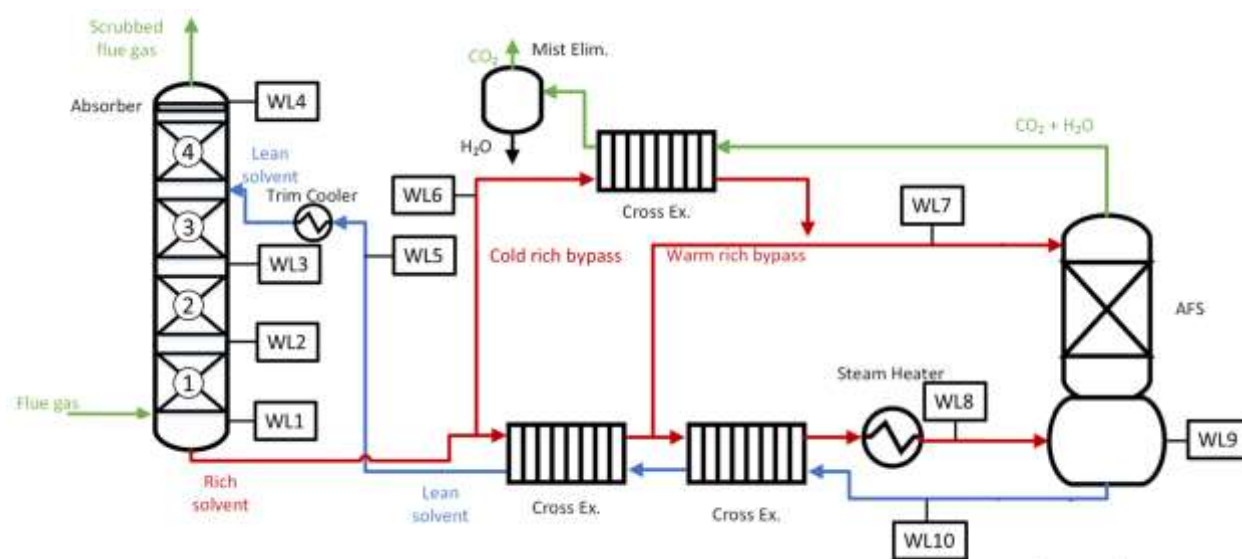


**Figure 1.** Process flowsheet of the NCCC pilot plant highlighting locations of coupon weight loss (WL) measurements: absorber sump (WL1), between absorber beds 1 and 2 (WL2), between absorber beds 2 and 3 (WL3), absorber top (WL4), cold lean stream (WL5), cold rich bypass (WL6), warm rich bypass (WL7), hot rich stream (WL8), stripper sump (WL9), and hot lean stream (WL10).

### 2.3 Coupon batching schedule

In each campaign, coupons were inserted and removed in four chronological batches (Tables 1 and 2). This schedule allowed more coupons to be examined and permitted an investigation of whether corrosion conditions changed over the course of the campaign. In the 2018 campaign, the

coupons in the absorber and in the Advanced Stripper were changed out at the same time, while in 2019 only the coupons in the Advanced Stripper were batched, and there was only one batch in the absorber.

**Table 1.** Calendar illustration of coupon batches in the 2018 campaign

NCCC 2018 Campaign							
	February	March	April	May	June	July	August
Batch 1							
Batch 2							
Batch 3							
Batch 4							

Green sections represent periods of piperazine operation, black sections represent periods when coupons were inserted but the plant was shut down, and the yellow section represents the period of simple stripper operation.

**Table 2.** Calendar illustration of coupon batches in the 2019 campaign

NCCC 2019 Campaign						
		February	March	April	May	June
Absorber						
AFS	Batch 1					
	Batch 2					
	Batch 3					
	Batch 4					

Green sections represent periods of piperazine operation, black sections represent periods when coupons were inserted but the plant was shut down.

### 3. Results & Discussion

#### 3.1 Temperature effect on stainless steel corrosion

Figure 2 shows the relationship between stainless steel corrosion and temperature. Three levels of fluid velocity at the measurement locations are also shown in the plot. The temperature and velocity were measured during the plant operation and were averaged over the batch period. Details of each data point are given in Supporting Information. At low temperature locations (40

°C), corrosion of 316L was minimal, but 316L became vulnerable as the temperature increased. The corrosion rate followed the Arrhenius dependence, and the activation energy of 316L corrosion in 5 m PZ was calculated as 80 kJ/mol. The high corrosion rate suggests that 316L is not an ideal construction material for a PZAS™ unit. Vulnerability of 316L has not been extensively reported in literature because other amines typically operate at 120 °C, where 316L also demonstrated acceptable performance in PZ.

304 and 2205 both showed great corrosion resistance even at high temperature locations. The corrosion rates were seldom above 10 µm/yr. Such a difference between the corrosion performance of 304 and 316L was not expected because these alloys have similar compositions, and they are usually interchangeable in real plant designs. A pilot-scale study showed similar findings in a system operating with 30 wt % MEA. 316L corrosion was measured to be up to 800 µm/yr in the hot lean stream exiting the stripper sump, which operated at 120 °C, while 304 had a corrosion rate lower than 25 µm/yr at comparable conditions.<sup>23</sup> There are limited data on the comparative corrosion behavior of 304 and 316L in PCCC processes, and the cause of the differences between the two is still unclear.

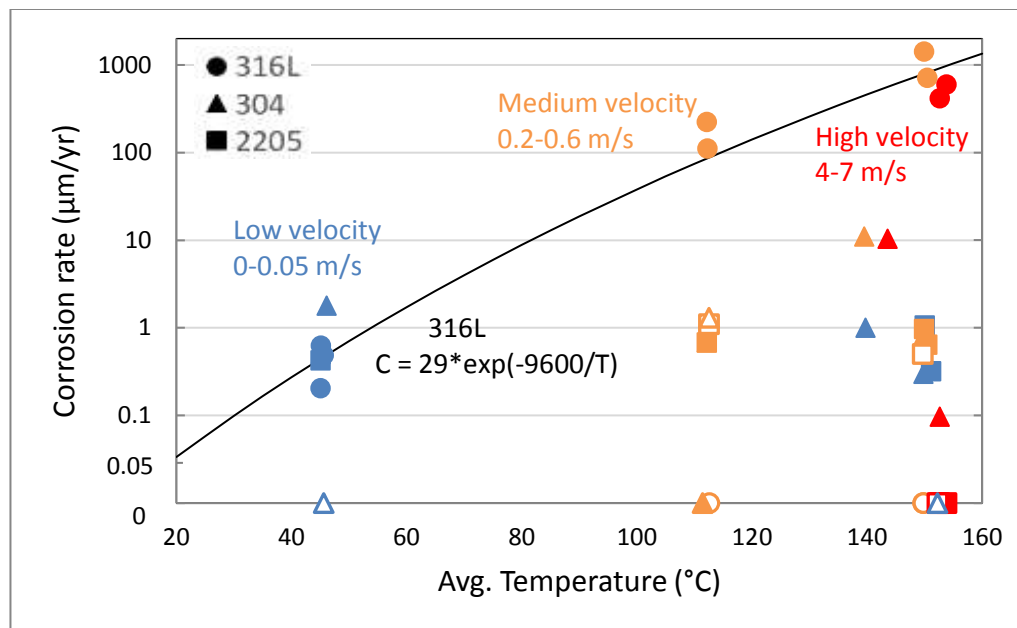


**Figure 2.** Stainless steel (●: 316L, ▲: 304, and ■: 2205 duplex) corrosion rates during the 2019 campaign. Blue points are low fluid velocity (0–0.05 m/s) locations, orange points are medium velocity (0.2–0.6 m/s) locations, and red points are high velocity (4–7 m/s) locations. Corrosion rate is shown on a complex y-axis (0–0.1 µm/yr: linear-scale; >0.1 µm/yr: log-scale). Open points show the rates measured when the carbon adsorption bed was operating. The solid curve shows the Arrhenius dependence of 316L corrosion rates excluding the data with the carbon bed.

### 3.2 Effect of PZ degradation on 316L corrosion

Figure 3 compares 316L corrosion measured in the 2018 and 2019 campaigns. At cold locations, including the absorber locations and the cold rich bypass in the Advanced Stripper, 316L in both campaigns worked well. As temperature increased to 116 °C, the corrosion behavior of 316L in 2019 is greater than that in 2018. In 2018, there were some periods when corrosion was much lower than that measured in 2019 at comparable temperatures, and sometimes it was as high. The difference in 316L corrosion in the two campaigns might be due to the accumulation of PZ degradation products. Fresh PZ solvent was used at the beginning of the 2018 campaign, and after 2100 hours of operation the solvent was drained and stored until loaded into the system again when the 2019 campaign started. Therefore, the solvent used in the 2019 campaign had higher levels of

degradation products, some of which might be corrosive to 316L. During the fourth coupon batch period in 2019, an activated carbon adsorption bed was added to the process to remove PZ degradation products. The corrosion measurement showed that 316L corrosion was extremely low at all locations, even in the hot rich and hot lean pipes where the corrosion was up to 1400  $\mu\text{m}/\text{yr}$  without the carbon bed operation. These results suggest that PZ degradation has an effect on corrosion of 316L, and removal of the degradation products can result in significant decrease in solvent corrosivity. A similar effect of MEA degradation on 316L corrosion has been reported in the literature.<sup>15,16</sup> Although the exact PZ degradation products causing the increase in solvent corrosivity have not been identified, the carbon bed adsorption may be an effective method for mitigating 316L corrosion.

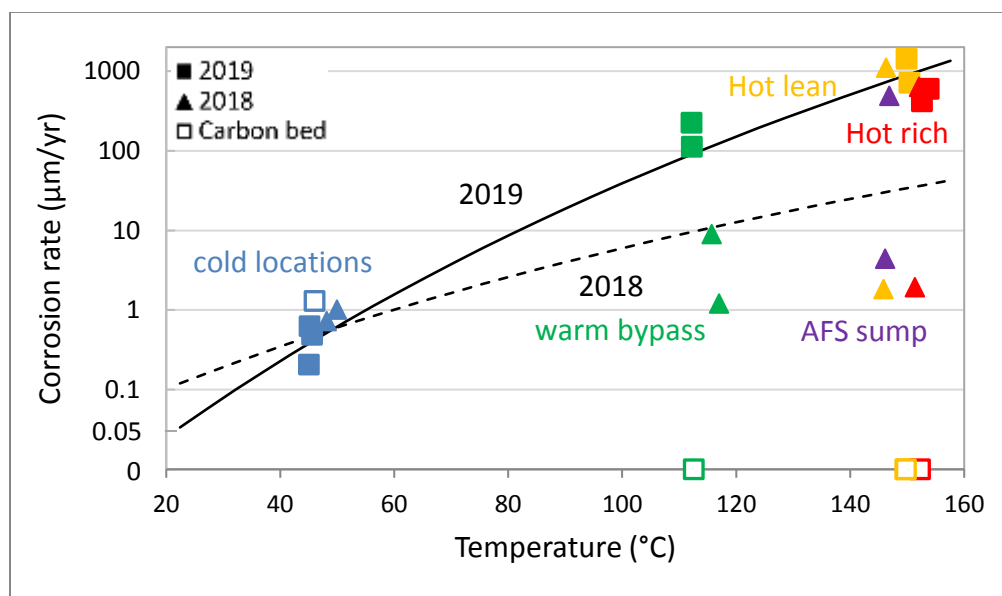


**Figure 3.** 316L corrosion during the 2018(▲) and 2019 (■) campaigns. Blue points are measurements in the cold locations, green points are in the warm bypass, yellow points are in the hot lean stream, red points are in the hot rich stream, and purple points are in the stripper sump. Corrosion rate is shown on a complex y-axis (0–0.1  $\mu\text{m}/\text{yr}$ : linear-scale; >0.1  $\mu\text{m}/\text{yr}$ : log-scale). Open points show the rates measured when the carbon adsorption bed was operating. The solid curve shows the Arrhenius dependence of 316L corrosion rates in 2019 excluding the data with the carbon bed, and the dashed curve shows the temperature dependence of 316L corrosion in 2018.

### 3.3 Effect of temperature and velocity on carbon steel corrosion

Figure 4 shows the corrosion of C1010 carbon steel measured in both campaigns as a function of temperature. The effect of temperature on C1010 corrosion was apparently weaker than its effect on 316L. Corrosion rates measured in the warm bypass (116 °C) were similar to those in the cold pipes, which include the cold bypass and the cold lean pipe (40 °C). At the three locations where the temperature was between 140 and 155 °C, corrosion rates varied widely. The carbon steel in the hot rich stream experienced the highest corrosion (up to 9600  $\mu\text{m}/\text{yr}$ ). The corrosion rate in the hot lean stream was lower but still significant (up to 900  $\mu\text{m}/\text{yr}$ ). The carbon steel in the stripper sump experienced much lower corrosion (up to 10  $\mu\text{m}/\text{yr}$ ) compared to the other two high temperature locations. Siderite protective films are believed to play a significant role in carbon steel corrosion, and the weak temperature effect on the corrosion rate can be driven by several factors:

1.  $\text{FeCO}_3$  solubility is lower at elevated temperature,<sup>29,30</sup> increasing the driving force for precipitation of siderite protective films.
2. Kinetics of siderite formation are faster at higher temperatures.
3. Oxidation of Fe is faster at higher temperatures, but this is less relevant because the rate of corrosion is limited by siderite formation

Therefore, although corrosion rates are normally higher at higher temperatures, due to the faster formation of the siderite protective film, carbon steel can be better protected, and corrosion can be lower.

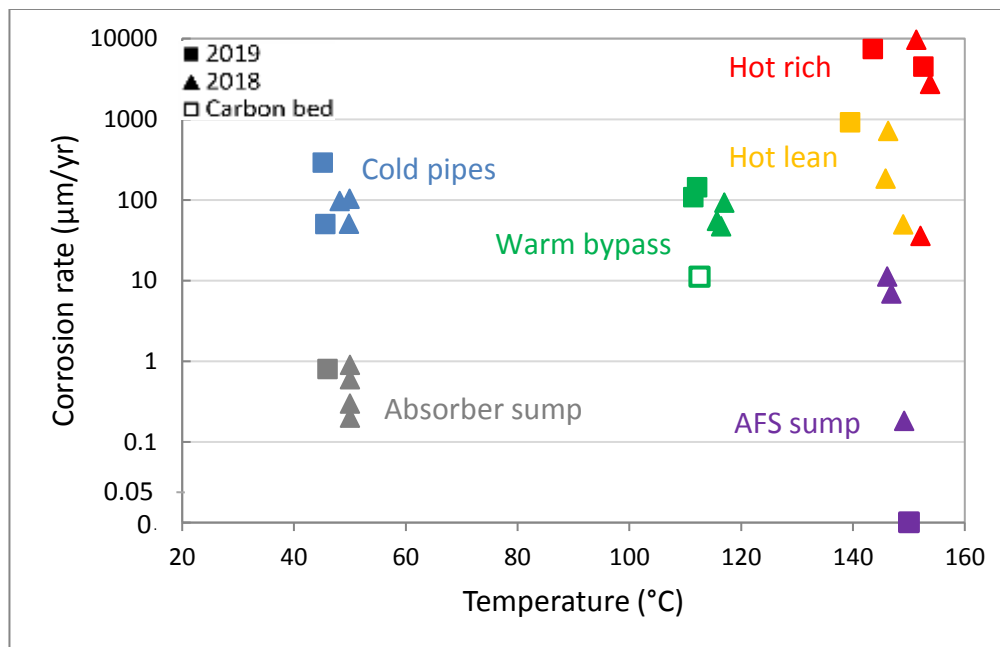


**Figure 4.** C1010 corrosion during the 2018(▲) and 2019 (■) campaigns. Blue points are measurements in the cold pipes (cold bypass and cold lean pipe), grey points are in the absorber sump, green points are in the warm bypass, yellow points are in the hot lean stream, red points are in the hot rich stream, and purple points are in the stripper sump. Corrosion rate is shown on a complex y-axis (0–0.1  $\mu\text{m}/\text{yr}$ : linear-scale; >0.1  $\mu\text{m}/\text{yr}$ : log-scale). Open points show the rates measured when the carbon adsorption bed was operating.

The wide variation of carbon steel corrosion rates at similar temperature can be explained by the effect of fluid velocity. In the absorber and stripper sumps, the liquid was almost stagnant, and thus these two locations are classified as low velocity locations. High velocity locations, on the other hand, refer to all the pipe locations, including the cold pipes, warm bypass, hot rich pipe and hot lean pipe. At these locations, the fluid velocity was estimated from the flow measurements and varied from 0.03 to 6.5 m/s. The highest flow was measured in the hot rich pipe because the fluid was flashing inside. Detailed velocities at each location are given in Table S1 in Supporting Information. High velocity locations had higher corrosion than low velocity locations regardless of temperature. High fluid velocity might exacerbate carbon steel corrosion because it removes the protective siderite layer, prevents formation of a compact, nonporous layer, or alters the structure of siderite crystals. In the stripper sump, where the liquid was hot but stagnant, carbon steel was

well protected and might outperform 316L at the same condition. At the low temperature locations, no siderite film was observed, which resulted in higher corrosion.

All C1010 coupons were covered by siderite films except the ones at those cold locations. The identification of siderite was done with powder XRD. The following figures show the SEM micrographs of the siderite layers on representative C1010 coupons retrieved from the pilot plant. Figure 5(a) shows the coupon taken from the stripper sump during Batch 3 in 2019. A crystalline, regular layer was observed, and the crystals had a cubic shape. The low corrosion rate at this location ( $<1 \mu\text{m}/\text{yr}$ ) shows that this layer was protective. Figure 5(b) shows the surface of the Batch 2 C1010 coupon taken from the warm rich bypass in 2019. The coupon was also covered by a crystalline siderite layer, but these crystals were triangular and smaller in size. The corrosion rate was  $107 \mu\text{m}/\text{yr}$ , suggesting the layer also provided some protection, while the protection was not as effective as that in the stripper sump.

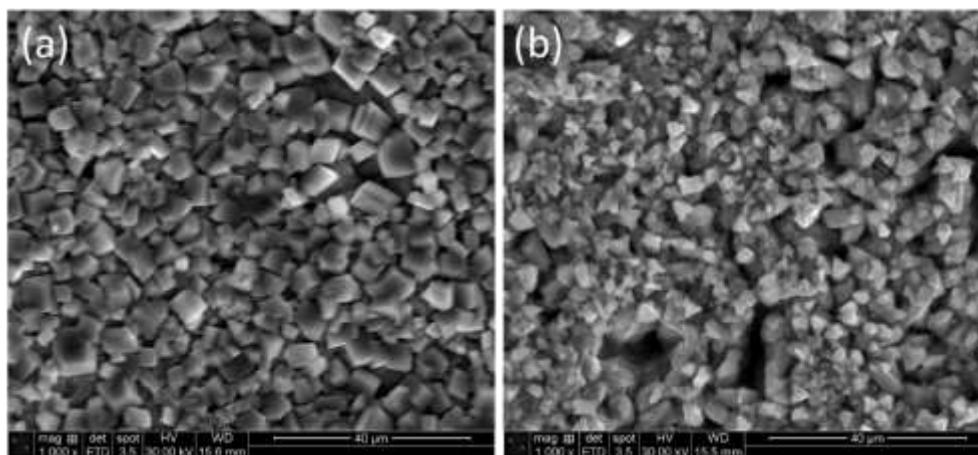


**Figure 5.** SEM micrographs of protective siderite layers on (a) the Batch 3 C1010 coupon in the stripper sump and (b) the Batch 2 C1010 coupon in the warm bypass.

Although all C1010 coupons taken from the warm and hot locations had siderite layers, some of the layers did not protect the steel. Figure 6 shows two C1010 coupons from the hot rich stream

that were not protected, one of which was from Batch 2 during the 2019 campaign, and the other from Batch 3 in 2018. The siderite films on these two coupons look very different from the protective ones shown previously and also different from each other. The coupon from the 2018 campaign had very large pyramidal crystals, and the film on the 2019 coupon had similar pyramidal structures but with a branching feature. These two coupons experienced very high corrosion (over 2500  $\mu\text{m}/\text{yr}$ ). The films on the coupons in the hot rich pipe and the stripper sump formed at comparable temperatures (150 °C) but performed differently. The lack of film protectiveness in the hot rich pipe is partially due to the flashing, high-velocity flow at this location, which altered the precipitation mechanism of siderite and caused the degradation of protection.

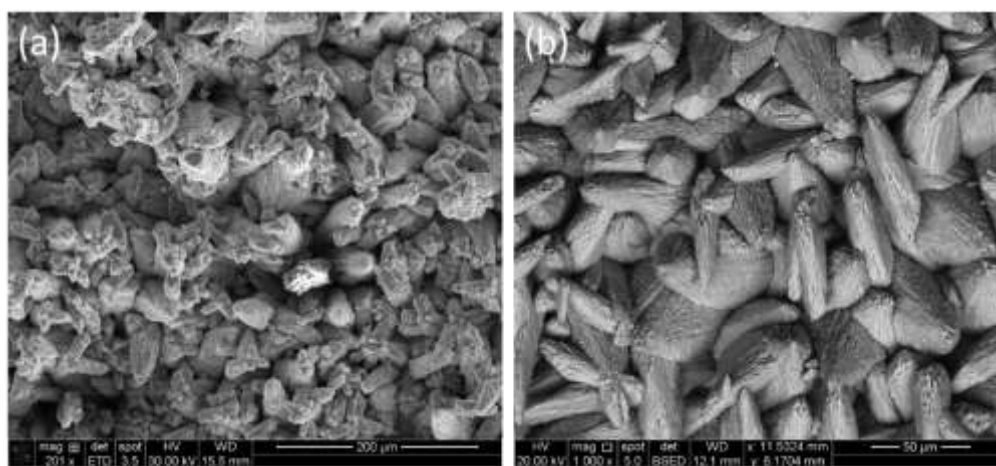


**Figure 6.** SEM micrographs of non-protective siderite layers on (a) the Batch 2 C1010 coupon in the hot rich pipe during the 2019 campaign and (b) the Batch 3 C1010 coupon in the hot rich pipe during the 2018 campaign.

### 3.4 Corrosion of nickel-based alloys

Nickel-based alloys are usually believed to be more corrosion-resistant than stainless steel; therefore Hastelloy<sup>®</sup> C276 and Inconel<sup>®</sup> 625 coupons were tested in the Advanced Stripper during the 2019 campaign and investigated as alternatives for stainless steel. Figure 7 shows the corrosion

rate of these Ni-based alloys as a function of temperature. Despite anecdotally good performance in industry with these alloys, they were surprisingly vulnerable in PZ, especially at high temperature. Similar to 316L, the Ni-based alloys showed corrosion strongly dependent on temperature, and the dependence followed the Arrhenius equation. The activation energy of corrosion of the alloys in PZ was calculated as 93 kJ/mol. Figure 8 shows a C276 coupon and the surface of the coupon under SEM. The area surrounding the holes was covered by Teflon™ washers during measurement. The liquid could be trapped in the gap between alloy and washer, and thus this area was exposed to a different corrosion environment. The bulk surface of the coupon looked etched and uneven under SEM, and there was a clear boundary between the bulk surface and the area under washers. Energy-dispersive X-ray spectroscopy (EDS) was used to measure the alloy compositions in these two regions, as given in Table 3. The bulk surface had a composition similar to the original composition of the alloy, but the area under washers had a Nickel content lower than the original value by 10 wt %. The decrease in Ni content suggests Ni had been selectively dissolved by PZ in this area. Although the dissolution of Ni was not observed on the bulk surface of the alloy and may not be representative for the major part of the pipe, it suggests that crevice corrosion is possible at joints between pipes and equipment if these Ni-based alloys are chosen as construction materials for a PCCC process using PZ.

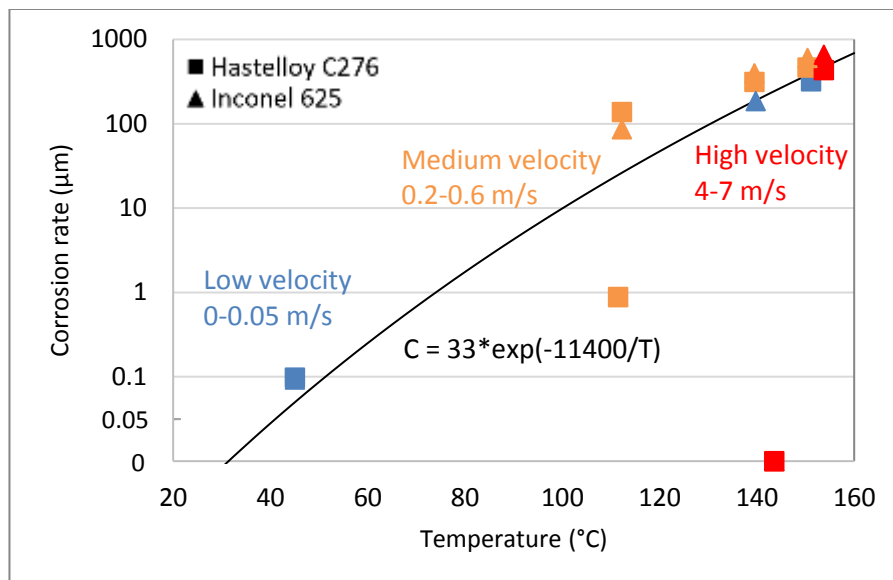


**Figure 7.** Corrosion of Hastelloy® C276 (■) and Inconel® (▲) during the 2019 campaign. Blue points are low fluid velocity (0–0.05 m/s) locations, orange points are medium velocity (0.2–0.6 m/s) locations, and red points are high velocity (4–7 m/s) locations. Corrosion rate is shown on a complex y-axis (0–0.1 µm/yr: linear-scale; >0.1 µm/yr: log-scale).

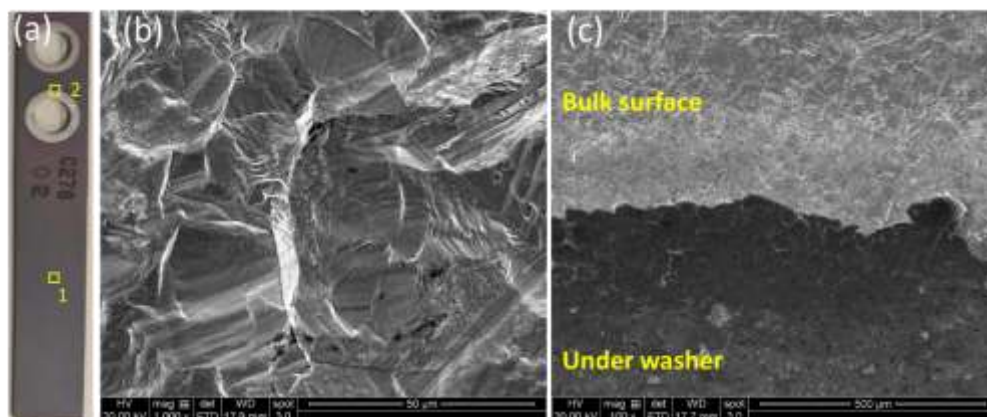


**Figure 8.** (a) Photo of a C276 coupon highlighting two locations imaged with SEM, (b) SEM micrograph of spot 1, and (c) SEM micrograph of spot 2.

**Table 3.** EDS measurement of surface alloy compositions of Hastelloy® C276 before and after experiment

Original (wt %)	Corroded bulk surface (wt %)	Corroded area under washers (wt %)

Ni	57	58.4	48.2
Cr	15.5	15.1	20.9
Fe	5.5	6.9	6.6
Mo	16	13.6	12.5

#### 4. Conclusions

- (1) 316L stainless steel experienced higher corrosion than 304 stainless steel and 2205 duplex stainless steel, and the corrosion rate showed strong dependence on temperature. The vulnerability of 316L was not expected and is related to the uniquely high operating temperature of PZ.
- (2) Degraded PZ also exacerbated 316L corrosion, and removal of PZ degradation products using a carbon adsorption bed significantly reduced corrosion.
- (3) 304 and 2205 performed well at all locations and can be good alternative construction materials for a PZ system.
- (4) Carbon steel corrosion showed a weak temperature effect because the corrosion was more dependent on protection by a siderite film. The protectiveness of the films was related to fluid velocity. Regular, crystalline films formed in stagnant fluid and provided better protection. High-velocity flow might alter the precipitation mechanism of siderite or damage the film and thus result in non-protective films.
- (5) Ni-based alloys did not perform well due to selective dissolution of Ni into PZ in some narrow gaps between alloy and washers.

Author Information

Corresponding author

\*Email: [gtr@che.utexas.edu](mailto:gtr@che.utexas.edu). Tel.: +01-512-471-7230; fax: +01-512-471-7060

## Acknowledgements

This material is based on work supported in part by the Department of Energy under Award Number DE-FE0005654. This report was prepared as an account of work sponsored by an agency of the United States Government. Neither the United States Government nor any agency thereof, nor any of their employees, makes any warranty, express or implied, or assumes any legal liability or responsibility for the accuracy, completeness, or usefulness of any information, apparatus, product, or process disclosed, or represents that its use would not infringe privately owned rights. Reference herein to any specific commercial product, process, or service by trade name, trademark, manufacturer, or otherwise does not necessarily constitute or imply its endorsement, recommendation, or favoring by the United States Government or any agency thereof. The views and opinions of authors expressed herein do not necessarily state or reflect those of the United States Government or any agency thereof.

Financial support was also provided by the Texas Carbon Management Program, the CO<sub>2</sub> Capture Project, and the National Carbon Capture Center (NCCC).

Karen Farmer from AECOM; Andrew Sexton from Trimeric Corporation; and the NCCC team from Southern Company played major roles in the design, construction, and operation of the pilot plant.

## References

- (1) Metz, B.; Davidson, O.; de Coninck, H.; Loos, M.; Meyer, L. A. *IPCC Special Report on Carbon Dioxide Capture and Storage, first published ed.*; Cambridge University Press: Cambridge, United Kingdom, 2005.
- (2) Pacala, S.; Socolow, R. Stabilization Wedges: Solving the Climate Problem for the Next 50 Years with Current Technologies. *Science* **2004**, *305* (5686), 968–972. <https://doi.org/10.1126/science.1100103>.
- (3) Rochelle, G. T. Amine Scrubbing for CO<sub>2</sub> Capture. *Science* **2009**, *325* (5948), 1652–1654. <https://doi.org/10.1126/science.1176731>.
- (4) Rochelle, G. T.; Wu, Y.; Chen, E.; Akinpelumi, K.; Fischer, K. B.; Gao, T.; Liu, C.-T.; Selinger, J. L. Pilot Plant Demonstration of Piperazine with the Advanced Flash Stripper. *Int. J. Greenh. Gas Control* **2019**, *84*, 72–81. <https://doi.org/10.1016/J.IJGGC.2019.03.014>.
- (5) Lin, Y.-J.; Rochelle, G. T. Approaching a Reversible Stripping Process for CO<sub>2</sub> Capture. *Chem. Eng. J.* **2016**, *283*, 1033–1043. <https://doi.org/10.1016/j.cej.2015.08.086>.
- (6) Gunasekaran, P.; Veawab, A.; Aroonwilas, A. Corrosivity of Single and Blended Amines in CO<sub>2</sub> capture Process. *Energy Procedia* **2013**, *37*, 2094–2099. <https://doi.org/10.1016/j.egypro.2013.06.088>.
- (7) Gunasekaran, P.; Veawab, A.; Aroonwilas, A. Corrosivity of Amine-Based Absorbents for CO<sub>2</sub> Capture. *Energy Procedia* **2017**, *114*, 2047–2054. <https://doi.org/10.1016/j.egypro.2017.03.1339>.
- (8) Zheng, L.; Landon, J.; Zou, W.; Liu, K. Corrosion Benefits of Piperazine as an Alternative CO<sub>2</sub> Capture Solvent. *Ind. Eng. Chem. Res.* **2014**, *53* (29), 11740–11746.

<https://doi.org/10.1021/ie501346z>.

- (9) Zheng, L.; Landon, J.; Matin, N. S.; Li, Z.; Qi, G.; Liu, K. Corrosion Behavior of Carbon Steel in Piperazine Solutions for Post-Combustion CO<sub>2</sub> Capture. *ECS Trans.* **2014**, *20*, 81–95.
- (10) Liu, C.-T.; Fischer, K. B.; Rochelle, G. T. Corrosion of Carbon Steel by Aqueous Piperazine Protected by FeCO<sub>3</sub>. *Int. J. Greenh. Gas Control* **2019**, *85*, 23–29. <https://doi.org/10.1016/j.ijggc.2019.03.027>.
- (11) Campbell, K. L. S.; Zhao, Y.; Hall, J. J.; Williams, D. R. The Effect of CO<sub>2</sub>-Loaded Amine Solvents on the Corrosion of a Carbon Steel Stripper. *Int. J. Greenh. Gas Control* **2016**, *47*, 376–385. <https://doi.org/10.1016/j.ijggc.2016.02.011>.
- (12) Zheng, L.; Matin, N. S.; Landon, J.; Thomas, G. A.; Liu, K. CO<sub>2</sub> Loading-Dependent Corrosion of Carbon Steel and Formation of Corrosion Products in Anoxic 30 wt.% Monoethanolamine-Based Solutions. *Corros. Sci.* **2016**, *102*, 44–54. <https://doi.org/10.1016/j.corsci.2015.09.015>.
- (13) Zheng, L.; Landon, J.; Matin, N. S.; Thomas, G. A.; Liu, K. Corrosion Mitigation via a pH Stabilization Method in Monoethanolamine-Based Solutions for Post-Combustion CO<sub>2</sub> capture. *Corros. Sci.* **2016**, *106*, 281–292. <https://doi.org/10.1016/j.corsci.2016.02.013>.
- (14) Billingham, M. A.; Lee, C.-H.; Smith, L.; Haines, M.; James, S. R.; Goh, B. K. W.; Dvorak, K.; Robinson, L.; Davis, C. J.; Peralta-Solorio, D. Corrosion and Materials Selection Issues in Carbon Capture Plants. *Energy Procedia* **2011**, *4*, 2020–2027. <https://doi.org/10.1016/j.egypro.2011.02.083>.

- (15) Fytianos, G.; Grimstvedt, A.; Knuutila, H.; Svendsen, H. F. Effect of MEA's Degradation Products on Corrosion at CO<sub>2</sub> Capture Plants. *Energy Procedia* **2014**, *63*, 1869–1875. <https://doi.org/10.1016/j.egypro.2014.11.195>.
- (16) Fytianos, G.; Ucar, S.; Grimstvedt, A.; Hyldbakk, A.; Svendsen, H. F.; Knuutila, H. K. Corrosion and Degradation in MEA Based Post-Combustion CO<sub>2</sub> Capture. *Int. J. Greenh. Gas Control* **2016**, *46*, 48–56. <https://doi.org/10.1016/j.ijggc.2015.12.028>.
- (17) Kittel, J.; Idem, R.; Gelowitz, D.; Tontiwachwuthikul, P.; Parrain, G.; Bonneau, A. Corrosion in MEA Units for CO<sub>2</sub> Capture: Pilot Plant Studies. *Energy Procedia* **2009**, *1* (1), 791–797. <https://doi.org/10.1016/j.egypro.2009.01.105>.
- (18) Tanthapanichakoon, W.; Veawab, A.; McGarvey, B. Electrochemical Investigation on the Effect of Heat-Stable Salts on Corrosion in CO<sub>2</sub> Capture Plants Using Aqueous Solution of MEA. *Ind. Eng. Chem. Res.* **2006**, *45*, 2586–2593. <https://doi.org/10.1021/ie050575a>.
- (19) Rooney, P. C.; DuPart, M. S. Effect of Heat Stable Salts on MDEA Solution Corrosivity. *Hydrocarb. Process.* **1997**, *76* (4), 65.
- (20) Fischer, K. B.; Daga, A.; Hatchell, D.; Rochelle, G. T. MEA and Piperazine Corrosion of Carbon Steel and Stainless Steel. *Energy Procedia* **2017**, *114*, 1751–1764. <https://doi.org/10.1016/j.egypro.2017.03.1303>.
- (21) Cousins, A.; Ilyushechkin, A.; Pearson, P.; Cottrell, A.; Huang, S.; Feron, P. H. M. Corrosion Coupon Evaluation under Pilot-Scale CO<sub>2</sub> Capture Conditions at an Australian Coal-Fired Power Station. *Greenh. Gases Sci. Technol.* **2013**, *3* (3), 169–184. <https://doi.org/10.1002/ghg.1341>.

- (22) Hjelmaas, S.; Storheim, E.; Flø, N. E.; Thorjussen, E. S.; Morken, A. K.; Faramarzi, L.; deCazenove, T.; Hamborg, E. S. Results from MEA Amine Plant Corrosion Processes at the CO<sub>2</sub> Technology Centre Mongstad. *Energy Procedia* **2017**, *114*, 1166–1178. <https://doi.org/10.1016/j.egypro.2017.03.1280>.
- (23) Khakharia, P.; Mertens, J.; Huizinga, A.; DeVroey, S.; Sanchez Fernandez, E.; Srinivasan, S.; Vlugt, T. J. H.; Goetheer, E. Online Corrosion Monitoring in a Postcombustion CO<sub>2</sub> Capture Pilot Plant and Its Relation to Solvent Degradation and Ammonia Emissions. *Ind. Eng. Chem. Res.* **2015**, *54* (19). <https://doi.org/10.1021/acs.iecr.5b00729>.
- (24) Hwang, G. S.; Stowe, H. M.; Paek, E.; Manogaran, D. Reaction Mechanisms of Aqueous Monoethanolamine with Carbon Dioxide: A Combined Quantum Chemical and Molecular Dynamics Study. *Phys. Chem. Chem. Phys.* **2015**, *17* (2), 831–839. <https://doi.org/10.1039/c4cp04518a>.
- (25) Li, W.; Landon, J.; Irvin, B.; Zheng, L.; Ruh, K.; Kong, L.; Pelgen, J.; Link, D.; Figueroa, J. D.; Thompson, J. Use of Carbon Steel for Construction of Post-Combustion CO<sub>2</sub> Capture Facilities: A Pilot-Scale Corrosion Study. *Ind. Eng. Chem. Res.* **2017**, *56* (16), 4792–4803. <https://doi.org/10.1021/acs.iecr.7b00697>.
- (26) Fischer, K. B. Corrosion of Stainless and Carbon Steel in Aqueous Amine for CO<sub>2</sub> Capture. Ph. D. Dissertation, The University of Texas at Austin, Austin, TX, 2019.
- (27) Gao, T.; Selinger, J. L.; Rochelle, G. T. Demonstration of 99% CO<sub>2</sub> Removal from Coal Flue Gas by Amine Scrubbing. *Int. J. Greenh. Gas Control* **2019**, *83*, 236–244. <https://doi.org/10.1016/j.ijggc.2019.02.013>.

- (28) Selinger, J. L. Pilot Plant Modeling of Advanced Flash Stripper with Piperazine. M. S. thesis, The University of Texas at Austin, Austin, TX, 2018.
- (29) Sharma, S. S.; Fischer, K. B.; Rochelle, G. Fe<sup>2+</sup> Solubility and Siderite Formation in Monoethanolamine and Piperazine Solvents. 2018, presented at 14th International Conference on Greenhouse Gas Control Technologies, Melbourne, Australia, 21-25 October.
- (30) Sun, W.; Nešić, S.; Woollam, R. C. The Effect of Temperature and Ionic Strength on Iron Carbonate (FeCO<sub>3</sub>) Solubility Limit. *Corros. Sci.* **2009**, *51* (6), 1273–1276. <https://doi.org/10.1016/j.corsci.2009.03.009>.

# Supporting Information for

## Corrosion by Aqueous Piperazine at 40-150 °C in Pilot Testing of CO<sub>2</sub> Capture

*Ching-Ting Liu, Kent B. Fischer, and Gary T. Rochelle\**

The University of Texas at Austin, McKetta Department of Chemical Engineering, 200 E Dean  
Keeton St. Stop C0400, Austin, TX 78712, USA.

\*Corresponding author

Email: [gtr@che.utexas.edu](mailto:gtr@che.utexas.edu)

Tel.: +01-512-471-7230; fax: +01-512-471-7060

**Table S1.** Summary table of corrosion measurements in the absorber at the NCCC pilot plant

Campaign	Location	Batch Descriptor	Batch operating hours	Approx. Temperature (°C)	Mean velocity (m/s)	Corrosion rate (µm/yr)		
						316L	304	C1010
NCCC 2019	Absorber sump	-	1979	50	0	0		298
	Bed 1-2	-	1979	50	0	0.5		278
	Bed 2-3	-	1979	50	0	0.2	0.5	0.8
	Absorber top	-	1979	50	0	0.2	0.2	0
	Cold lean	-	1979	50	0.36	0.0	18	140
NCCC 2018	Absorber sump	2	388	50	0	0.5		0.9
		3	879	50	0		0.1	0
		4	363	50	0	0.6		0.6
	Bed 1-2	2	388	50	0			
		3	879	50	0	0.1		0.3
		4	363	50	0	0.5		0.2
	Absorber top	2	388	50	0			
		3	879	50	0			5
		4	363	50	0			
	Cold lean	2	388	50	0.50			
		3	879	50	0.50	0.4		108
		4	363	50	0.50	1		210

**Table S2.** Summary table of corrosion measurements in the Advanced Stripper at the NCCC pilot plant

Campaign	Location	Batch descriptor	Batch operating hours	Temperature (°C)	Mean velocity (m/s)	Qualitative Loading	Corrosion rate (µm/yr)					
							316L	304	C1010	2205	C276	I625
NCCC 2019	Hot lean	1	225	150	0.44	lean	711				464	604
		2	390	139	0.60	lean		11	910		314	397
		3	400	150	0.55	lean	1429			1.0		
		4	964	150	0.54	lean	0.0	0.8		0.5		
	Hot rich <sup>i</sup>	1	225	154	6.46	lean	597			0.0	433	656
		2	390	144	5.72	lean		10	7431		0.0	0.0
		3	400	153	4.83	lean	417	0.1	4463	0.0		
		4	964	152	4.83	lean	0.0	0.0		0.0		
	Warm bypass	1	225	112	0.25	rich	112			0.0	137	86
		2	390	111	0.30	rich		0.0	107		0.9	0.9
		3	400	112	0.24	rich	223	0.7	143	0.7		
		4	964	113	0.24	rich	0.0	1.3	11	1.1		
	Cold bypass	1	225	45	0.03	rich	0.2			0.4	0.1	0.1
		2	390	45	0.05	rich	0.6	0.5	291			
		3	400	46	0.03	rich	0.5	0.0	50			
		4	964	46	0.03	rich	1.3	1.8				
	Stripper sump	1	225	151	0.00	lean				0.3	318	
		2	390	140	0.00	lean		1.0				186
		3	400	150	0.00	lean			0.0	1.1		
		4	964	150	0.00	lean	0.0	0.3				
NCCC 2018	Hot lean	2	388	146	0.53	lean	1095					
		3	879	149	0.43	lean		0.5	711			
		4	363	146	0.54	lean	1.8		49			
		2	388	152	0.87	lean	629		184			
	Hot rich <sup>i</sup>	3	879	154	0.73	lean		198	36			
		4	363	151	0.91	lean	1.9		2729			
		2	388	116	0.26	rich	9.0		9621			
		3	879	116	0.21	rich		0.3	55			
	Warm bypass	4	363	117	0.27	rich	1.2		47			
		2	388	48	0.05	rich	0.7		92			
		3	879	50	0.05	rich		0.0	97			
		4	363	50	0.05	rich	1.0		50			
	Stripper sump	2	388	147	0.00	lean	489		103			
		3	879	149	0.00	lean		0.6	0.2			
		4	363	146	0.00	lean	4.4		11			

<sup>i</sup>The hot rich stream was flashing, and part of the CO<sub>2</sub> was in the gas phase; therefore, the liquid phase had a CO<sub>2</sub> loading in the “lean” region.

# PZ emissions from PZAS™ on Natural Gas Combined Cycle

Quarterly Report for October 1 – December 31, 2019

by Korede Akinpelumi

Supported by

Carbon Capture Project 4

McKetta Department of Chemical Engineering

The University of Texas at Austin

January 31, 2020

## **Abstract**

Coal is rapidly being replaced by natural gas for electricity generation and future advances in CO<sub>2</sub> capture technologies must demonstrate reliable operations from Natural Gas Combined Cycles (NGCC). Solvent emissions in the scrubbed gas challenge long-term operations of amine-based CO<sub>2</sub> capture units and must be monitored and managed below 1 ppm. Although long-term solvent emissions from coal have been reported, the literature is sparse for NGCC. The gas application presents a unique opportunity for emissions control due to the differences in flue gas composition and absorber operating conditions. In this work, solvent emissions are reported for CO<sub>2</sub> capture under NGCC conditions in the pilot plant at the National Carbon Capture Center (NCCC) using the Piperazine Advanced Stripper (PZAS™). Emissions from changes in solvent intercooling configurations and operation of the direct contact cooler were measured. Wash tower performance was evaluated through continuous gas sampling on the absorber and wash tower gas outlets. The NGCC capture conditions appear to suppress emissions even at significant aerosol nuclei penetration. PZ emissions averaged 0.7 ppm and were much lower than the previous coal campaign. The intercooling configurations did not affect emissions. Although the introduction of hot inlet gas caused a five-fold increase in emissions, the emissions were still below 1 ppm. On average, the wash tower removed 94% of the PZ entering from the absorber.

## **Introduction**

Flue gases from fossil fuel-based power plants are the major concentrated CO<sub>2</sub> sources in the United States. The capture of CO<sub>2</sub> from these plants is an important solution to meeting energy demand in an economical and sustainable manner. Natural Gas Combined-Cycle (NGCC) plants have replaced coal as the major electricity generation source and contribute a third of total U.S. energy-related CO<sub>2</sub> emissions (EIA, 2019). Future advances in the CO<sub>2</sub> capture technologies must demonstrate reliable CO<sub>2</sub> capture operations from NGCC.

Solvent emissions in the CO<sub>2</sub>-scrubbed gas are a concern for amine-based CO<sub>2</sub> capture units and must be monitored and managed below 1 ppm. Pilot studies have shown that emissions are largely influenced by the flue gas composition and absorber operating conditions. SO<sub>2</sub>, SO<sub>3</sub>, and fly ash in the flue gas nucleate aerosol on which the solvent condenses. Absorber operating conditions also play a critical role in creating or mitigating emissions in the presence of aerosols (Akinpelumi

et al., 2019; Bade et al., 2015). These factors are important because the flue gas composition and absorber conditions differ for CO<sub>2</sub> capture from NGCC and coal. Firstly, NGCC flue gas has a lower CO<sub>2</sub> content which reduces the partial pressure driving force for absorption and requires lower lean loading for equivalent capture to coal. Because amines are more volatile at lower lean loading, this can affect the mass transfer of species from gas to aerosol. Also, because of the lower CO<sub>2</sub>, the NGCC flue gas requires a lower liquid to gas (L/G) ratio which shifts the temperature bulge higher up the absorber compared to capture from coal. The magnitude and location of the temperature bulge can influence the supersaturation of the upward streaming gas and nucleation of aerosols. Intercooling configurations can affect the temperature bulge location and thus have significant effects on solvent volatility and emission control. Lastly, the NGCC flue gas has a cleaner composition with a lower concentration of aerosol nuclei. The absence of significant concentrations of SO<sub>2</sub>, SO<sub>3</sub>, and fly ash should result in much lower amine emissions.

Although long-term emissions from capture from coal have been reported, the literature is sparse for NGCC. A bench-scale emissions study of capture from varying inlet CO<sub>2</sub> showed that an initial increase of inlet CO<sub>2</sub> to 4% doubled PZ emission, while further increases in inlet CO<sub>2</sub> had negligible effects (Fulk and Rochelle, 2014). Beaudry (2018) found that higher inlet CO<sub>2</sub> increased the mean diameter of aerosols. Although both studies show that inlet CO<sub>2</sub> can have some effect on solvent emission, they only demonstrated instantaneous changes in CO<sub>2</sub> over a short duration of 30 minutes. The experiments were also not under optimal capture conditions and the solvent loading and concentration was not tracked. Pilot studies with 90% capture over extended periods must be conducted for NGCC to monitor solvent emissions.

This work reports solvent emissions over extended periods of capture from NGCC using the PZAS<sup>TM</sup> process. The emission trends during the NGCC campaign were compared to a previous coal campaign at the National Carbon Capture Center (NCCC). The effect of intercooling configurations and use of the direct contact cooler (DCC) on emissions were investigated. This work also evaluated wash tower performance through continuous emissions sampling upstream and downstream of the wash tower.

### ***Test System and Methods***

The Pilot Solvent Test Unit (PSTU) at the NCCC was run with the PZAS<sup>TM</sup> from February 14 to May 20, 2019. Flue gas containing 12% CO<sub>2</sub> from the coal boiler was diluted with air to 4% CO<sub>2</sub> to simulate NGCC conditions. Two intercooling configurations were tested: In-and-out (IO) and Pump-around (PA). The DCC was bypassed for certain periods of the campaign and hot inlet gas at 76°C was fed directly to the absorber. The PZAS<sup>TM</sup> process overview and test runs for this campaign are reported by Gao and Rochelle (2019). Figure 1 shows the flue gas pretreatment processes at the NCCC. Ca(OH)<sub>2</sub> (hydrated lime) injection rates are critical to SO<sub>3</sub> removal (Akinpelumi et al., 2019) and were monitored throughout the campaign.

The NCCC absorber consists of 3 beds of packing. For this campaign the first two beds of the NCCC absorber were used for absorption while the 3<sup>rd</sup> bed was operated dry. Two Fourier transform Infrared Spectroscopy (FTIR) analyzers continuously measured PZ, CO<sub>2</sub>, H<sub>2</sub>O, and NH<sub>3</sub> at the absorber and wash tower gas outlets. The continuous measurement of gas compositions upstream and downstream of the wash tower provided real-time evaluation of the wash tower performance and was a significant improvement on previous campaigns at the NCCC where one analyzer was used alternately for both sample locations. There were periods of sampling discontinuities due to condensation issues on the probes and sampling lines.

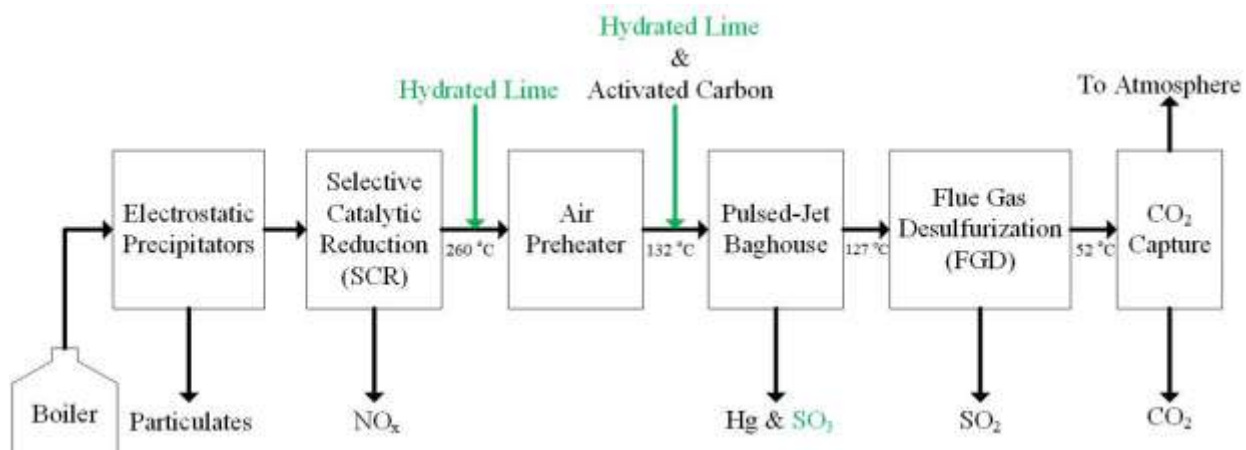


Figure 1: Flue gas treatment steps at NCCC Gaston Unit 5

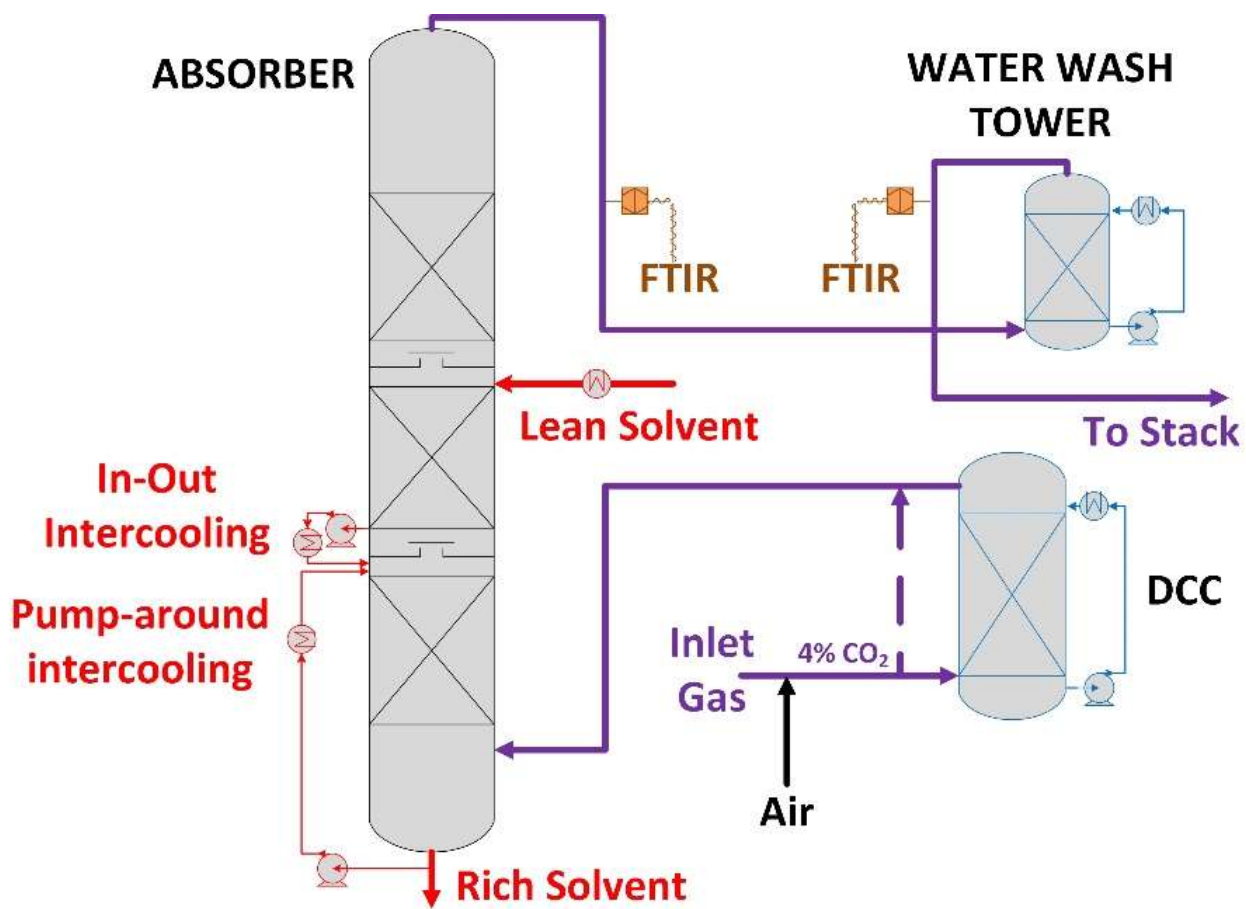
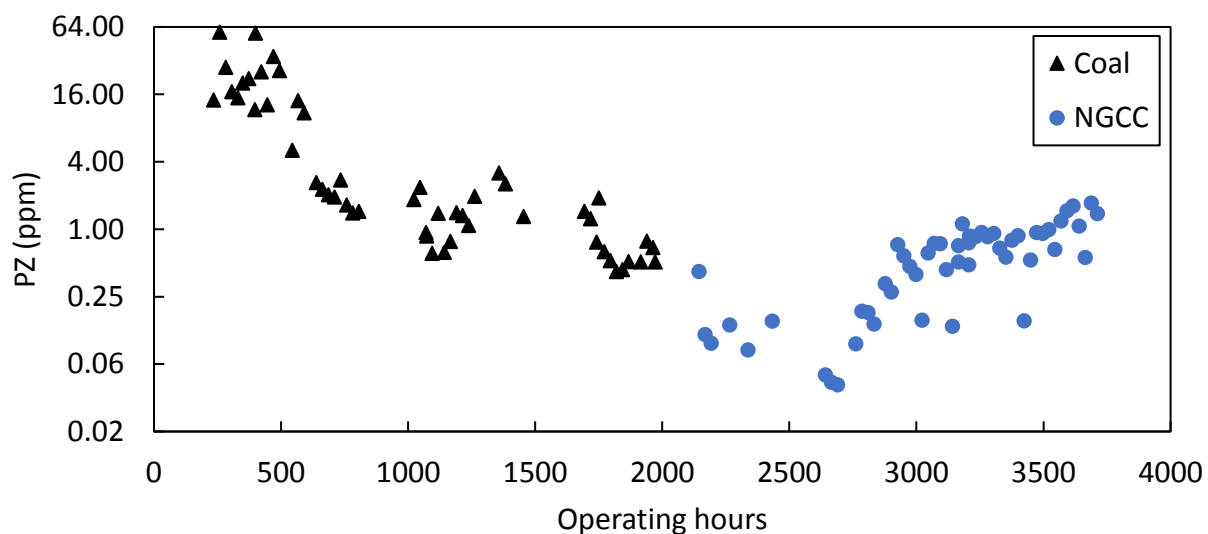


Figure 2: PSTU absorber gas sampling system

## Results and Discussions

### Emissions trends from Coal and NGCC Campaigns

The coal and NGCC campaigns each lasted about 2000 hours with brief periods during which the capture plant was shut down. The data points in Figure 3 represent daily average PZ in the wash tower gas outlet without filtering for steady state operations. While this helps to analyze emissions from an operational standpoint, it could introduce outliers resulting from unsteady operations during process changes. PZ emissions ranged from 5–60 ppm during the first 600 hours of the coal campaign and <4 ppm for the balance of the coal campaign. Emissions during the NGCC campaign were much lower with <0.4 ppm for the first 800 operating hours and <1.7 ppm for the balance of the campaign. The NGCC campaign average PZ emission was 0.7 ppm.



**Figure 3: Emission trends from 2018 Coal and 2019 NGCC campaigns. Each data point represents daily average PZ from wash tower outlet.**

Akinpelumi et al. (2019) interpreted the first period of excessive emissions during the coal campaign to be due to  $\text{SO}_3$  penetration from a suboptimal lime rate upstream of the baghouse (Figure 4). The lime rates during the NGCC campaign were low, similar to the first half of the coal campaign, and suggestive of significant  $\text{SO}_3$  penetration. However, the PZ emissions were much lower than might be expected at such implied  $\text{SO}_3$  penetration levels. It is likely the PZ emissions were low because the flue gas (and  $\text{SO}_3$ ) was diluted by a factor of three to get the 4.3%  $\text{CO}_2$  for NGCC conditions. The dilution would significantly reduce the concentration of inlet aerosol nuclei, resulting in low outlet PZ emissions. It is also possible that the capture conditions of NGCC suppressed emissions at high  $\text{SO}_3$  penetration.

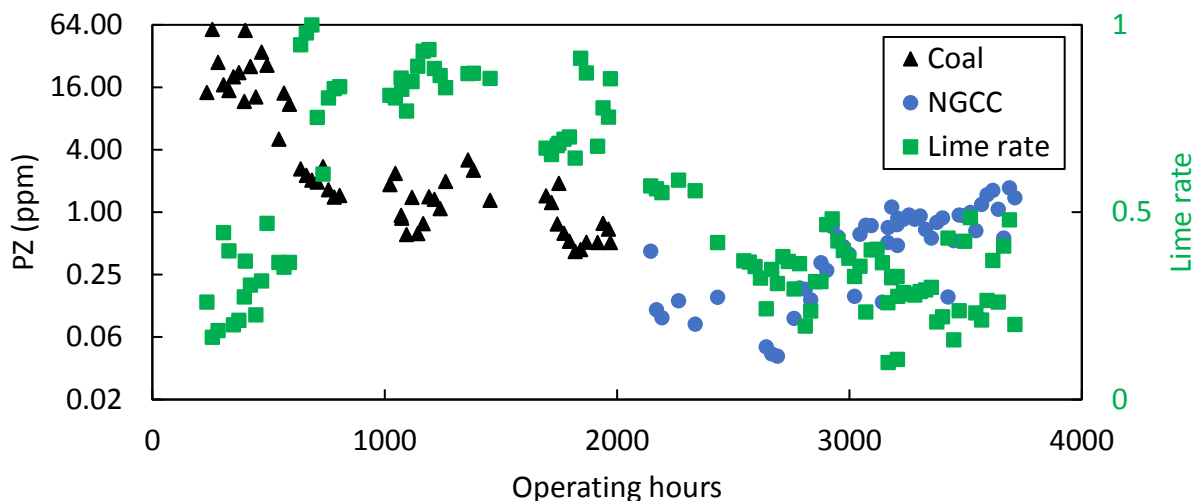


**Figure 4: Effect of lime rate on emissions during coal and NGCC campaigns. Lime rate was normalized to maximum injection during both campaigns. All datapoints represent daily averages.**

### Emissions from NGCC Steady-State Operations

PZ measurements at the absorber and wash tower gas outlet were extracted for 36 and 56 steady-state runs respectively out of a total of 75. Analyzing emissions during steady-state operations helps remove outliers from process disruptions. PZ emissions from the wash tower across all steady-state runs were below 3 ppm with an average of 0.72 ppm (Figure 5). This average is consistent with that obtained from the unsteady state (daily averaged) results. PZ emissions from the absorber appear to belong to two distinct sets: the first with a maximum of 0.4 ppm and the second with an average of 11 ppm. Figure 6 shows that the step change in emissions for the absorber gas corresponds to the bypass of the DCC. This bypass also resulted in a five-fold increase in PZ exiting the wash tower (Table 1). Changing the intercooling configuration did not have any significant effect on emissions. When the DCC was bypassed, the inlet gas at 76 °C was introduced to the absorber resulting in a potential for aerosol formation due to quenching of hot gas with cold solvent (Bade et al., 2015). The lean solvent temperature throughout the test period was constant at 40 °C and no major changes in process operations that might explain the increase in emissions were identified. It is however possible that the low PZ absorber outlet could be an artifact of the FTIR sampling technique at the beginning of the campaign. Probe failure and condensation were observed at the absorber sampling port at the beginning of the campaign and were only corrected at a later stage in the campaign. Nevertheless, even if the absorber data at the start of the campaign are discarded, the increase in wash tower PZ might still be indicative of aerosol formation due to quenching with PZ.

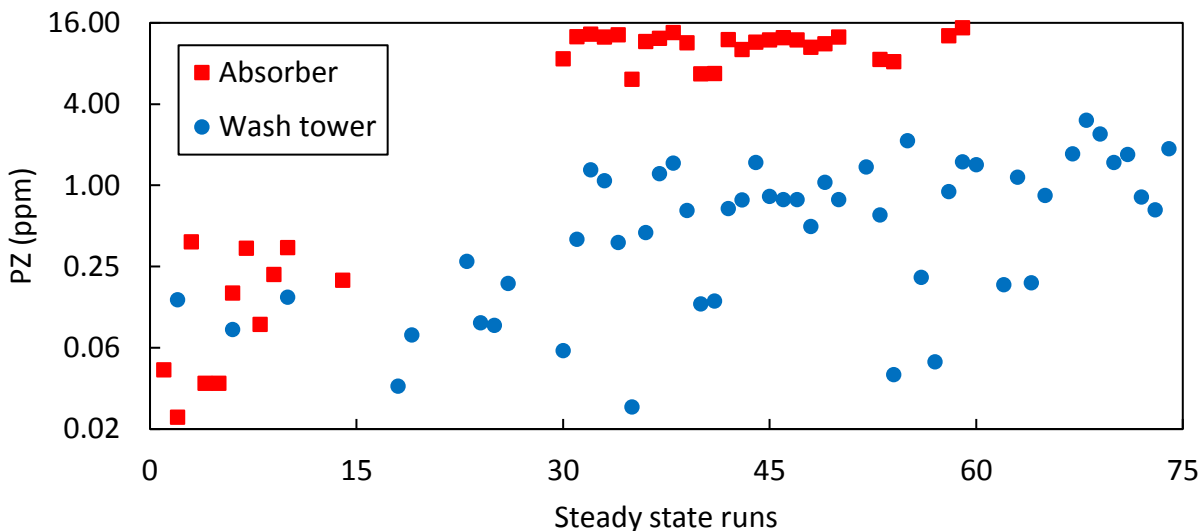


**Figure 5: PZ emissions from absorber and wash tower gas outlets for steady-state operations during NGCC campaign.**

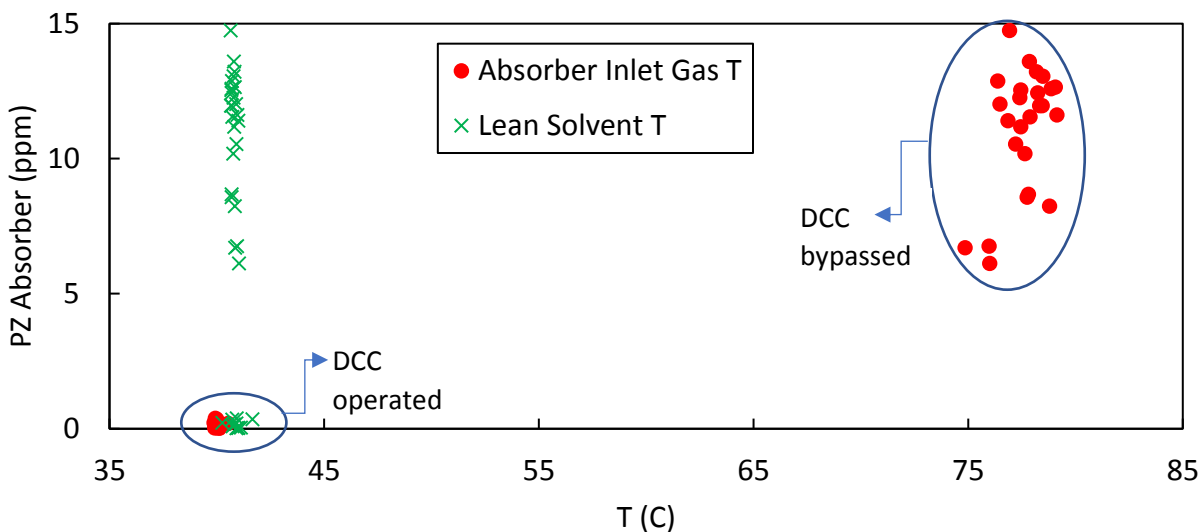


**Figure 6: Effect of bypassing DCC on PZ emissions during NGCC campaign. Lean solvent T was set to 40 °C and remained unchanged throughout the campaign. PZ data point represents hourly steady state averages of PZ in absorber gas outlet.**

**Table 1: Average PZ emissions from absorber configurations tested**

DCC	Intercooling (IC)	PZ Wash tower Gas outlet (ppm)	PZ Absorber Gas outlet (ppm)
ON	IO	0.11	0.15
	PA	0.15	0.27
OFF	PA	0.75	11.1

## Wash Tower Performance

The continuous measurement of gas compositions upstream and downstream of the water wash provides real-time evaluation of the wash tower performance. For this analysis, steady-state runs 41–70 were chosen as reliable PZ data from both absorber and wash tower outlets. Wash tower removal efficiency was defined as the fraction of PZ removed from the gas entering the wash tower. Figure 7 shows an inverse correlation between PZ entering wash tower and wash tower removal efficiency. On average, a removal efficiency of 94% was obtained. This means that about 6% of PZ entering the wash tower was emitted. These high removal rates suggest that the emissions were mostly vapor and not aerosol.

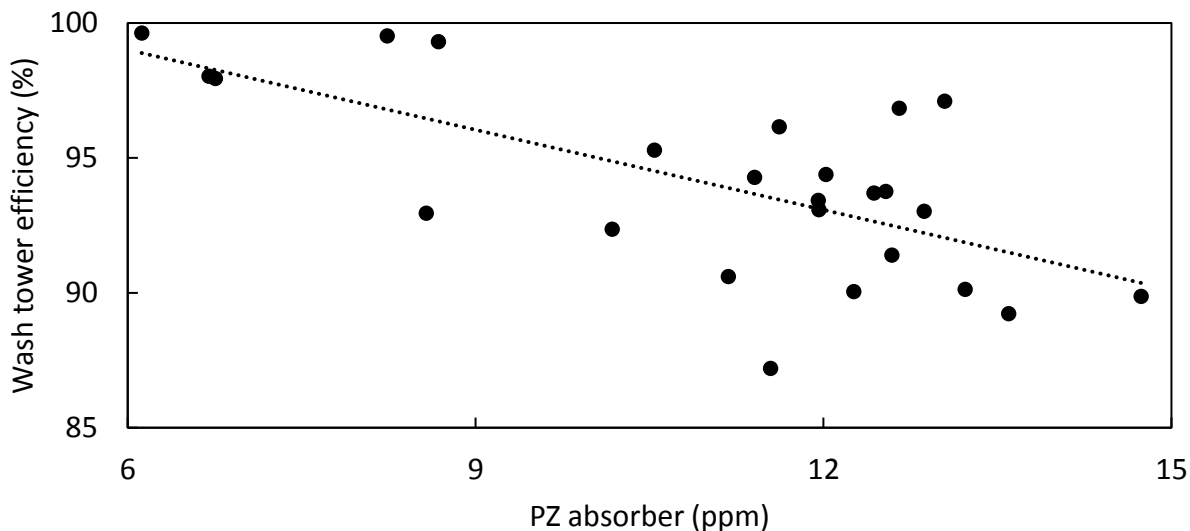


**Figure 7: Evaluation of wash tower performance during NGCC campaign with DCC bypassed. Each data point represents steady-state averages (runs 41–70) of PZ in absorber gas outlet.**

## Conclusions

1. Piperazine emissions averaged 0.7 ppm with <0.3 ppm for the first 600 operating hours and <1.7 ppm for the balance of the NGCC campaign.
2. Overall, the PZ emissions during the NGCC campaign were lower than the previous coal campaign. This reduced emission was expected and is likely due to the dilution of residual SO<sub>3</sub> at the flue-gas air mixing point particular to the NGCC campaign.
3. Although PZ emissions increased by a factor of 5 when the DCC was bypassed, the emissions were still below 1 ppm. This increase could have resulted from the nucleation of aerosols during quenching of the hot inlet gas in the absorber.
4. Solvent intercooling configurations did not significantly affect PZ emissions.
5. The wash tower efficiency was found to be inversely correlated with PZ: Higher absorber gas PZ resulted in lower wash tower efficiency. On average, only 6% of PZ entering the wash tower was emitted. This suggests that most of the PZ entering the wash tower was vapor, not aerosol.

## References

- Akinpelumi K, Saha C, Rochelle GT. "Piperazine aerosol mitigation for post-combustion carbon capture". *International Journal of Greenhouse Gas Control*, 2019;91,102845.
- Bade OM, Woodhouse S, Gorset O, Andersson V. "Method for mist control". 2015; US9180404B2.
- Beaudry M. *Aerosol measurement and mitigation in CO<sub>2</sub> capture by amine scrubbing*. The University of Texas at Austin. Ph.D. Dissertation. 2018.
- Fulk SM, Rochelle GT. "Quantification of Gas and Aerosol-phase Piperazine Emissions by FTIR Under Variable Bench-scale Absorber Conditions". 2014; 63,871–883.
- Gao T, Rochelle GT. "CO<sub>2</sub> absorption from gas turbine flue gas by aqueous piperazine with intercooling". *Industrial & Engineering Chemistry Research*. 2019. Accepted manuscript.
- U.S. Energy Information Administration (EIA). "Energy-Related Carbon Dioxide Emissions". 2019. [https://www.eia.gov/environment/emissions/carbon/pdf/2018\\_co2analysis.pdf](https://www.eia.gov/environment/emissions/carbon/pdf/2018_co2analysis.pdf)

# Piperazine Oxidation in PZAS<sup>TM</sup> Configuration

Yuying Wu<sup>a</sup>, Gary T. Rochelle<sup>a,\*</sup>

<sup>a</sup>*McKetta Department of Chemical Engineering,  
The University of Texas at Austin, 200 E. Dean Keeton St., C0400, Austin, TX 78712-1589*

---

## Highlights

5 m PZ tested for 4100 hrs with coal-fired flue gas and with simulated NGCC flue gas  
PZ oxidized at 0.1 kg PZ/ton CO<sub>2</sub> in coal case, and 0.3 kg PZ/ton CO<sub>2</sub> in NGCC case  
Carbon bed demonstrated to remove degradation products and reduce oxidation rate  
PZAS<sup>TM</sup> configuration and low NO<sub>2</sub> in flue gas mitigated oxidation

## Abstract

Piperazine (PZ) has shown promise as an amine scrubbing solvent to reduce CO<sub>2</sub> emissions due to its high CO<sub>2</sub> absorption rate, capacity, and thermal stability (Freeman et al., 2009). From February to June 2019, a pilot plant campaign was run for 2100 hours at the National Carbon Capture Center (NCCC) using 5 m slightly degraded PZ with simulated NGCC flue gas equivalent to a 0.64 MW NGCC plant. PiperaZine with the Advanced Stripper (PZAS<sup>TM</sup>) and a baghouse were used throughout the campaign, and N<sub>2</sub> sparging was applied at the bottom of the absorber.

The cumulative NH<sub>3</sub> production of the NCCC 2019 campaign was 180 mmol/kg over the 2100 hours, indicating a PZ oxidation rate of 0.07 mmol/kg/hr, equivalent to 0.3 kg PZ/tonne of CO<sub>2</sub>. Total formate and Ethylenediamene (EDA) were found to accumulate faster at lower temperature, probably due to their lower degradation rate. Carbon bed treating removed Cr selectively, and reduced NH<sub>3</sub> production from 0.1 mmol/kg/hr to 0.056 mmol/kg/hr after 400 hrs of operation.

*Keywords:* CO<sub>2</sub>; piperazine; degradation; oxidation; pilot plant

---

## 1. Introduction

Piperazine (PZ) is a superior second generation (2G) solvent for amine scrubbing in post-combustion CO<sub>2</sub> capture (Freeman et al., 2009). PZ has good thermal stability, allowing the stripper to operate at higher temperature and pressure to reduce the overall energy cost. However, the degradation of PZ can cause environmental issues and economic losses. The production of volatile products such as NH<sub>3</sub> and volatile amines can cause environmental problems (Kohl and Nielsen, 1997). The production and degradation of nitrosamines also make it necessary to understand the composition of degradation products (Nielsen et al., 2013). Only 70% of N and 30% of C products have been identified in bench-scale experiments (Nielsen, 2018), so the possibility of unknown toxic products remains. Economically, oxidation not only causes amine loss, but can also raise problems such as foaming and corrosion (Kohl and Nielsen, 1997). The accumulation of degradation products can increase the viscosity of the solvent, reducing the heat transfer performance in heat exchangers (Nielsen, 2019). Therefore, regular solvent reclaiming is required to keep the solvent relatively clean. Oxidation is expected to be a more significant cause of PZ loss than thermal degradation

(Freeman, 2011), so this work focuses on the oxidation of PZ. In cyclic systems, PZ can be oxidized to produce ammonia, ethylenediamine (EDA), 2-piperazinol (PZOH), and heat stable salts such as formate (Nielsen, 2018).

PZ can react with dissolved oxygen absorbed from the flue gas and carried to the high-temperature part of the heat exchanger and stripper in a cyclic system. Degradation products may catalyze this reaction, causing the degradation rate to increase over time (Cousins, 2015).

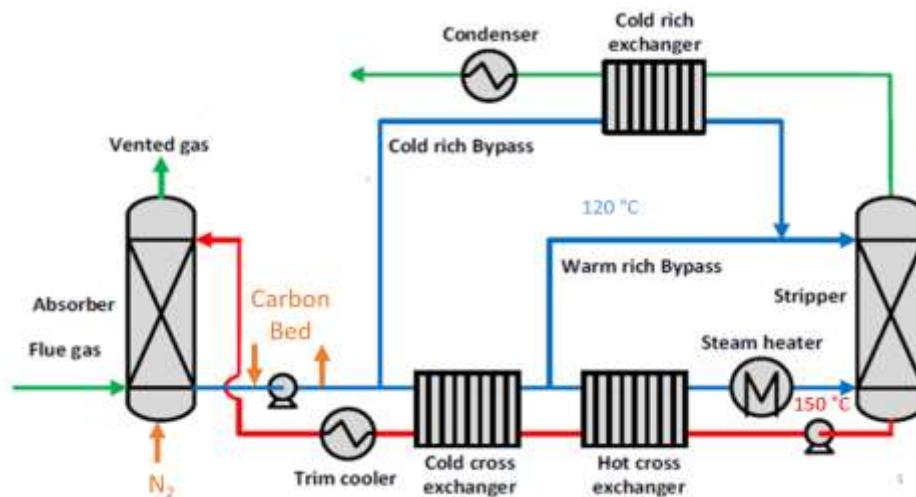


**Figure 1. Configuration of PZAS™ in the NCCC 2018-2019 Campaign**

From February to June 2019, a pilot plant campaign was run at the National Carbon Capture Center (NCCC) using 5 m PZ as solvent. The solvent experienced 2100 hours of operation in the previous NCCC campaign, and is slightly degraded, containing 5.3 mmol/kg total formate (Rochelle et al., 2019). The flue gas contained 4% CO<sub>2</sub> and 15% O<sub>2</sub>, equivalent to a 0.64 MW NGCC plant. The PZAS™ process, shown in Figure 1, and a baghouse in the parent plant was used throughout the campaign, and N<sub>2</sub> sparging was applied at the bottom of the absorber. Starting in this campaign, the solvent experienced another 2100 operating hours. The campaign started with 300-hrs at 150 °C stripper temperature, followed by 60 hrs at 160 °C. From 2460 to 2850 hrs, the stripper temperature was lowered to 140 °C, and the long-term operation at 150 °C stripper temperature started at 2850 hrs. At 3570 hrs, a carbon bed was activated to test the effect of removing degradation products and oxidation catalysts. LiOH and KHPO<sub>4</sub> were used as tracers to correct for water balance fluctuations and human error in the analytical process.

The oxidative degradation was studied and compared with previous pilot plant results using PZ, including results from Pilot Plant 2 (PP2), the Separations Research Program (SRP) in Austin, TX, and CSIRO Tarong in Queensland, Australia. PP2 used a slipstream of real flue gas from a coal-fired boiler, which had been treated with selective catalytic reduction and flue gas desulfurization to reduce SO<sub>x</sub> and NO<sub>x</sub>. 8 m PZ was used, and the campaign used a simple stripper operating from 120 °C to 150 °C (Nielsen, 2018). SRP treated a synthetic flue gas equivalent to 0.1–0.2 MW, typically consisting of air and 12 kPa CO<sub>2</sub> at 350 to 500 ACFM. 5 to 8 m PZ was used, and both simple stripper and advanced stripper configurations were tested. The stripper temperature was controlled at 150 °C (Nielsen, 2018). CSIRO Tarong is designed to capture up to 90% of the CO<sub>2</sub> in a 0.1 MW slipstream of coal flue gas from the Tarong Power Station. In late 2012 through early 2013, a campaign was conducted to test the effectiveness of 8 m PZ. Initially, 856 hours of parametric testing were performed to optimize energy performance. After these tests, the plant was

operated at steady-state conditions for 425 hours at a stripper operating temperature of 125 °C, followed by 421 hours at 155 °C to determine the effects of stripper temperature on energy performance and degradation (Cousins, 2015).

The identified degradation products of PZ are listed in Figure 2 in the order of production. Total formate concentration and NH<sub>3</sub> production rate were used to estimate the oxidation extent and rate of PZ oxidation.

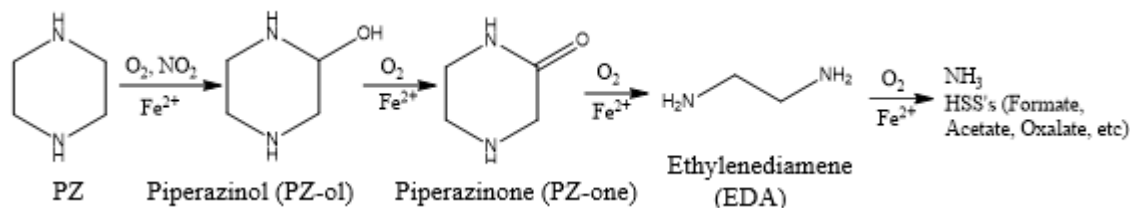


**Figure 2. Degradation products of PZ (Nielsen, 2018)**

In this campaign, the stripper temperature was changed from 140 °C to 160 °C, and the relationship between temperature and oxidation products was studied. The system was then operated at normal conditions, and the oxidation behavior was studied in the long-term test. In the latter half of the campaign, a carbon bed was used to remove catalytic metals and oxidation products to mitigate oxidation. Important degradation product results including total formate and dissolved Fe were compared with previous campaigns using PZ.

## 2. Analytical Methods

### 2.1. FTIR

The composition of gas (water, NH<sub>3</sub>, CO<sub>2</sub>, and PZ) from the absorber outlet and water wash outlet was quantified using hot gas FTIR. When analyzing gas emissions, continuous measurements were taken every minute.

### 2.2. Cation IC

PZ and other degradation products were quantified with cation chromatography (Dionex ICS2100). The eluent consisted of methanesulfonic acid (MSA) and deionized water. The procedure started with 5.5 mM MSA, increasing to 38.5 mM MSA during the run. The separation of ions was performed in an IonPac GC 17 guard column and an IonPac CS 17 analytical column. A chromatograph was created of the conductivity change in the solution (Freeman, 2011). The samples were gravimetrically diluted to 10000X, and PZ eluted at 33 minutes during a total runtime of 50 minutes.

### 2.3. Anion IC

Heat stable salts including formate, acetate, sulfate, and oxalate generated from PZ degradation were quantified with anion chromatography (Dionex ICS-3000). The eluent contained KOH and water. The separation of ions occurred in an IonPac AG15 guard column and an IonPac AS15 analytical column. A chromatograph was created of the conductivity change in the solution (Freeman, 2011). The samples were gravimetrically diluted to 100X, and the formate peak elutes at 9.2 minutes during a total run of 25 minutes.

### 2.4. ICP-OES

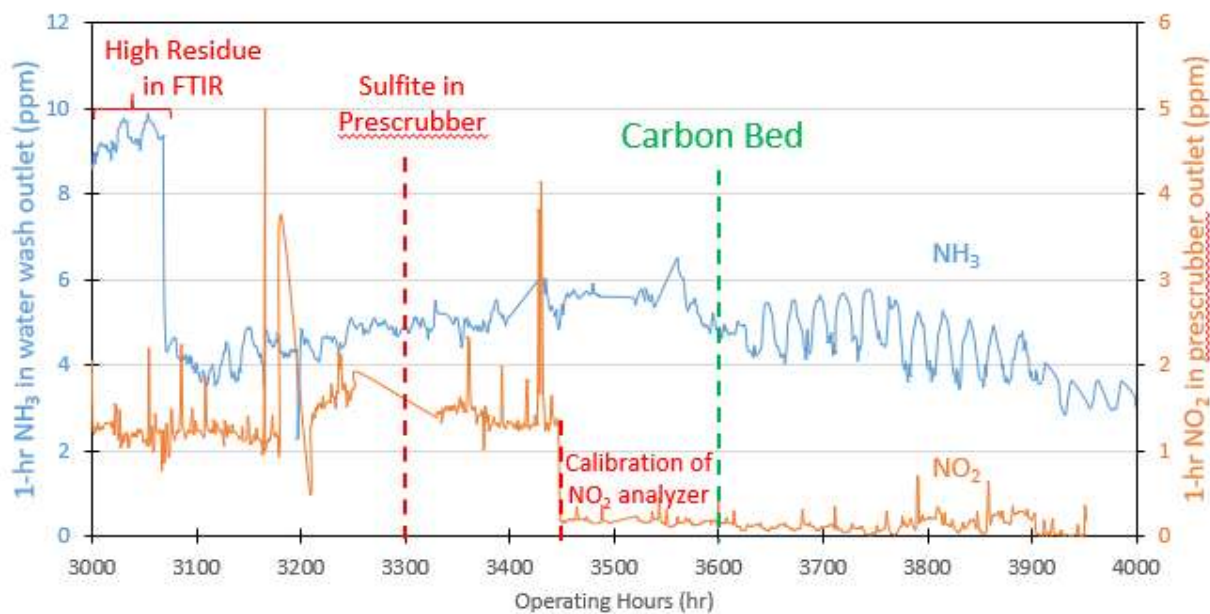
ICP-OES was used to analyze metals by the specific wavelength of UV light emitted in argon plasma flame at 7000K. Varian 10-ES Axial ICP-OES (Varian Inc., Palo Alto, CA) was used for this analysis (Nielsen, 2018). The system was controlled through ICP Expert II<sup>®</sup> software. 0.32 mL samples were diluted into 8 mL with 2 wt % nitric acid to allow for multiple analyses, and standards between 0.5 ppm and 25 ppm were prepared fresh for each series. For each element, three wavelengths with the highest intensity were used, and four measurements were performed at each wavelength.

### 3. Discussion and Results



**Figure 3. Visual Effects of Solvent by Carbon Bed**

After 3600 hrs of operation, the carbon bed was turned on to mitigate oxidation by removing degradation products. The carbon bed treated a slipstream of rich solvent that was taken from the rich pump discharge and returned to the rich storage tank before the rich pump. As shown in Figure 3, the solvent color changed significantly from dark brown to light yellow. After 9 days of operation, the solvent color was very close to that of the fresh solvent, indicating some degradation or corrosion products have been removed.

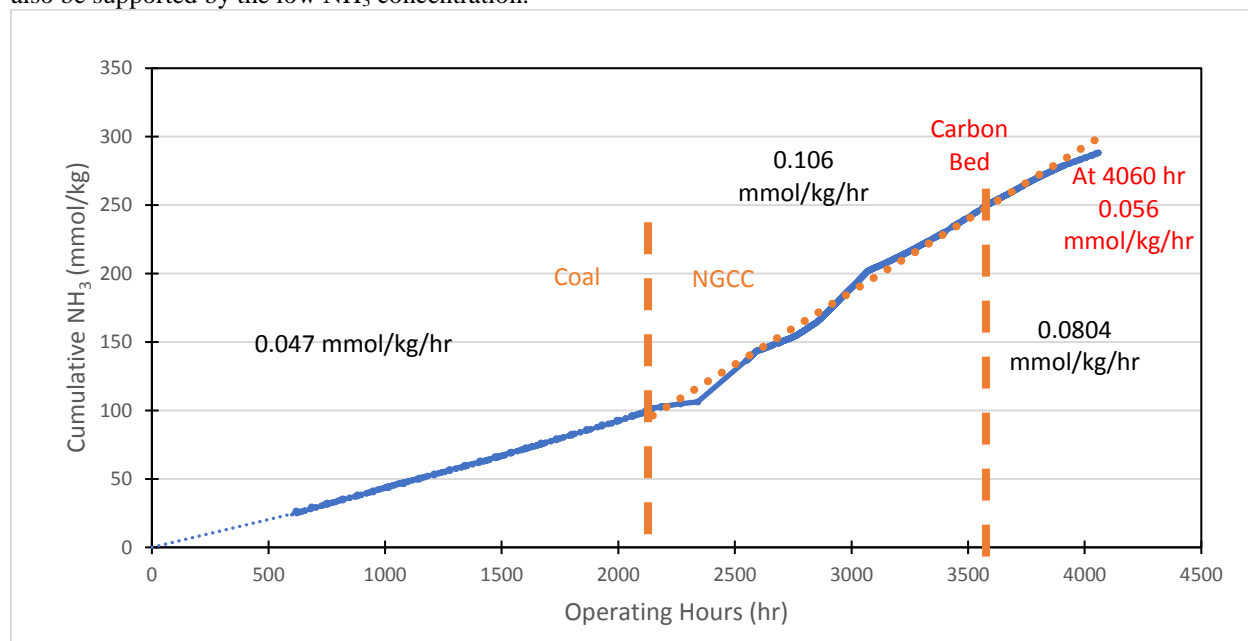


\* NO Concentration relatively stable at 50 ppm

**Figure 4. NH<sub>3</sub> Production Rate in water wash outlet and the NO<sub>2</sub> concentration in absorber inlet**

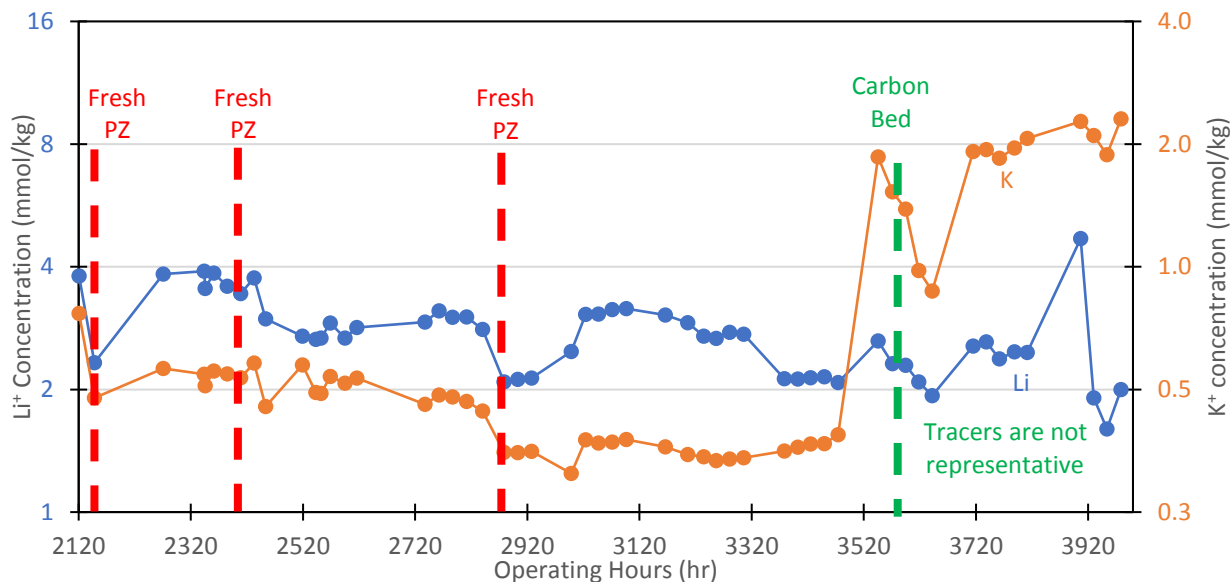
The NH<sub>3</sub> concentration in the water wash gas outlet was monitored continuously, shown as the blue curve in Figure 4. Based on the results from previous bench-scale experiments, 1 mol of PZ will oxidize into 1 mol of NH<sub>3</sub>, thus the NH<sub>3</sub> production rate can represent the PZ oxidation rate (Nielsen, 2017). Before 3100 hours, the FTIR results were believed to be inaccurate due to high NH<sub>3</sub> residue. Between 3100 and 3500 hours, the NH<sub>3</sub> concentration increased steadily to 6 ppm as the solvent became more degraded. When the carbon bed was turned on, the NH<sub>3</sub> concentration

began to decrease, and reached 3.5 ppm after 400 hours. This trend showed that oxidation was mitigated by using the carbon bed, which could remove oxidation catalysts for PZ or its degradation products. The  $\text{NH}_3$  production rate fluctuated diurnally between 3600 and 4000 hours, which was most probably due to the change in  $\text{NH}_3$  solubility in water due to temperature difference between day and night. The  $\text{NO}_2$  concentration was also shown as orange in Figure 4. Previously,  $\text{NO}_2$  was found to oxidize PZ (Fine, 2015), and bench-scale results showed that 1 mol of  $\text{NO}_2$  oxidizes 1.5 mol PZ by modelling  $\text{NO}_2$  with addition of  $\text{NaNO}_2$  (Nielsen, 2018). The apparent  $\text{NO}_2$  was high at 3 ppm from 3000 to 3450 hours despite the fact that sulfite was added to the prescrubber at 3300 hrs. However, when the  $\text{NO}_2$  analyzer was calibrated at 3450 hrs, the  $\text{NO}_2$  decreased to  $<0.2$  ppm. As a result, it is believed that the high  $\text{NO}_2$  results were due to inaccurate analyzer results, and the actual  $\text{NO}_2$  was always low during the campaign. This reasoning is also supported by the low  $\text{NH}_3$  concentration.



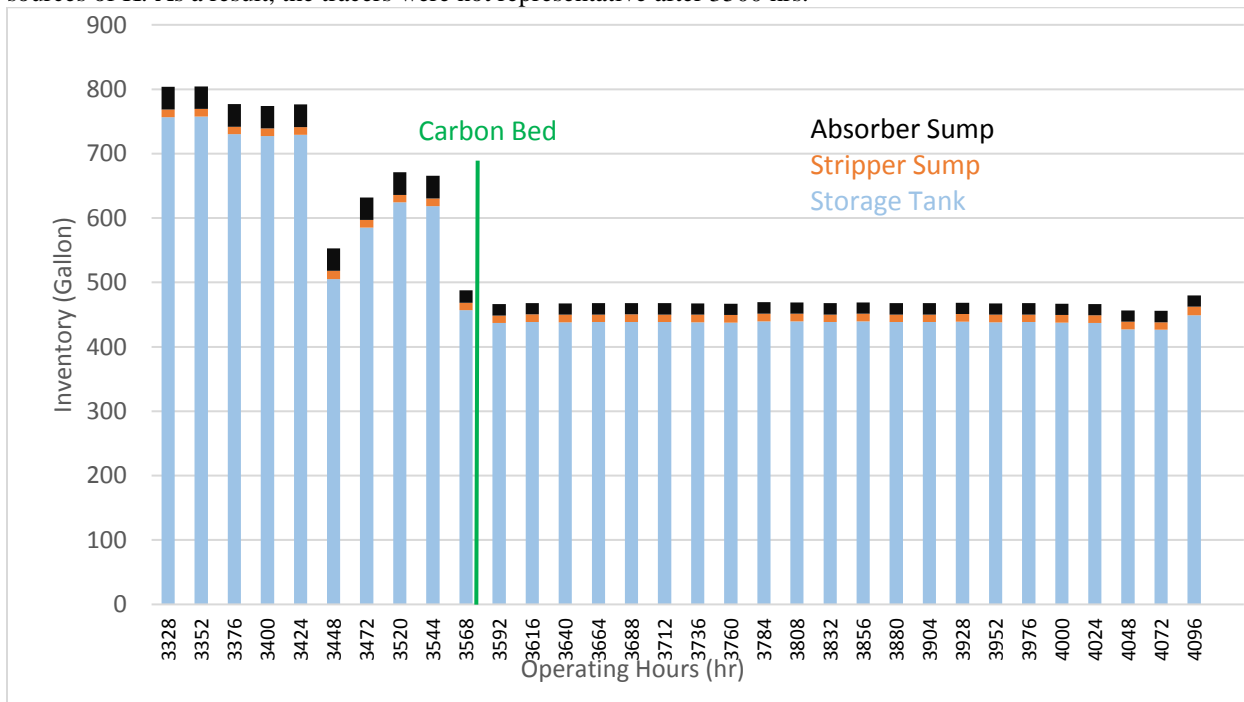
**Figure 5. Cumulative  $\text{NH}_3$  over the NCCC 2018–2019 Campaign**

Figure 5 shows the cumulative  $\text{NH}_3$  production in 4200 hrs of operation. During the coal campaign, the  $\text{NH}_3$  production rate was relatively constant at 0.047 mmol/kg/hr, corresponding to an oxidation rate of 0.1 kg PZ/ton  $\text{CO}_2$  captured. After the NGCC campaign started, the  $\text{NH}_3$  production rate increased to 0.106 mmol/kg/hr, corresponding to an oxidation rate of 0.3 kg PZ/ton  $\text{CO}_2$ . This may be because the NGCC condition is more oxidizing due to a higher oxygen content in the flue gas. After the carbon bed was turned on, the  $\text{NH}_3$  production decreased, and the rate was estimated as 0.056 mmol/kg/hr at the end of the campaign. If the campaign had continued with the carbon bed on, more catalysts may have been removed, and the  $\text{NH}_3$  rate may have continued to decrease. The average rate when the carbon bed was turned on was 0.0804 mmol/kg/hr.



**Figure 6. Tracer Concentrations in NGCC Campaign**

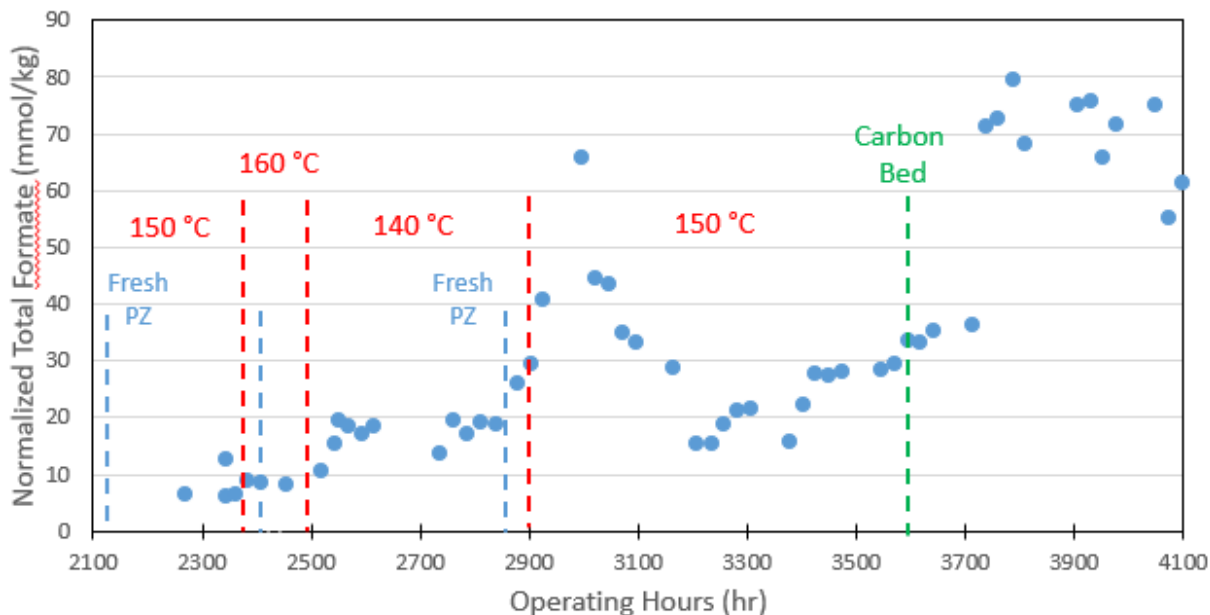
In order to correct for water balance and human error during sampling, transportation, and analysis, two tracers, LiOH and  $\text{KH}_2\text{PO}_4$ , were added at the start of the campaign, and concentrations of degradation products and PZ were corrected based on the tracer concentrations. The Li and K concentrations are shown in Figure 6. At 2130, 2400, and 2880 hrs, fresh PZ was added, and both tracers showed an immediate drop in concentration. Before 3300 hrs, the two tracers behaved similarly, indicating that the inventory can be represented by the tracers. However, starting at 3500 hrs, K increased much more significantly than Li, and the ratio of the tracer concentrations deviated from the initial ratio of LiOH and  $\text{KH}_2\text{PO}_4$  added into the solvent, indicating that the carbon bed could have introduced external sources of K. As a result, the tracers were not representative after 3500 hrs.



**Figure 7. Estimated Inventory in Absorber Sump, Stripper Sump, and Storage Tank**

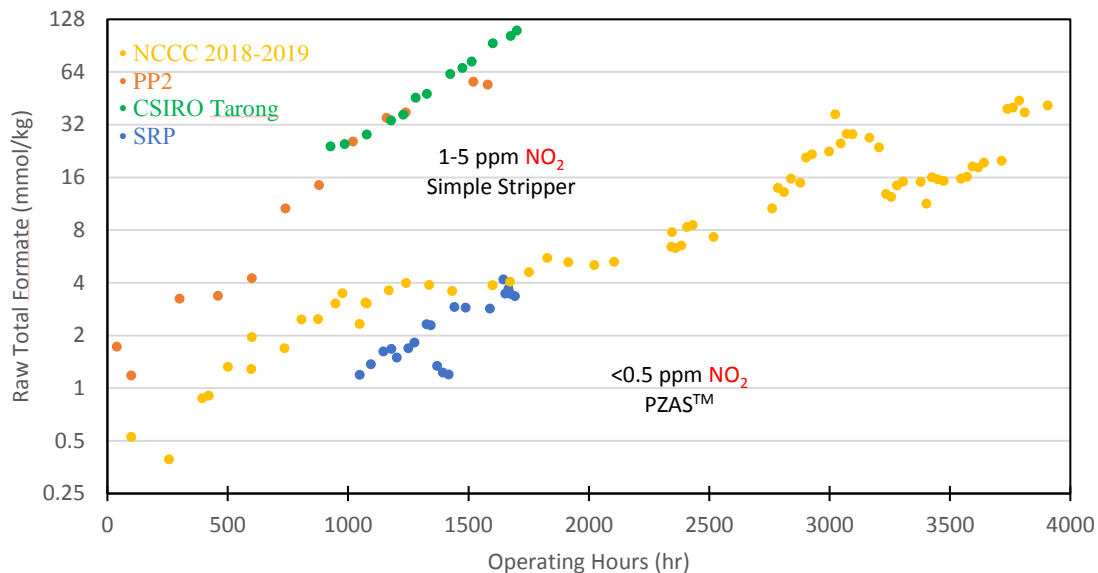
Without the tracer data, the inventory in the rich storage tank, the absorber sump, and the stripper sump were estimated to keep track of the total inventory of solvent. As shown in Figure 7, the total inventory stayed relatively

constant after the carbon bed was turned on at 3570 hrs. While the inventory of packing, heat exchangers, and piping was not included, it was assumed that the inventory in these parts stayed constant. As a result, the water balance was assumed to be constant, and no corrections were made based on the tracers over this time period.



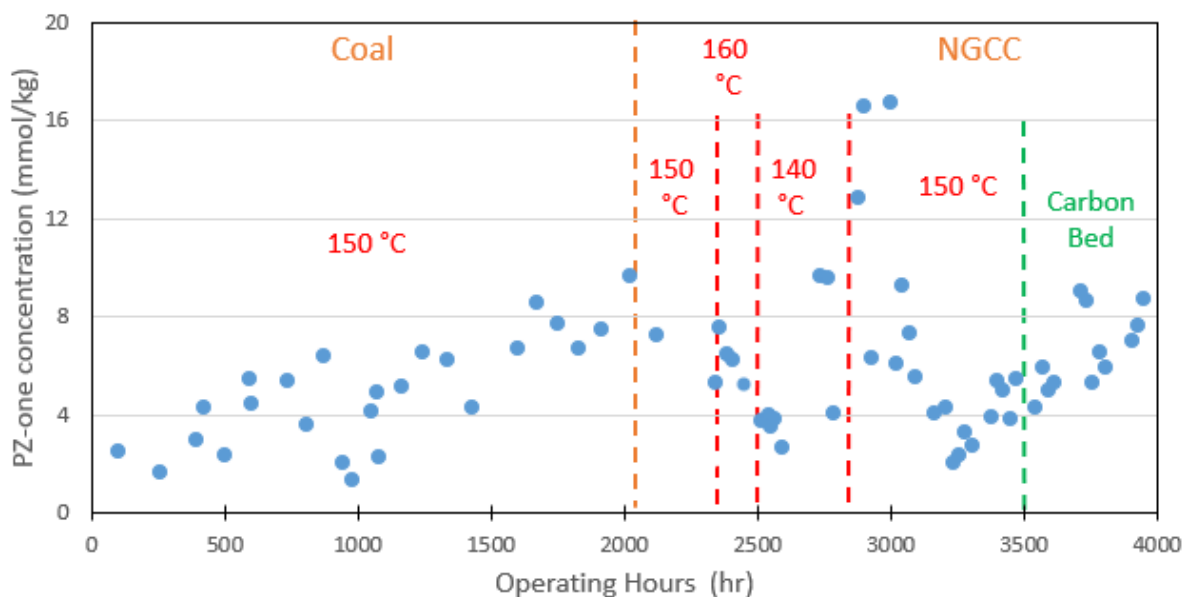
**Figure 8. Normalized Total Formate in NGCC Campaign**

Total formate was used as an important indication of PZ oxidation extent (Nielsen, 2017). Figure 8 shows the normalized total formate concentration. When the stripper temperature was high at 150 °C and 160 °C, the total formate concentration stayed low. However, when the temperature was reduced to 140 °C, the total formate concentration increased at an accelerated rate. This suggests that formate can degrade into other products, and the low temperature resulted a low degradation rate, causing the accumulation of total formate. After the stripper temperature was raised back to 150 °C, the degradation rate of formate increased, causing the concentration of formate to decrease until equilibrium was reached. When the carbon bed was turned on, there was a step increase followed by some fluctuations in the total formate concentration. This increase may be due to existing formate from the carbon bed; it is unlikely that it is due to oxidation.



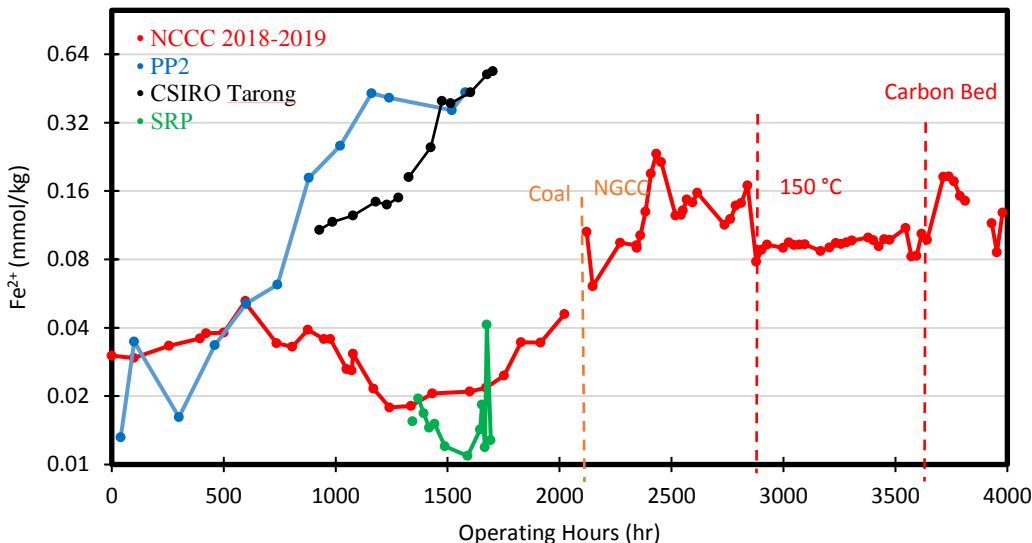
**Figure 9. Comparison of Raw Total Formate from NCCC 2018–2019, PP2, CSIRO, and SRP Campaigns**

Figure 9 shows the total formate in the NCCC 2018–2019 campaign and previous pilot plant campaigns using 5 m PZ. The total formate production rate in NCCC 2018–2019 and SRP is much slower than in the other two pilot plants. The main difference is that NCCC and SRP used the PZAS<sup>™</sup> advanced stripper and had low NO<sub>2</sub> in flue gas; the other two campaigns used a simple stripper and had a relatively high inlet NO<sub>2</sub>.



**Figure 10. Normalized PZ-one Concentration in NCCC 2018-2019 Campaign**

PZ-one is an early degradation product of PZ and usually accumulates when the solvent is clean and decomposes when the solvent becomes more degraded (Nielsen, 2018). As seen in Figure 10, PZ-one increases steadily until 2100 hrs. PZ-one decreased when the temperature increased to 160 °C, and then increased significantly when the temperature decreased to 140 °C. This observation indicates that the degradation of PZ-one is highly temperature-dependent. After the temperature was reduced to 150 °C, PZ-one decreased again due to a higher degradation rate. After the carbon bed was turned on, PZ-one increased at a rate similar to that at the start of the campaign, indicating that the catalysts that were formed during the operation to oxidize PZ-one were removed by the carbon bed.



**Figure 11. Raw Fe Comparison of NCCC 2018–2019, PP2, CSIRO, and SRP Campaigns**

As shown in Figure 11, the Fe concentration fluctuated between 2100 and 2900 hrs due to changes in temperature, which may affect the oxidation. Between 2900 and 3500 hrs, the system was operated under a constant stripper temperature of 150 °C, and the Fe was increasing slowly but steadily, similar to the trend of  $\text{NH}_3$  concentration. This relationship was also seen in the NCCC 2018 campaign (Rochelle et al., 2019). After the carbon bed was turned on, Fe increased and then fluctuated, indicating that the carbon bed is not useful for removing Fe. Compared to the other campaigns, the Fe in the NCCC 2018–2019 campaign is still low, which is consistent with the observations of low degradation products, possibly due to low  $\text{NO}_2$  in flue gas and the PZAS<sup>TM</sup> configuration.

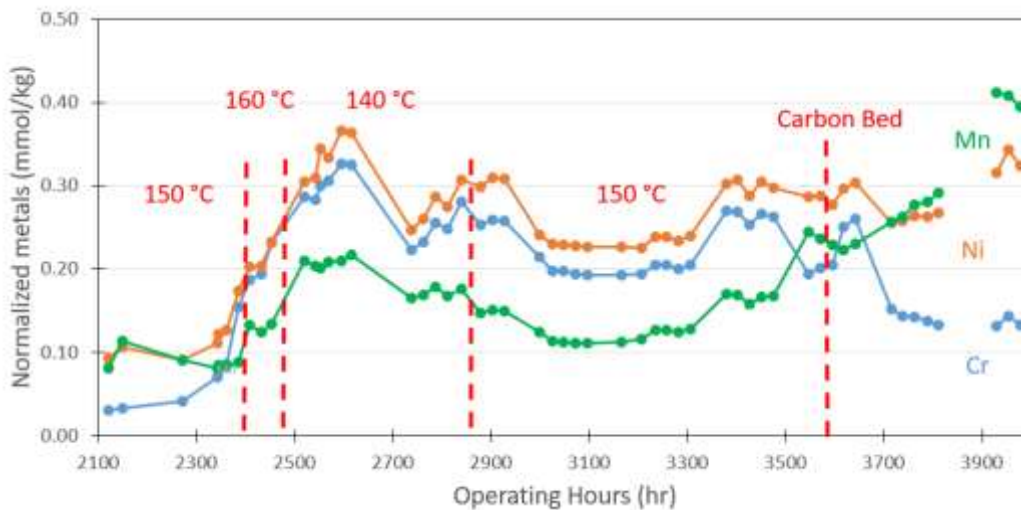


**Figure 12. Cr, Ni, and Mn Concentration in the NCCC 2018–2019 Campaign**

Figure 12 shows the concentration of other stainless steel metals including Cr, Ni, and Mn. Before the carbon bed was turned on, they showed similar behavior, indicating that the concentration changes were mainly due to corrosion. After the carbon bed was turned on, the Mn and Ni still increased, but the Cr concentration decreased steadily, which may be a result of Cr being selectively removed by the carbon bed.

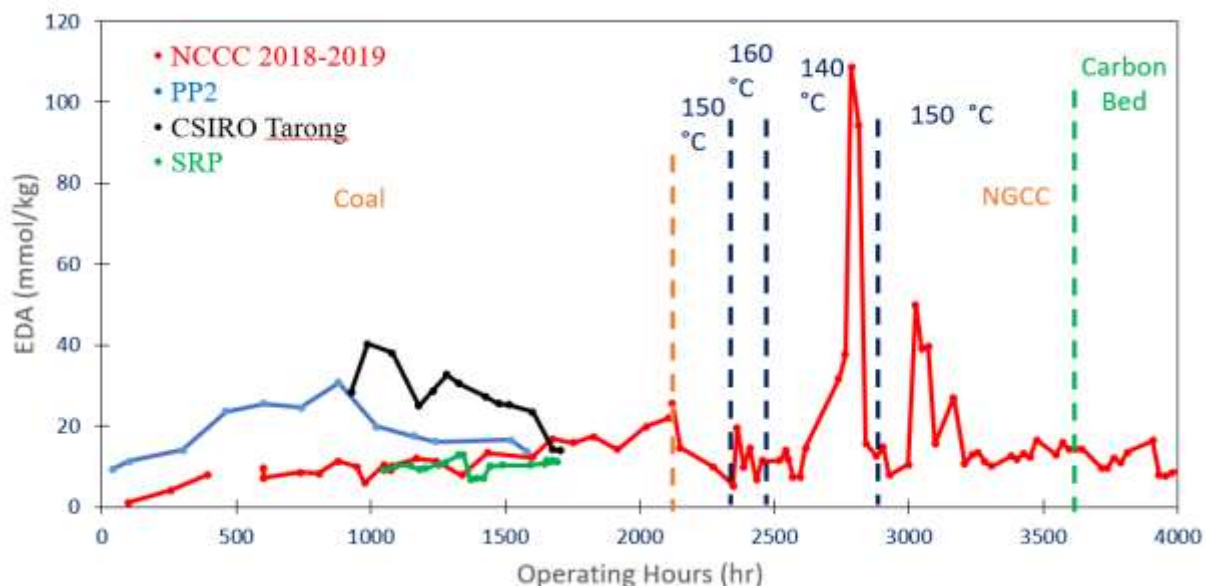


**Figure 13. Raw EDA Comparison of NCCC 2018–2019, SRP, CSIRO, and PP2 Campaigns**

The raw ethylenediamine (EDA) concentration is shown in Figure 13, compared to results from other pilot plants using PZ. When the temperature is high at 150 °C and 160 °C, the EDA concentration stays low. However, when the temperature is reduced to 140 °C, the EDA concentration increases significantly. Since EDA can be thermally degraded into 2-imidazolidone, the increase at the low temperature can be due to the shift of equilibrium towards formation of EDA. In all the 150 °C operation ranges of the four campaigns, the EDA concentration decreases after reaching 20 to 40 mmol/kg/hr, indicating that EDA may be in equilibrium with its degradation products at this concentration.

#### 4. Conclusions

1. The carbon bed removes oxidation catalysts and reduces  $\text{NH}_3$  production rate.
2. The carbon bed does not remove Fe, but selectively removes Cr.
3. PZ in the NCCC campaign oxidized at a slower rate compared to the CSIRO and PP2 campaigns, possibly due to use of the PZAS<sup>TM</sup> and the absence of  $\text{NO}_2$  in inlet gas. The total  $\text{NH}_3$  production was 280 mmol/kg over 4200 hrs of operation. The PZ oxidation rate was estimated to be 0.1 kg PZ/ton  $\text{CO}_2$  for the coal condition, and 0.3 kg PZ/tonne  $\text{CO}_2$  for the NGCC condition.
4. EDA reaches equilibrium with its degradation products at 20 to 40 mmol/kg at 150 °C. The concentration increases significantly when the temperature is low.

#### Acknowledgements

This work was supported by the  $\text{CO}_2$  Capture Project and the Texas Carbon Management Program.

#### References

- Cousins A., Nielsen P.T., Huang S., Cottrell A., Chen E., Rochelle G.T., Feron P.H. Pilot-scale evaluation of concentrated piperazine for  $\text{CO}_2$  capture at an Australian coal-fired power station: Duration experiments. *Greenhouse Gases: Science and Technology* 2015;5(4):363–73. doi:10.1002/ghg.1507.
- Fine N.A. Nitrosamine Management in Aqueous Amines for Post-Combustion Carbon Capture, Ph.D. dissertation, University of Texas at Austin. 2015.
- Freeman S.A., Dugas R., Wagener D.H., Nguyen T., Rochelle G.T. Carbon dioxide capture with concentrated, aqueous piperazine.

- International Journal of Greenhouse Gas Control* 2010; 4(2):119–24. doi:10.1016/j.ijggc.2009.10.008.
- Freeman S.A. Thermal Degradation and Oxidation of Aqueous Piperazine for Carbon Dioxide Capture. Ph.D. dissertation, University of Texas at Austin. 2011.
- Kohl A.L., Nielsen R.B. Gas purification. 1997.
- Nielsen P.T., Li L., Rochelle G.T. Piperazine Degradation in Pilot Plants. *Energy Procedia* 2016;37:1912–23. doi:10.1016/j.egypro.2013.06.072.
- Nielsen P.T., Rochelle G.T. Effects of Catalysts, Inhibitors, and Contaminants on Piperazine Oxidation. *Energy Procedia* 2017;114:1919–29. doi:10.1016/j.egypro.2017.03.1323.
- Nielsen P.T. Oxidation of Piperazine in Post-Combustion Carbon Capture. Ph.D. dissertation, University of Texas at Austin. 2018.
- Rochelle G.T., Wu Y., Chen E., Akinpelumi K., Fischer K.B., Gao T., Liu C.T., Selinger J.L. Pilot Plant Demonstration of Piperazine with the Advanced Flash Stripper. *International Journal of Greenhouse Gas Control*, 84, 72–81. doi: 10.1016/j.ijggc.2019.03.

## Appendix

### A1. Common Name, IUPAC Name and CAS Number of the Degradation Products

Common Name	IUPAC Name	CAS Number
Piperazine	Piperazine	110-85-0
Piperazinol	(2R)-piperazin-2-ol	
Piperazinone	piperazin-2-one	5625-67-2
Ethylenediamine	1,2-Ethanediamine	107-15-3
Formaldehyde	Methanal	50-00-0
Formate	methanoate	